EXPLORING THE ELECTRON COMPONENT IN INCOHERENT SCATTER FROM THE IONOSPHERE

A Dissertation

Presented to the Faculty of the Graduate School

of Cornell University

in Partial Fulfillment of the Requirements for the Degree of

Doctor of Philosophy

by

Asti Bhatt

February 2010

EXPLORING THE ELECTRON COMPONENT IN INCOHERENT SCATTER FROM THE IONOSPHERE

Asti Bhatt, Ph.D.

Cornell University 2010

Small thermally-induced fluctuation in the ionospheric electron density present a scattering cross-section, if probed with a radar frequency higher than the plasma frequency. This technique, known as the incoherent scattering from the ionosphere, is a well-established field of study now. Since the conception of this field of study in 1958, numerous theoretical and experimental efforts have led the way to the high precision ionospheric research we have today. The theory of the incoherent scatter is highly robust. Recent advances in the radar hardware and computing technology have made it possible to probe the ionosphere using the full extent of this theory. In the effort presented here, high spectral resolution incoherent scatter experiments have been used to, for the first time, fully understand the theoretical predictions concerning the electron component of incoherent scatter. The two resonance lines that constitute the electron component are called the gyro line and the plasma line, and are greatly affected by the presence of the earth's geomagnetic field. The experiments described here present the first unambiguous measurements of the gyro line with high spectral resolution in the incoherent scatter spectrum. Plasma line experiments presented here show the existence of frequency gaps that were predicted in the early days of incoherent scatter theory, but never observed. High latitude plasma line measurements are presented here to show that using the plasma line technique, the

gravity waves in the thermosphere can be detected. The intention here is to observe all the components of the incoherent scatter and apply them to understand ionospheric processes.

BIOGRAPHICAL SKETCH

Asti Nimittaben Bhatt was born August 15, 1979 in Ahmedabad, India. She received the Bachelor of Engineering in Electronics and Communications from The Dharamsinh Desai Institute of Technology of Gujarat University in 2001 and the Master of Science in Electrical Engineering from the Utah State University in 2004. She worked as a Research Assistant at the Space Dynamics Lab at the Utah State University and both as a Research and a Teaching Assistant in the School of Electrical and Computer Engineering at Cornell University. She served as the Student Representative for the RF Ionospheric Interactions Workshop from 2005-2008. She worked as an intern at the Patni Computer Systems in Mumbai, India, and the SRI International in Menlo Park, California. She is a member of the American Geophysical Union and an incoherent person overall.

This thesis is dedicated to my parents (Nimitta and Ashvin) and my grandparents (Sarla and Narhari) who made me who I am.

ACKNOWLEDGEMENTS

The road to this thesis began with my participation in the Polar Aeronomy and Radio Science summer school held at Arecibo, Puerto Rico in 2004 during the summer before my first semester at Cornell. Several experiments, coherent and incoherent discussions, and travels to far off worlds later this thesis has found its form. Along the way I have had the opportunity to work for and alongside a great group of people whose contributions I would like to acknowledge here.

I feel deeply privileged to have as my graduate advisor, Prof. Mike Kelley, whose guidance, support, encouragement and hands-off approach has made my time at Cornell special, and who has taught me not only science but also valuable life skills. I am thankful for his friendship throughout this process. I am grateful to my graduate committee members, Prof. Don Farley and Prof. Dave Hysell, who were always available, and have helped me through teaching excellent classes, group meetings, and valuable discussions. I would also like to acknowledge Prof. Seyler for teaching difficult concepts and Prof. Swartz for useful discussions.

I especially thank Laurie Shelton for her unending kindness and Scott Coldren for always being there to help. I also thank my colleagues at MIT's Haystack Observatory for their support while I finished writing, Anthea Coster in particular.

I thank my collaborators at Arecibo Observatory, Mike Sulzer, without whom this thesis would not have been possible, Nestor Aponte, who always helped

in these experiments regardless of the hour of night, and Sixto Gonzaléz for his support and encouragement. I also thank my collaborators at SRI International, Mike Nicolls, who has been a friend and a collaborator since Cornell and whose insights have been invaluable, Craig Heinselman, for providing opportunities for working with AMISR data and helping me understand radar systems, and Mary McReady for her constant support.

I feel lucky to have excellent friends and colleagues. Elizabeth Kendall, who has been a mentor and a lifelong friend even by being on the other coast; Alex Cerruti, who started scaring-Asti-through-loud-noises, a tradition that was continued by Brady O'Hanlon, also known as Mr. Fix-it; Erik Lundberg, who I have enjoyed walking the same road home with in cold to freezing Ithaca weather; Rudy Cuevas, SPP's resident Salsa guru; Camilo Ramos and Esayas Shume, who introduced me to the diverse life in Ithaca and Collegetown Bagels. Ithaca will also remind me of friends and roommates who introduced me to the larger Cornell and Ithaca community and made my time in Ithaca extra special.

Finally, a family that has been a huge part of my journeys. My mother, for putting me on this path and enthusiastically being a part of my life abroad; my father, for teaching me to stay the course; my grandmother, for constantly encouraging to study harder; my grandfather, for having faith in all my endeavors; and Vatsal-Kavita-Arnav, for being a family I can call a home away from home.

TABLE OF CONTENTS

LIST OF FIGURES

CHAPTER 1

INTRODUCTION

1.1 Ionosphere and Radio Science

The earth's ionosphere is a region of charged particles in the upper atmosphere from 60 to beyond 1000 km. It is considered the natural plasma laboratory. Energy from the Sun's ultraviolet rays ionizes neutral gases creating the ions and the electrons during the day time, which recombine in the absence of the Sun. Depending on the neutral density that varies with the altitude, the degree of the ionization changes.

In 1902, Oliver Heaviside proposed the existence of a conducting layer in the earth's upper atmosphere that would allow multi-hop transmission of the electromagnetic waves. It was termed the Kennelly-Heaviside layer. Sir Edward Appleton confirmed the existence of the ionosphere in 1927, for which he was awarded the Nobel Prize in 1947. This discovery was followed by several theoretical and experimental investigations in radio propagation. The development of radio also helped further discover the nature of the ionosphere as a non-linear medium.

The ionosphere is divided in three primary regions. The division is based on the concentration of the neutral particles, which determines the collision frequency between the charged particles and the neutrals. The regions are called D, E,

and F, in the order of most to least neutral density (Fig. 1.1). The D region is mostly responsible for absorbing the electromagnetic waves during the active solar-geomagnetic conditions that increase the collision frequency. The E region is essentially a thin layer around 100 km that was the first to be named (E for Electric). This region gets most affected by meteors and auroral precipitation. F-region is where the peak of the electron density occurs depending on the time of the day. The electron density falls off above the altitude of the peak.

To ensure the collective behavior for the plasma, the criterion $N_e\lambda_{de}^3 \gg 1$ should be satisfied, where N_e is the electron density and λ_{de} is the electron Debye length. The system scale length should also be much greater than the Debye length. Both of these conditions hold true for the ionospheric plasma. The Debye length for electrons is defined as,

$$\lambda_{de} = \sqrt{\epsilon_0 k_B T_e / N_e e^2}, \tag{1.1}$$

where ϵ_0 is the free space permittivity, k_B is the Boltzmann's constant, T_e is the electron temperature, and e is the charge of a single electron. In the ionosphere, typical N_e is $10^8 - 10^{12}/m^3$ and the electron temperature is of the order of a few hundred to well beyond a $1000^\circ K$. The Debye length is generally of the order of a few mm or cm, while the scale lengths are of the order of a few km. The ions and the electrons follow a Maxwellian velocity distribution (*Chen*, 1984).

Since the process of ionization depends strongly on the Sun, any changes in the Sun's energy output are reflected in the ionosphere. The earth also has a dipole geomagnetic field, which magnetizes the ionospheric plasma. Being the buffer

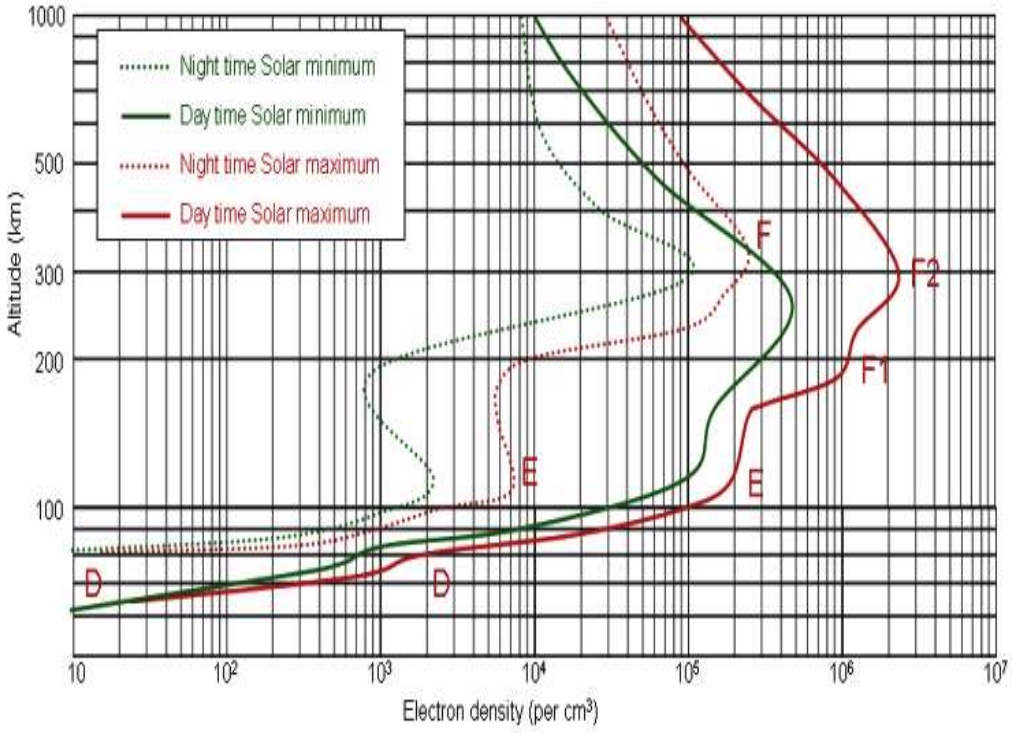

Figure 1.1: A typical ionospheric electron density profile showing various regions of the ionosphere for solar maximum and solar minimum conditions. The experiments described in this thesis have been done in the solar cycle leading up to a deep solar minimum. The region below the F layer peak frequency is known the 'bottomside ionosphere' while that above the F peak is known as the 'topside ionosphere'.

zone between the magnetosphere and the lower atmosphere, the ionosphere gets affected by the processes in both of these regions. The temperature and the pressure changes in the lower atmosphere can drive buoyancy waves (also known as gravity waves) all the way up to the thermosphere, which in turn affect the ionospheric electron density. The geomagnetic field of the earth affects these plasma processes profoundly and creates very clear distinction between the equatorial, the mid-latitude, and the high-latitude ionospheres.

The science of Radio Detection and Ranging (RADAR) started to develop during the World War II. Various types of radars were developed for civilian and military use to detect hard targets like aircrafts. This thesis is concerned with radar scattering from electrons in the ionosphere, which present a soft, volume target. The expression for the received power from a monostatic radar for a volume scatterer is,

$$P_R = \frac{P_T G_T A_{eff} V \sigma_{radar}}{16\pi^2 R^2}, \tag{1.2}$$

where P_R = Received power, P_T = Transmitted power, G_T = Transmitter gain, A_{eff} = Antenna effective area, V = Scattering volume, σ_{radar} = Radar scattering cross section per unit volume and R = Radar range. The basics of incoherent scatter in particular are discussed in the following sections.

1.2 Incoherent scattering from the ionosphere

The ions and the electrons in the ionosphere have random thermal velocities, which results into a weak scatter. This scatter, known as "incoherent" scatter due to the uncorrelated motions of the electrons, is a very useful diagnostic tool for the ionosphere.

1.2.1 Beginnings

In 1958, a Cornell University professor W. E. Gordon conceived the idea that if a radar with a large enough area and power is built, the combined scatter from the multiple scatterers (electrons) with very small cross-sections can be observed (*Gordon*, 1958). The frequency of the radar would be much higher than the maximum plasma frequency in the ionosphere to ensure that the waves pass through the plasma without perturbing it, except for a weak scatter from spatial density fluctuations. These density fluctuations contain information about the ionospheric plasma. It is important to note that the electrons present a "soft" volume target, as opposed to a "hard" target like an airplane. The scattering volume for the electrons would fill the radar beam and change with the radar range. The Doppler shift due to the thermal motion of these electrons can be used to infer the electron temperature. The idea was soon tested (*Bowles*, 1958). However, the observed signals indicated that the echoes had a Doppler broadening in the range of the ion thermal velocities rather than the electron thermal velocities. Since the ions are much heavier than the electrons, they move much more slowly and the Doppler frequency range is smaller. These results encouraged several authors to develop the theory of the thermal density fluctuations in a plasma. Within a few years of the conception of this idea, the theory for a non-magnetized plasma was almost fully developed (e.g., *Dougherty and Farley*, 1960; *Fejer*, 1960; *Salpeter*, 1960; *Rosenbluth and Rostoker*, 1962). The magnetic field was included in the theory soon after (e.g., *Hagfors*, 1961; *Salpeter*, 1961). The refinements in the theory now include the effects of the ion and electron collisions, unequal ion and electron temperature, multiple ion species, and particles with a non-Maxwellian velocity distribution.

Along with the theoretical work, the efforts for building the required instrumentation were already underway. The first measurements began in 1961 with a 50 MHz radar at the Jicamarca Radio Observatory (11°57′ N, 76°52′ W) near Lima, Peru. A 430 MHz spherical dish radar with a diameter of 300 m was constructed at Arecibo (18°20′ N, 66°45′ W) in Puerto Rico and began operations in 1963. The initial measurements of the scattered power indicated differences between the theory and the observations. This was solved when *Bowles et al.* (1962) showed that the theory and the experiments used the values of the radar cross-section differing by 4π. It was shown that the required receiver bandwidth was much smaller due to the slower ion velocities, which meant that the total received noise was also much less. So the radars did not need to have as large a receiving area as was initially proposed by Gordon in order to get a better signal-to-noise ratio.

1.2.2 Basic theory

In the case of incoherent scattering, the incident field on the particles is much larger than the scattered field from each individual particle and hence unaffected by any loss in the scattering power due to multiple scatterers. The incoherent scattering cross section is proportional to the ionospheric electron density. The electron density fluctuations leading to the incoherent scatter have been treated with both microscopic and macroscopic mathematical approaches. The microscopic approach, widely known as the dressed particle approach, con-

siders a test ion in the plasma. This ion is surrounded by a cloud of electrons that create a potential distribution around the test ion that is different from the free space potential. This is known as Debye shielding and the electron cloud is called the Debye cloud. Beyond a few Debye lengths the test ion is completely shielded from the rest of the plasma, since the Debye cloud acts as the charge neutralizer. The cloud is essentially a statistical effect that has an excess of electrons and a deficiency of ions. This is the result of electrons and ions with slightly perturbed orbits, due to the presence of the test ion, getting attracted and repealed respectively from the test ion. If this test ion is moving, it would have a velocity comparable to the mean ion thermal velocity. The shielding by the ions will be reduced if the test ion is faster than those. Electrons are faster and can move with the test ion, and hence largely make up the cloud. This way very fast test ions will be almost completely shielded by the electrons, which from the scattering standpoint act as a slow electron. The scattering cross-section of these ions is four times that of a test ion at rest. However, the ions have a Maxwellian velocity distribution and there are fewer fast ions. This means that there are fewer fast ions with a higher scattering cross-section per shielded ion, and more slow ions with a lower scattering cross-section. This results in a double humped spectrum with the peaks corresponding to the positive and the negative ion thermal velocities.

The macroscopic approach treats the density fluctuations rather than treating individual particles. These fluctuations are described by a Fourier series of acoustic-like waves and their statistical properties are then calculated. The normal wave modes resulting from this approach can be described as waves trav-

eling in opposite directions creating resonances at the positive and negative Doppler frequencies. For example, the above mentioned double hump spectrum can be explained as the scatter from up and down going Ion Acoustic waves. Similarly, the electron Langmuir waves create peaks at the positive and the negative Langmuir frequency offsets (Figure 1.2). These approaches have been treated in detail in *Rosenbluth and Rostoker* (1962) (dressed particle) and *Dougherty and Farley* (1960) (wave approach using the Nyquist theorem) and the followup papers.

Both these approaches lead to the same final result. In this text we are interested in the role of the electrons on the incoherent scatter spectrum. Since the experimental results described in this thesis were first predicted by *Salpeter* (1961), we will use the expression for intensity of the electron density spectrum for a constant wave vector **k** derived therein and later used for numerical calculations by *Perkins* (1963). This expression is derived from the following two equations - The incoherent scatter frequency spectrum can be expressed as $|Q_e(\omega)|^2$, where,

$$Q_e(\omega) = \int_0^\infty \rho_e(t) e^{(-i\omega+\eta)t} dt, \tag{1.3}$$

is the Laplace transform of,

$$\rho_e(t) = -e \sum_{j=1}^{N} e^{-ikz_j}, \tag{1.4}$$

which is the spatial Fourier transform of the electron charge density for a fixed wave vector **k** (*Salpeter*, 1961). Here k is the Bragg scattering wave number defined as $4\pi/\lambda$, λ is the radar wavelength $= c/f_0$, f_0 being the radar operating

frequency and c being the speed of light; z is parallel to k and z_j refers to the position of the jth electron. The magnetic induction and retardation are neglected to simplify matters. η is an infinitesimal positive constant of the order $(2\tau)^{-1}$, τ being the finite experiment time over which $|Q_e(\omega)|^2$ may be obtained. An important parameter is $\phi = \frac{\pi}{2} - \alpha$, where α is the angle between the radar wave vector $\mathbf{k}$ and the earth's geomagnetic field, $\mathbf{B}$. Other variables to be used in following analysis are defined as,

$\omega_{pe} = \sqrt{\frac{N_e e^2}{\epsilon_0 m_e}}$ is the radian electron plasma frequency;

$\Omega_e = \frac{eB}{m_e}$ is the radian electron gyro frequency;

$v_{the} = \sqrt{\frac{2k_B T_e}{m_e}}$ is the electron thermal velocity;

Some normalized frequencies -

$$a = \sqrt{2}\frac{\omega_{pe}}{k v_{the}} = \frac{1}{k\lambda_{de}}$$

$$\varepsilon = \frac{\Omega_e}{k v_{the}}$$

$$x = \frac{\omega}{k v_{the}}$$

For the intermediate angles (between 0 and $\pi/2$), $P(x)dx = (\eta/N_e e^2 \pi)|Q_e(x)|^2 dx$ is defined as follows, ignoring collisions and the bulk electron motion and considering ions and electrons in a complete thermodynamic equilibrium. (The full mathematical treatment to arrive at this result from 1.3 and 1.4 is given in *Salpeter* (1961).)

$P(x)dx =$

$$\frac{1}{\sqrt{\pi}\sin\phi|1-H_e-H_i|^2}\left[|1-H_i|^2\sum_{n=-\infty}^{\infty}\chi_{ne}e^{(-x_{ne}^2)}+|H_e|^2Z\sum_{n=-\infty}^{\infty}\chi_{ni}e^{(-x_{ni}^2)}\right]dx, \tag{1.5}$$

where

$$x_{ne}=\frac{(n\varepsilon-x)}{\sin\phi}, \tag{1.6}$$

and

$$H_e(x)=-a^2\sum_{n=-\infty}^{\infty}\chi_{ne}T_{ne}(x). \tag{1.7}$$

Here T_{ne} is related to the plasma dispersion function

$$Z(r)=i\sqrt{\pi}e^{-r^2}-r^{-1}f(r) \tag{1.8}$$

where

$$f(r)=2re^{-r^2}\int_0^r e^{t^2}dt \tag{1.9}$$

by

$$T_{ne}(x)=1+\frac{x}{\sin\phi}Z(x_{ne}) \tag{1.10}$$

and

$$\chi_{ne}=\exp\left(-\frac{\cos^2\phi}{2\varepsilon^2}\right)I_n\left(\frac{\cos^2\phi}{2\varepsilon^2}\right). \tag{1.11}$$

The ion components of the above equations, namely, x_{ni}, T_{ni}, χ_{ni} and H_i can be found by replacing ε with ε_i However, we are not very concerned about the ion components as will be made clear later in this chapter. Note that for $\phi=\frac{\pi}{2}$, the

motion of the particles along the magnetic field lines is unaffected by the magnetic field, i.e. $\chi_{ne} = \chi_{ni} = 0$ and all magnetic field effects disappear.

I_n is the modified Bessel function of the first kind and is defined as -

$$I_n(t) = \left(\frac{t}{2}\right)^n \sum_{m=0}^{\infty} \frac{\left(\frac{t^2}{4}\right)^m}{m!\Gamma(n+m+1)}, \tag{1.12}$$

where $\Gamma(a) = \int_0^\infty e^{-t} t^{a-1} dt$ is the Gamma function.

The resultant IS spectrum can be categorized in two components (see figure 1.2) - an ion component and an electron component. The ion component indicates motion of the ions and is visible in the spectrum at the center frequency with two humps at the positive and the negative Doppler frequencies for the ion acoustic waves. These are pressure waves with compression and rarefaction and velocity corresponding to the sound speed in the plasma. The acoustic frequency in the plasma can be given as $k(k_B T_e/m_e + \gamma_i k_B T_i/m_i)$, where γ_i is the ratio of specific heat capacities. In essence, this wave mode depends solely on the thermal motions of the particle and has equal phase and group velocities (*Chen*, 1984). The broad shape of the ion "line" is due to the collisionless damping of the ion acoustic waves from the wave interacting with the ions having lower phase velocities than the wave, also known as the ion Landau damping. A detailed treatment of the Landau damping can be found in any standard plasma physics text (e.g, *Chen*, 1984).

The electron component consists of two different wave modes on the electrosta-

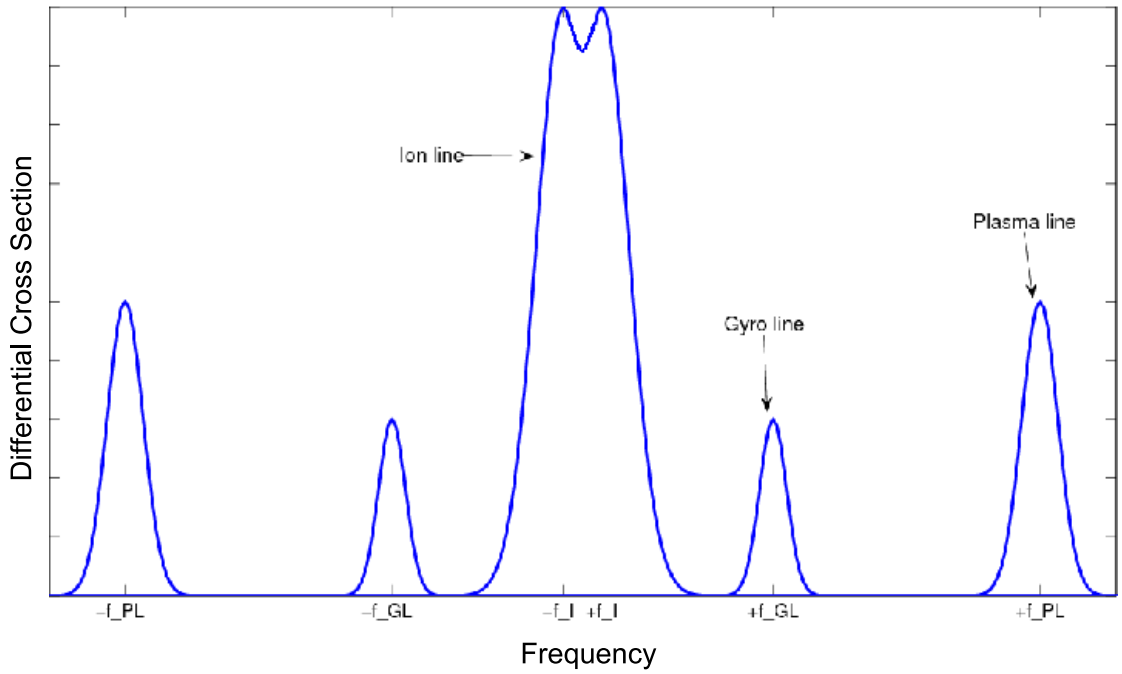

Figure 1.2: A typical incoherent scatter spectrum with a double humped ion line in the middle, and the gyro line (GL) and the plasma line (PL) make up the electron component of the spectrum. Experimentally, the electron lines are much weaker (about 3 orders of the magnitude less) than the ion line.

tic branch of the Whistler mode waves. The experiments described in this thesis are concerned with the resonance lines in the spectrum owing to these wave modes. These modes have almost no contribution from the ions and results from purely electron motion. These are fast electrons and are fewer in numbers, so the scatter from these electrons is not as strong as from the ions. The energy in the electron component is $k^2\lambda_{de}^2$ less than the energy in the ion line.

The plasma and the gyro lines make the electron component and are two roots of the dispersion relation for the magnetized plasma. We are particularly in-

terested in the electron component at low electron densities. Analytical expressions for these lines can be arrived at after approximating several terms in the equation 1.2. The first approximation is to ignore the ion component in the equation 1.2, since the ion contribution is negligible in generating these resonances. This approximation is valid as long as $m_e/m_i \ll \sin^2\phi$ and ($m_e \ll m_i$), which is true everywhere except at equatorial latitudes where $\mathbf{k}$ may be perpendicular to $\mathbf{B}$. The ions are mostly unaffected by the magnetic field or the angle ϕ. This reduces equation 1.2 to the following form.

$$P(x) = \frac{1}{\sqrt{\pi}\sin\phi}\frac{1}{|1-H_e|^2}\left[\sum_{n=-\infty}^{\infty}\chi_{ne}e^{(-x_{ne}^2)} + |H_e|^2\right]. \tag{1.13}$$

The above function will display resonances wherever the denominator goes to zero. The denominator has both real and imaginary parts. Revisiting the expression for H_e,

$$\begin{aligned} H_e(x) &= -a^2\textstyle\sum_{n=-\infty}^{\infty}\chi_{ne}T_{ne}(x) \\ &= -a^2\textstyle\sum_{n=-\infty}^{\infty}\chi_{ne}\left[1+\frac{x}{\sin\phi}\left(\frac{f(x_{ne})}{x_{ne}} - i\sqrt{\pi}\exp(-x_{ne}^2)\right)\right] \\ &= -a^2\textstyle\sum_{n=-\infty}^{\infty}\left[\chi_{ne}\left(1+\frac{x}{\sin\phi}\frac{f(x_{ne})}{x_{ne}}\right) - i\sqrt{\pi}\frac{x}{\sin\phi}\chi_{ne}\exp(-x_{ne}^2)\right] \\ &= \Re H_e + i\Im H_e \end{aligned}$$

For parameters related to experiments at Arecibo and the low frequency regime that we are interested in, $|x_{ne}| \gg 1$ (see fig 1.3). (There are some contributions to the spectrum at low frequencies when $|x_{ne}| \leq 1$ that will be discussed in Chapter 3.) This makes the exponential term in $\Im H_e$ very small compared to $\Re H_e$. Other parameters a and ε are graphed in figure 1.4 for the same electron density range as in figure 1.3, along with $a^2/2\varepsilon^2$. Since $\Im H_e \ll \Re H_e$, $P(x)$ will display resonances wherever $Y(x) = 1 - \Re H_e = 0$. $Y(x)$ is the dispersion relation

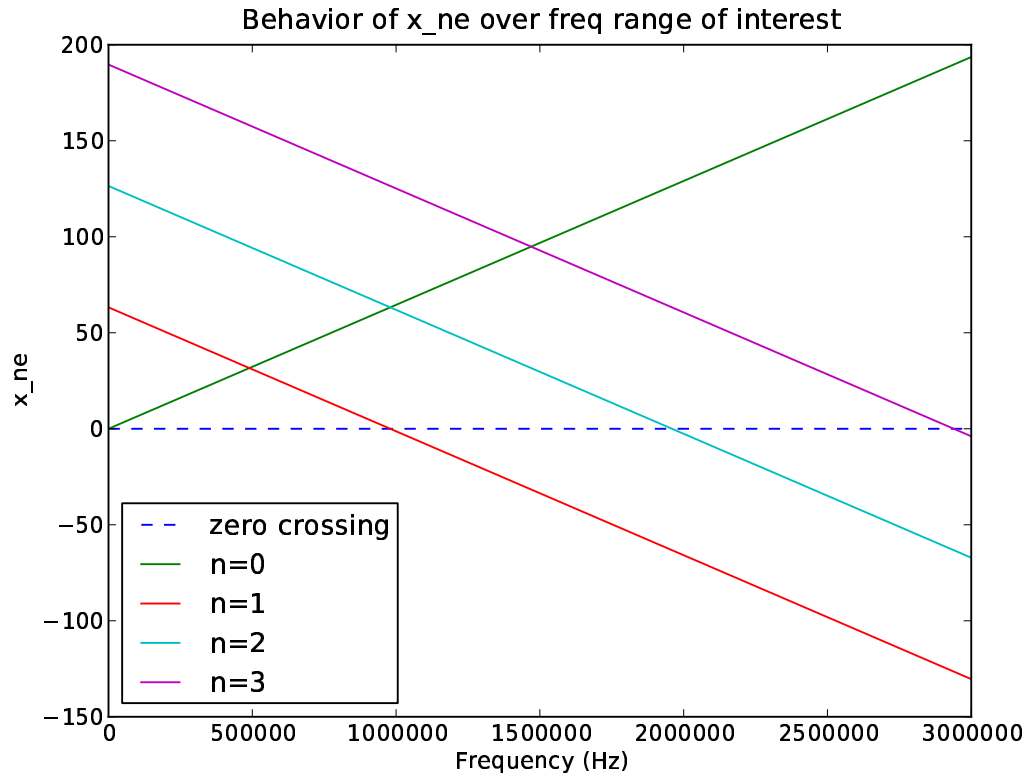

Figure 1.3: x_{ne} plotted for n = 0, 1, 2 and 3 over the frequency range of our interest 0-3 MHz. The points where x_{ne} crosses zero, depict the gyro harmonics. P(x) displays interesting behavior at these locations. Note that x_{ne} is dimensionless.

for the magnetized plasma and is given as -

$$Y(x) = 1 + a^2 \sum_{n=-\infty}^{\infty} \chi_{ne} \left[1 + \frac{x}{\sin\phi} \frac{f(x_{ne})}{x_{ne}} \right]. \tag{1.14}$$

Two roots of this dispersion relation are the gyro line and the plasma line. Let us first arrive at analytical expressions for these electron lines for normal ionospheric conditions, which implies that we ignore all higher order terms

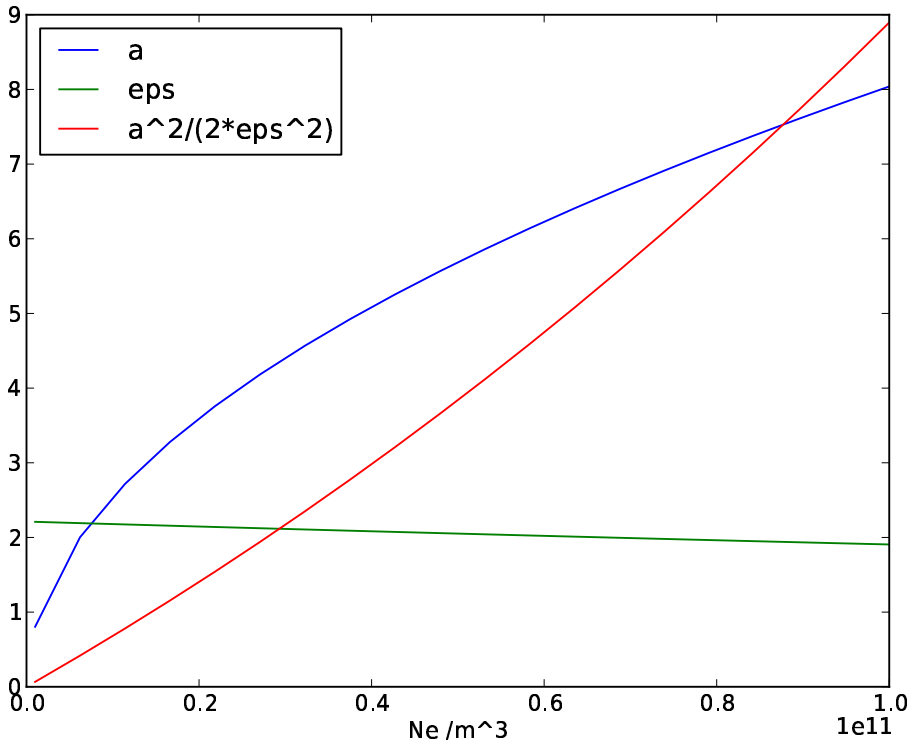

Figure 1.4: a, ε and $a^2/2\varepsilon^2$ are plotted for the density/frequency range of interest ($1 \times 10^9 < N_e < 1 \times 10^{11}$). Simplifications of various expressions here are based on how large these values are compared to 1. Note that all the quantities plotted here are dimensionless.

($|n| > 1$) in $Y(x)$. For the case of ionosphere over Arecibo, where $\varepsilon \approx 2$ as shown in figure 1.4, the exponential term in $\chi_{ne} \ll 1$ and we can series expand it, considering series expansions of $e^{-t} = 1 - t + t^2/2! - ...$ and bessel functions ($I_0(t) = 1 + t^2/4 + t^4/64 + ...$ and $I_1(t) = t/2 + t^3/16 + t^5/384 + ...$), leaves us with the following approximations -

$$\chi_{0e} = 1 - \frac{\cos^2\phi}{2\varepsilon^2} + \frac{\cos^4\phi}{8\varepsilon^4} - ... \tag{1.15}$$

$$\chi_{1e} = \frac{\cos^2\phi}{4\varepsilon^2} - \frac{\cos^4\phi}{4\varepsilon^4} + ... \tag{1.16}$$

However, for the reasons mentioned above, the higher order terms in both the above expressions will be negligible and we can safely ignore those, leaving only the first two terms in χ_{0e} and the first term in χ_{1e}. $f(r)$ in the plasma dispersion relation is a tabulated function that for $|r| \gg 1$ can be written as an asymptotic series expansion,

$$f(r) = 1 + \frac{1}{2r^2} + \frac{3}{4x^4} + ...$$

which allows for the following approximations -

$$f(x_{0e}) = 1 + \frac{1}{2x_{0e}^2}, \tag{1.17}$$

and

$$f(x_{1e}) = 1. \tag{1.18}$$

The higher order terms for $n = 0$ and $n = 1$ give extremely small contributions and can be safely neglected. Also note the identity (*Salpeter*, 1961),

$$\sum_{n=-\infty}^{\infty} J_n^2(r) = \sum_{n=-\infty}^{\infty} \chi_{ne} = 1$$

Putting these approximations in equation for $H_e(\omega)$ and taking the real part of it -

$$\begin{aligned}
\Re He &= -a^2 \textstyle\sum_n \chi_{ne} - a^2 \sum_n \chi_{ne} \frac{x}{\sin\phi} \frac{f(x_{ne})}{x_{ne}} \\
&= -a^2 \left(1 + \left(1 - \frac{\cos^2\phi}{2\varepsilon^2}\right) \frac{x}{\sin\phi} \frac{1+1/2x_{0e}^2}{x_{0e}} + \frac{\cos^2\phi}{4\varepsilon^2} \frac{x}{\sin\phi} \frac{1}{x_{1e}}\right) \\
&= a^2 \left[\frac{\cos^2\phi \sin^2\phi}{4\varepsilon^2 x^2} - \frac{\sin^2\phi}{2x^2} - \frac{\cos^2\phi}{2\varepsilon^2}\left(1 - \frac{x}{2(\varepsilon - x)}\right)\right]
\end{aligned}$$

The first term in the above expression has, for all x, a value that is much less than the rest of the terms and can be ignored. The expression for $Y(x) = 1 - \Re He$, after explicitly putting in the condition that $|x|$ and $|x - n\varepsilon|$ are $\gg 1$, results in the following expression -

$$Y(x) = 1 - \frac{a^2}{\varepsilon^2}\left[\frac{\frac{x^2}{\varepsilon^2} - \sin^2\phi}{\frac{x^2}{\varepsilon^2}(\frac{x^2}{\varepsilon^2} - 1)}\right]. \tag{1.19}$$

Converting $Y(x)$ into $Y(\omega)$ and equating the above equation to 0 gives the resonances in the incoherent scatter spectrum.

$$\frac{\omega_p^2}{\Omega_e^2}\left(\frac{\omega^2/\Omega_e^2 - \sin^2\phi}{\omega^2/\Omega_e^2(\omega^2/\Omega_e^2 - 1)}\right) = 1 \tag{1.20}$$

Denoting $b = \omega/\Omega_e$,

$$b^4(\Omega_e^2) - b^2(\Omega_e^2 + \omega_p^2) + \omega_p^2 \sin^2\phi = 0$$

$$b^2 = \pm\frac{1}{2\Omega_e^2}\left(\Omega_e^2 + \omega_p^2 \pm \sqrt{(\Omega_e^2 + \omega_p^2)^2 - 4\Omega_e^2\omega_p^2 \sin^2\phi}\right),$$

which in turn gives,

$$\omega^2 = \pm\frac{1}{2}\left(\Omega_e^2 + \omega_p^2 \pm \sqrt{(\Omega_e^2 + \omega_p^2)^2 - 4\Omega_e^2\omega_p^2 \sin^2\phi}\right) \tag{1.21}$$

The above expression gives two pairs of resonance lines, one with the frequency higher than the other. Since the first term in the square root is much smaller than the second term, we can expand the square root,

$$\omega^2 = \pm\frac{1}{2}\left(\Omega_e^2 + \omega_p^2 \pm (\Omega_e^2 + \omega_p^2)\left(1 - \frac{2\Omega_e^2\omega_p^2 \sin^2\phi}{(\Omega_e^2 + \omega_p^2)^2}\right)\right)$$

The larger root here gives the expression for the plasma line frequency,

$$\omega_{PL}^2 = \omega_p^2 + \frac{\Omega_e^2}{\Omega_e^2 + \omega_p^2}(\Omega_e^2 + \omega_p^2 \cos^2\phi). \tag{1.22}$$

and the smaller root the expression for the gyro line frequency,

$$\omega_{GL}^2 = \frac{\Omega_e^2\omega_p^2 \sin^2\phi}{\Omega_e^2 + \omega_p^2}. \tag{1.23}$$

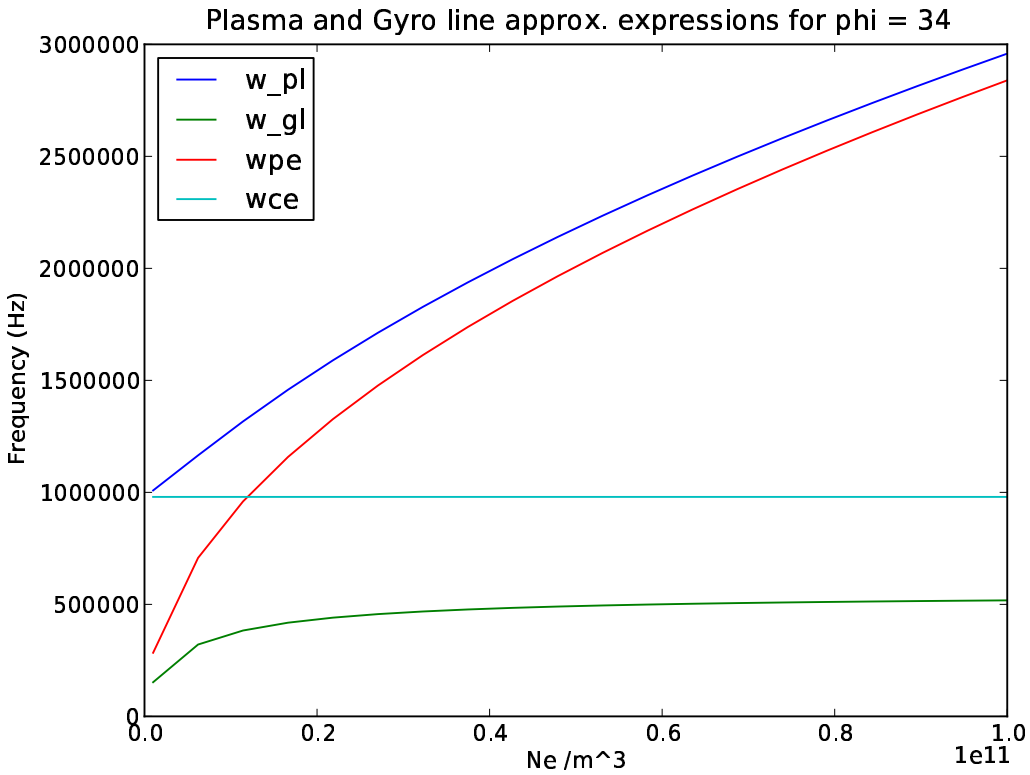

Figure 1.5: ω_{PL} and ω_{GL} from (1.22) and (1.23) are plotted here with ω_p and Ω_e with electron density ranging from $1 \times 10^9 - 10^{11}/m^3$ and $\phi = 34^o$ corresponding to the experiments conducted with Arecibo radar. $\mathbf{B = 35000nT}$ corresponding to the F region above Arecibo. Note that both ω_{PL} and ω_{GL} will be affected slightly if electron temperature term is included.

Figure 1.5 shows how these approximated frequencies vary with electron density ranging from $1 \times 10^9 - 10^{11}/m^3$. For the normal day time ionospheric conditions, where ω_p is larger than Ω_e, ω_{GL} can be approximated as $\pm\Omega_e \sin\phi$, which is the value that the ω_{GL} curve is shown to approach as the density increases. But during low electron density conditions, mainly dawn, dusk and night time, when ω_p is of the order of Ω_e, ω_{GL} starts following electron density more closely, an interesting fact that is the basis for Chapter 2.

From looking at figure 1.5, it is evident that the plasma line needs to be evaluated in three different domains, $\omega_p > \Omega_e$, $\omega_p \simeq \Omega_e$ and $\omega_p < \Omega_e$. As will be shown in later chapters, it is nearly impossible to detect the plasma line for $N_e < 1 \times 10^{10}/m^3$ with reasonable altitude and time resolution, even with the most sensitive incoherent scatter radar on the earth. The gyro line on the other hand can be reasonably detected for electron densities as low as $2 \times 10^9/m^3$. The analytical expression of plasma line for $\omega_p < \Omega_e$ is hence not derived here.

The electron temperature affects the width and the intensities of these lines much more than it does the frequencies. Intensity of each line can be evaluated by integrating the area under the line (*Salpeter*, 1961; *Perkins*, 1963),

$$I_\nu = \int_{-\infty}^{\infty} P(\omega) d\omega = \frac{k^2 v_{the}^2}{2\omega_p^2 (\frac{\partial Y}{\partial \omega}\omega)\big|_{\omega=\omega_\nu}}, \tag{1.24}$$

where ν is PL or GL. Using 1.19 to get $Y(\omega)$,

$$Y'(\omega) = -\frac{\omega_p^2}{\Omega_e^2}\left[\frac{2\omega/\Omega_e}{\omega^2/\Omega_e^2(\omega^2/\Omega_e^2 - 1)} + \frac{(\omega^2/\Omega_e^2 - \sin^2\phi)(4\omega^2/\Omega_e^2 - 2)}{\omega^3/\Omega_e^3(\omega^2/\Omega_e^2 - 1)^2}\right], \tag{1.25}$$

which gives the expression for intensity of the lines as,

$$I_\nu = \frac{2k^2 v_{the}^2}{\Omega_e^2} \left[\frac{\omega^2/\Omega_e^2 - \sin^2\phi}{\omega^2/\Omega_e^2(\omega^2/\Omega_e^2 - 1)} + \frac{\cos^2\phi}{(\omega^2/\Omega_e^2 - 1)} \right]_{\omega=\omega_\nu} \tag{1.26}$$

Substituting 1.22 and 1.23 for plasma and gyro lines respectively, we arrive at intensities graphed in figure 1.6. These intensity values need to be multiplied by physical experimental parameters to be compared with received intensities. These approximations do not compare well with the observed theory as far as comparing the trend goes. Note that the plasma line during the daytime at higher frequencies get significantly enhanced by the presence of high energy photoelectrons. These photoelectrons create a "bump" near the tail of the Maxwellian velocity distribution that give energy to the resonance line (*Yngvesson and Perkins*, 1968).

The equations 1.22 and 1.23 were arrived from the assumption that $\Omega_e \gg k v_{the}$. When Ω_e is of the same order as $k v_{the}$, equation 1.19 is further simplified giving (*Perkins*, 1963),

$$Y(x) = 1 - a^2 \left[\frac{1}{2x^2} + \frac{1}{x^4} \left(\frac{3}{4} + \frac{\varepsilon^2 \cos^2\phi}{2} \right) \right] \tag{1.27}$$

Equating this equation to zero gives the plasma line frequency that is equivalent to that of the Langumuir waves,

$$\omega^2 = \omega_p^2 + \frac{3}{2} k^2 v_{the}^2 + \Omega_e^2 \cos^2\phi, \tag{1.28}$$

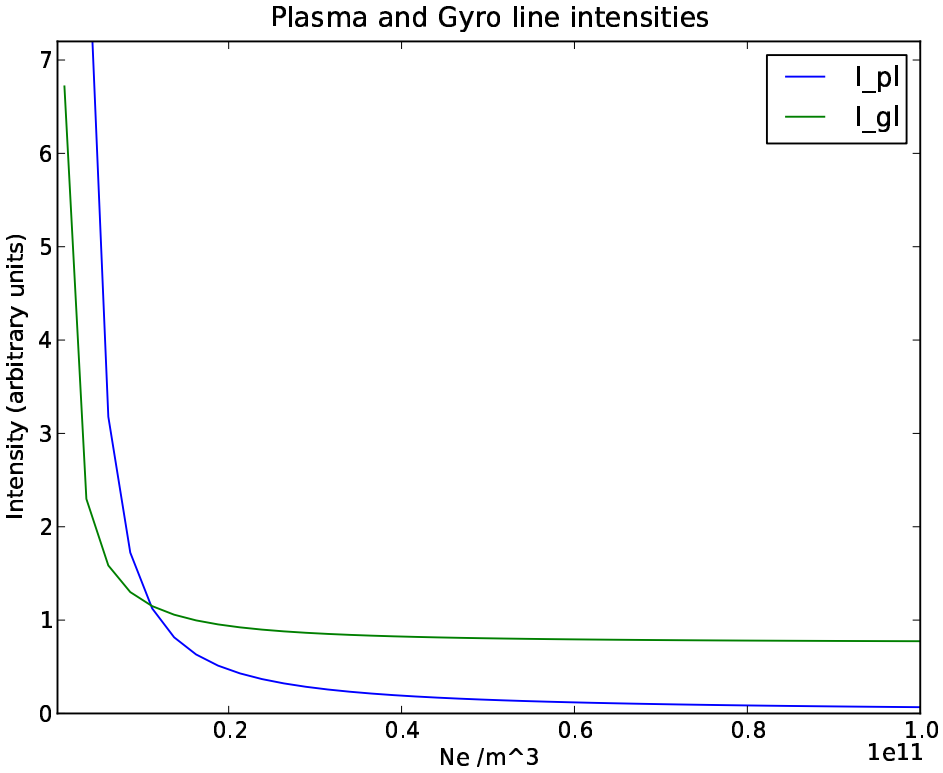

Figure 1.6: Plasma and gyro line intensities plotted using 1.26 for the frequencies in 1.22 and 1.23 respectively. The values are plotted for a range of electron density from 1×10^9 to $1 \times 10^{11}/m^3$. The intensities are plotted for the same parameters as those mentioned in the figure 1.5 and $T_e = 1000^o K$. These intensity values are dimensionless and need to be multiplied by physical parameters to be compared with experimental values.

which is somewhat more accurate than equation 1.22. The other root of this fails to give an accurate gyro line frequency however,

$$\omega^2 = \frac{3}{2}k^2 v_{the}^2 + \Omega_c^2 \cos^2\phi, \tag{1.29}$$

which under any circumstances does not work. A better analytical expression for the gyro line will be estimated in Chapter 2.

These same expressions (equations 1.23 and 3.1) can be also derived using the more widely used Gordeyev integral. Following the notation of *Farley et al.* (1961), the density fluctuation spectrum including only electron effects for a Maxwellian velocity distribution may be written as

$$\frac{\langle |n_e(\mathbf{k},\omega)|^2 \rangle}{N_e} = \frac{k^4\lambda_{de}^4}{\omega}\frac{\Re(y_e)}{|y_e + ik^2\lambda_{de}^2|^2} \tag{1.30}$$

or

$$\frac{\langle |n_e(\mathbf{k},\omega)|^2 \rangle}{N_e} = \frac{k^4\lambda_{de}^4}{\omega}\frac{\Re(y_e)}{\Re(y_e)^2 + [\Im(y_e) + k^2\lambda_{de}^2]^2} \tag{1.31}$$

where the effect of bulk electron motion has been neglected. In this equation y_e is the electron admittance function. The admittance function neglecting collisions can be written as

$$y_e = i + xJ(x) \tag{1.32}$$

The function $J(x)$ refers to a Gordeyev integral, which, when including the magnetic field effects but excluding collisions of all types, can be written as (*Farley et al.*, 1961)

$$J(x) = \int_0^\infty e^{-ixt - \varepsilon^{-2}\sin^2\alpha \sin^2 \frac{1}{2}xt - \frac{1}{4}t^2\cos^2\alpha} dt \tag{1.33}$$

where $\alpha = 90^o - \phi$, is the angle between k and $\mathbf{B}$. The Gordeyev integral may be interpreted as the one-sided Fourier transform of the single particle autocorre-

lation function (e.g., *Bernstein*, 1958; *Farley et al.*, 1961; *Sulzer and Gonzalez*, 1999; *Kudeki and Milla*, 2006).

Equating the denominator of (1.30) to zero corresponds to the dispersion relation for free oscillations (normal modes) in the plasma (*Farley et al.*, 1961). Since $Re(y_e)$ is very small, it can be shown that resonances occur when the following expression is satisfied:

$$\Im(y_e) + k^2\lambda_{de}^2 = \\ k^2\lambda_{de}^2 + \frac{\sin^2\alpha}{2(\varepsilon^2 - x^2)} + \frac{(\sin^2\alpha - 2\varepsilon^2)\cos^2\alpha}{4\varepsilon^2 x^2} = 0 \tag{1.34}$$

Two roots of this equation are the plasma and the gyro lines as given by 3.1 and 1.23 respectively. Both these resonance lines have unique properties that make them worth studying. Both their intensities combined are less by a factor of $k^2\lambda_{de}^2$ from the ion line, which makes them very hard to detect with an incoherent scatter radar.

Full spectrum analysis

The exercises above were to arrive at analytical expressions for the resonance lines. The analysis so far assumes $|n\varepsilon - x|/\sin\phi$ or $|n\Omega_e - \omega|/kv_{the}\sin\phi \gg 1$.

These results are a good approximation for daytime ionospheric conditions at mid to high latitudes. However, these results were arrived at after several series expansions and eliminating terms much smaller than others to simplify matters. As a result, they fail to accurately predict the behavior of plasma line primarily during low density conditions and at the electron gyro harmonics. Chapter 3 in this thesis addresses the plasma line response when the plasma frequency is close to the second electron gyro harmonic. With the advances in sophisticated computing tools, more accurate shape of the spectrum can be predicted without needing those approximations. The theoretical spectra throughout this thesis have been numerically calculated using a code written to calculate $P(x)$ multiplied by $\sqrt{\pi}\sin\phi$ from equation 1.5, in the MATLAB programming language. The analysis assumes $T_e = T_i$ and thermal electrons only and O_2^+ as the dominant ion. We ignore collisions and bulk motion. The magnetic field information is from International Geophysical Reference Field (IGRF). It then numerically sums n for -30 to 30, and calculates a spectrum over 1024 FFT points and the frequency range of interest. The code can evaluate $f(x_{ne})$ with the help of inherent error functions like *erfz*, and Bessel functions in χ_{ne} without having to eliminate higher order terms. The accuracy of the spectra calculated thus is limited only by the computing power of the machine the code runs on (a higher resolution FFT is possible for example). An example spectrum computed in this manner, which will be referred to as 'full spectrum analysis' or 'computed values' for the rest of this thesis, is shown in figure 1.7. Experimental high spectral resolution observations of both these lines have been presented in the following chapters. The sections below describe the radars used for these observations.

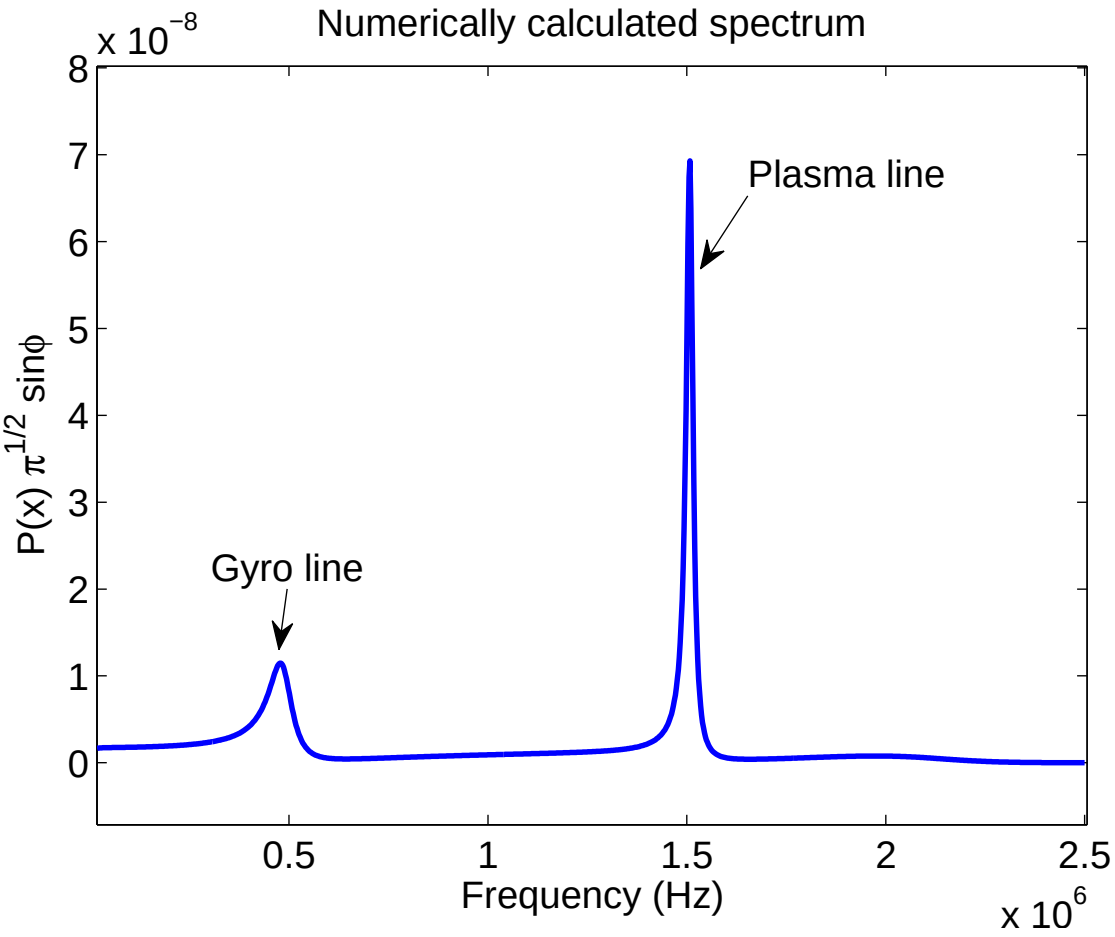

Figure 1.7: Electron component in the full IS spectrum calculated numerically for $N_e = 1.66 \times 10^{10}/m^3$, $T_e = 863^o K$, $B = 35000nT$, and $\phi = 30^o$ using equation 1.5. Note that $P(x)$ includes ions, which affect the spectral intensity here. Note that while $P(x)$ is the backscattered signal as observed by the radar in the units of Cross section $\cdot Hz^{-1}$ that needs to be multiplied by a frequency independent constant based on experimental conditions and radar parameters in order to be compared with actual received backscattered signal.

1.2.3 Instrumentation

Since the incoherent scatter was understood to be coming from the electron cloud around ions, which are much slower than the electrons, the receiving bandwidth requirement decreased drastically. This eliminated the requirement for a radar with a large area to ensure low noise, and resulted into the construction of several radar facilities around the world. Only the radars at Arecibo and Jicamarca remained the ones very large apertures. Among the other radars were, the 440 MHz Millstone Hill radar with a diameter of 68 m in 1963, the Stanford 1290 MHz parabolic antenna in California in 1965 (which was transferred to Chatanika, Alaska in 1971, and later to Søndre Strømfjord, Greenland in 1983), the EISCAT (European Incoherent SCATter) radar system in Norway, Sweden and Finland consisting parabolic reflectors and a parabolic cylinder and transmitting at 224 MHz and 924 MHz in 1980, the 47.5 MHz MU radar in Shigaraki, Japan, consisting of 475 yagi antenna elements in 1983, an additional 500 MHz parabolic dish radar within the EISCAT system in Svalbard, Norway in 1999, and lastly the 449 MHz phased array system known as AMISR (Advanced Modular Incoherent Scatter Radar) that began operations at Poker Flat, Alaska in 2006. Some other radar systems were built and later decommissioned in Europe (e. g. 935 MHz radar at St. Santin in France that operated from 1965 to 1987), but nevertheless contributed to our knowledge base while operating.

The operations at these radars over the years have helped perfect the ionospheric models by providing precise measurements of primarily the electron density and the ion and the electron temperatures. The individual exper-

iments performed at these radars have also helped validate important aspects of the kinetic theory of plasma, such as Landau damping (*Perkins et al.*, 1965). As noted above, most of the incoherent scatter theory had been developed in the 1960's and has been the basis for the later theoretical developments and the measurements based on them (e.g., *Farley et al.*, 1967; *Sulzer and Gonzalez*, 1999; *Woodman*, 2004; *Kudeki and Milla*, 2006; *Rodrigues et al.*, 2007b,a; *Nicolls et al.*, 2006; *Shume*, 2000; *Bhatt et al.*, 2006, 2008). In recent years, the IS radars have also been used extensively to detect the so called traveling ionospheric disturbances (TIDs) and other manifestations of the gravity waves in the thermospheric plasma (e.g., *Djuth et al.*, 2004; *Nicolls et al.*, 2004; *Vadas and Nicolls*, 2008). With the development of better radar and computer hardware and computing technology, better measurements requiring higher computational power from these systems can be expected.

The year 2006-2007 was marked as the International Polar Year (IPY) in the ionospheric radar community. Some of the radars mentioned above (Svalbard and AMISR) ran continuous operation during IPY, the data for which are in public domain through the Madrigal database access[*http://madrigal.haystack.mit.edu*]. The data presented in Chapter 4 of this thesis have been obtained with the Poker Flat IS radar during the IPY.

Arecibo Observatory

The Arecibo Observatory in Puerto Rico holds a unique position as the largest single dish radar/radio telescope in the world. The observatory carries out research in the areas of radio astronomy and planetary science in addition to the ionospheric studies. The radar has a 304.8 m spherical dish built into one of the many sinkholes in the island of Puerto Rico. The receiver assembly is located on a platform suspended some 150 m above the dish by cables from three concrete towers. The first feed was a line, since the rays reflected from a spherical surface form a focal line rather than a point. In 1997, a new Gregorian system was developed consisting of a secondary and a tertiary reflectors that are housed in a separate dome hanging alongside the line feed. The Gregorian system focuses the rays on a single point, thus enhancing the receiver sensitivity. The forward gain of the Gregorian system is 55.5 dB at 430 MHz. The platform has a circular azimuth and a bow-shaped elevation tracks, which allow the feeds to scan 360° in azimuth and $\pm$ 20° in elevation. This makes multi-point measurements possible.

In the field of ionospheric physics, the Arecibo radar has been instrumental in making the most sensitive measurements of the ionospheric parameters. It remains the most powerful incoherent scatter radar to date. It was the first radar to measure the electron component in the IS spectrum with high spectral and height resolution and infer the ionospheric electron density and temperature using those measurements. So far, it is the only radar where unambiguous, high precision gyro line measurements have been possible. The Arecibo Obser-

Figure 1.8: The Gregorian assembly in the front and the line feed in the back, hanging from the platform at Arecibo Observatory. Other elements in the figure are, the azimuth and the elevation tracks, the platform, the cables connecting to the dish below, and a catwalk from the ground to the platform.

vatory is operated by Cornell University under a cooperative agreement with the National Science Foundation.

1.3 Data Collection and Analysis

Data shown in chapters 2 and 3 of this thesis have been obtained using the Arecibo radar, and those in chapter 4 have been obtained using the Poker Flat IS radar. This section describes the experimental procedure used for data collection at these places.

1.3.1 Arecibo Experiments

The Arecibo data were taken for low electron density conditions. The goal of the first experiments was to observe the gyro line that was known to be very hard to detect above the noise floor (*Behnke and Hagen*, 1978). We transmitted a single long pulse 500 μs in length with an inter-pulse period (IPP) of 10 ms, giving a duty cycle of 5%. This IPP ensured the maximum unambiguous range of 1500 km ($cIPP/2$). No significant scatter compared to the E and the F region, is expected from ranges above that. A pulse length of 500 μs is equivalent to the range resolution ($\Delta R = c\tau/2$) of 75 km. Figure 1.9 shows the range-time diagram for this pulse mode also known as the "uncoded long pulse". Note in figure 1.9 that the range gates overlap in altitude by half the range resolution, which makes it extremely difficult to pinpoint the altitude where the signal may be coming from. The received signal is essentially integrated over the entire 75 km, which elevates the signal much more over the noise floor. A disadvantage is that it also introduces range smearing, which significantly broadens the resonance 'lines'. The data obtained with this method show same signal with different strengths in two consecutive range gates. Typical scale heights in the E and the bottom-side F regions are less than 75 km, and the received signal fails to reflect the electron density changes over one scale height. However, the scatter comes from electron waves and gets abruptly large when there are more electrons resonating at the phase velocity of the wave. This happens at the peaks and valleys in the ionospheric density profile. This is shown in fig. 1.10, which is taken from figure 1 in *Showen* (1995). These peaks and valleys are reflected in the resonance line intensities in the spectral analysis of the data. It is also known as a 'cutoff' method after sharp vertical lines observed at the point of

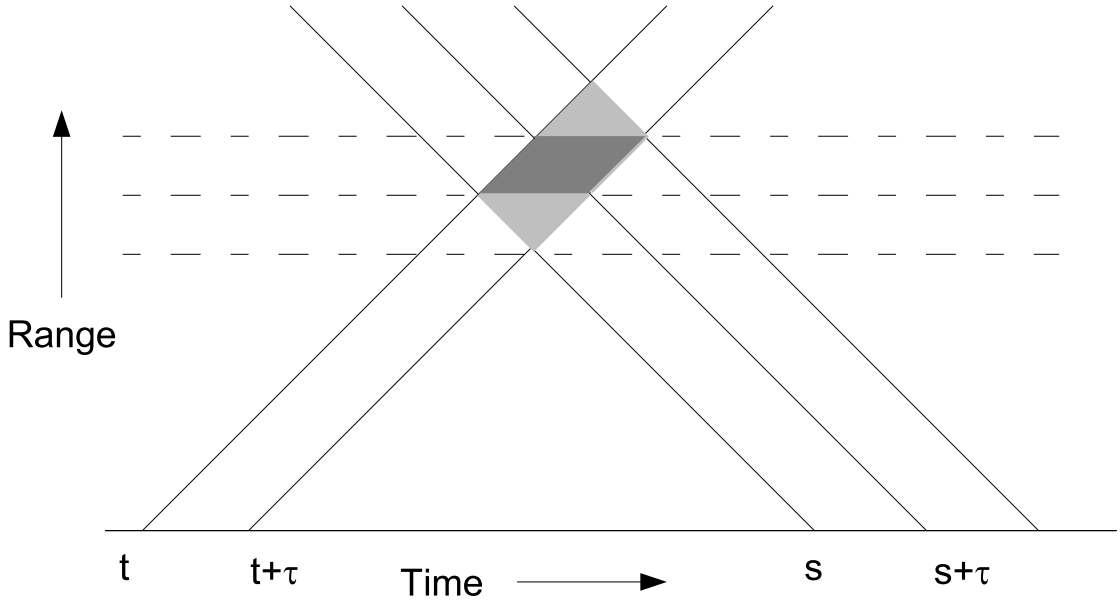

Figure 1.9: The range-time diagram showing the transmission mode used for Arecibo experiments. Here $\tau = 500\mu s$. Dashed lines show altitude slices. Lighter gray areas show unambiguous ranges, while the darker gray areas show range overlap. This is because the received signal was sampled as the same interval (τ) as the transmit signal. The received signal is integrated over an entire pulse length. The signal received from the darker gray regions come from the same altitude, hence showing an overlap of signals in consecutive range gates.

sharpest gradient in the electron density profile. If there are very thin density layers with sharp peaks and valleys with a scale height much smaller than the pulse length, they will be reflected quite precisely in the spectra. An advantage of transmitting a really long pulse like this is to The data shown in Chapter 3 and wave data in Chapter 4 resulted from this phenomenon.

The signal is received at the rate of 5 MHz. In some experiments, only one receiver channel was used with a 5 MHz bandwidth centered at 430 MHz, the

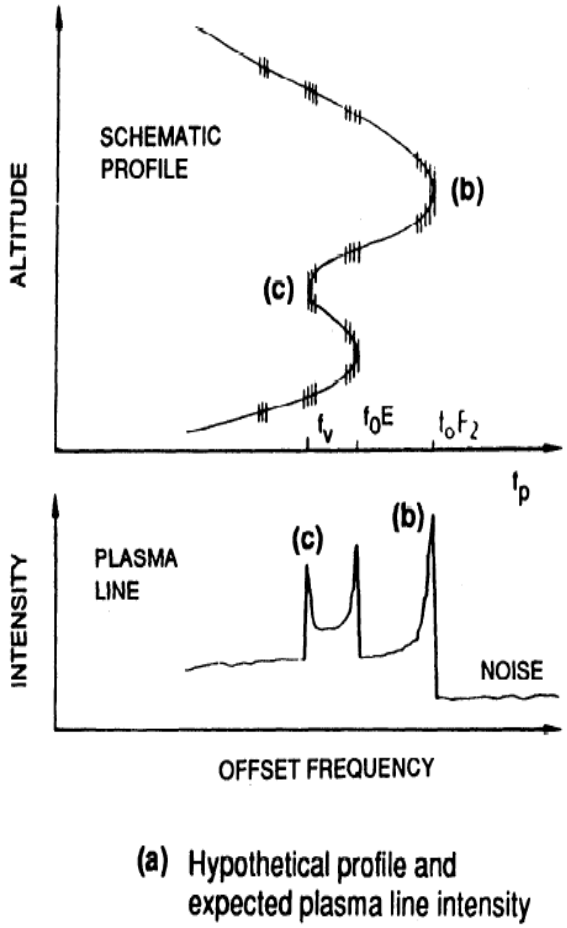

Figure 1.10: From Figure 1 in *Showen* (1995) showing the expected plasma lines at peaks and valleys of the electron density profile. Note the sharp edge of the plasma line where the electron concentration is highest in a small range of altitudes.

transmitter frequency. In later experiments displaying a 10 MHz bandwidth, two separate 5 MHz receiver channels were used for up and down shifted spectra. The two channels have slightly different gains, which is often apparent in the images showing experimental spectra. To get the spectra, the raw data are first divided into range gates. The number of range gates depends on the total number of samples collected by the receiver system. The old analog re-

ceiver system normally employed at Arecibo does not have a large enough data buffer or the data rate to store all the samples in one IPP. For experiments with 5 MHz total bandwidth (August 2004, December 2005), the data were taken on the analog system and only 6 range gates were obtained. The first four range gates span from 100 to 400 km. Above this, the F-region is in topside and the densities are low compared with the F-region. In recent years, a new digital receiver system using $Echotek^{TM}$ processors has been employed on experimental basis at Arecibo that is capable of receiving on multiple channels with a wider bandwidth. The experiments with total 10 MHz bandwidth were taken using this system with two separate 5 MHz channels centered at 2.5 MHz above and below the transmitter frequency.

The signal data come from E and F region altitude ranges, while the noise data come from averaging the range gates near the end of the 10 ms gate delay. No separate noise samples were taken in these experiments. The receiver filter is 1-to-1 matched to the transmitter pulse. No pulse compression technique was used for these experiments. Each sample is 200 ns long. A 1-D Fast Fourier Transform (FFT) is then applied to the complex signal in each range gate. The spectral resolution is 2.44 kHz. The power spectral density calculated thus is plotted over the 5 MHz bandwidth to get the entire spectrum after subtracting noise data from the signal data.

It is important to note here some problems with the data obtained for this thesis. Every radar has a "system constant" that takes into account inherent equipment variabilities and compensates for them. There are various ways to measure this constant. For a phased array like the Poker Flat IS radar for example, the system

constant is look-direction specific since the gain of a phased array varies with the look-angle. However, the Arecibo radar does not have a standard way of measuring the system constant, which is a problem. The system constant then plays a crucial role in measuring the absolute power of the received signal. The received power can be written as,

$$P_R = \frac{P_T \tau}{Range^2} K_{sys} \frac{N_e}{(1 + k^2\lambda_{de}^2)(1 + k^2\lambda_{de}^2 + T_e/T_i)} [Watts] \tag{1.35}$$

A bulk of this power resides in the the ion line and is proportional to the electron density. Here τ is the transmitted pulse length. To use the received power to estimate electron density, one must first calibrate for the system constant, K_{sys}. To calculate the system constant for individual experiments, this requires using independent measurements of electron density and electron and ion temperatures. The standard procedure is to use the electron density from an ionosonde, or a plasma line if there is one available with a reasonable altitude resolution (this is generally achieved by 'coding' the long pulse thus improving the range resolution to about 150 m (*Djuth et al.*, 1994)) that is a more precise measure of electron density than that from an ionosonde. Electron temperature one would get from fitting the spectral shape. The problem with calculating K_{sys} for our experiments is that the scatter is smeared over 75 km, and the only precise plasma lines we see are from peaks in layers that may or may not represent the true value of electron density. There are also no higher altitude resolution independent measurements of plasma or ion lines in order to optimize the temporal resolution. But in theory, one could interleave transmission modes to get such measurements and use those to get an estimate for overall electron density and

temperature. Another problem is that there is no standard calibration for power for these experiments. At some radars a calibration pulse of known power is injected in the transmitted signal that helps convert the received signal into Watts ($P_R = P_{Cal}(Signal - noise)/(Cal - noise)$). At Arecibo, such a calibration pulse is not used. So the power estimates are not entirely accurate. Some power estimation of the received signal will be attempted in the Chapter 2, but calculating absolute power for these experiments remains a problem.

5 MHz bandwidth is much wider compared to the standard ion line bandwidth of 250 kHz, which is what is usually observed with most radars. Such wider bandwidth is needed in order to observe the high frequency (compared to ion line) electron component behavior over changing geophysical conditions. Wider receiver bandwidth also means higher receiver noise (Noise = $k_B T_{sys}(BW)$), which can be detrimental to the detection of weak features in the spectrum. The system temperature of the Gregorian assembly is $\approx 80^o K$. The filter function for the new digital receiver channels at Arecibo is flat over almost the entire 5 MHz bandwidth and drops very rapidly at the ends, hence the noise bandwidth is almost 5 MHz. Since the Arecibo antenna has a physical area of $\pi(150^2)m^2$, the extremely high gain resulting from this helps elevate the signal level significantly above the noise floor. The effective aperture of the Gregorian system is pointing dependent, and is $\approx 0.3 \times 10^6 m^2$ at 430 MHz for angles between 15^o and 19^o, which gives 0.4 as a ratio of A_{eff} and A_{phys}. Note that Arecibo cannot point lower than 19.6^o off zenith. The noise performance of the Gregorian system is also better than the line feed since the received signal is focused on a single point instead of a line. The product of transmitter power and antenna aperture is directly proportional to the radar sensitivity. In comparison,

Poker Flat IS radar that transmits at a similar frequency and same transmitter power level as Arecibo has the area of 900 m^2 (when operated including all the array elements) that reduces the power-aperture product by at least two orders of magnitude. Other factors that affect the noise performance are hardware components integral to the mono-static radar transmitter/receiver assembly. This makes a significant difference in observing scatter from low-energy electron waves. While the Poker Flat radar can observe higher frequency plasma lines with a reasonable sensitivity, as shown in Chapter 4, the gyro line would be extremely difficult to detect even if the aspect angle requirement was met in theory (which it does not due to the radar being at polar latitudes). The Arecibo radar is so far the only facility where the gyro line has been unambiguously measured with a good enough accuracy to infer geophysical parameters.

1.4 Thesis objective

This thesis is an effort to use the full incoherent scatter spectrum, including the electron component to derive crucial ionospheric parameters during low electron density conditions. The ion line is primarily used for this purpose at every radar facility, which needs to be calibrated using the electron density from an external instrument like an Ionosonde. Some facilities have begun to make use of the plasma line to calculate absolute electron density to normalize the ion line. High altitude resolution plasma line measurements are only possible during the daytime, even at Arecibo. Chapter 2 in this thesis describes using the frequency of gyro line, the lesser known cousin of the plasma line, to obtain absolute elec-

tron densities during dawn, dusk, and most of the night time. The absolute temperature measurements at night still remain a problem. Chapter 3 in this thesis describes getting absolute electron temperature from a "split" in the plasma line at second electron gyro-harmonic, which at Arecibo is normally seen during the dawn hours, before the local sunrise. When observed with a long pulse, the plasma line comes from the region of maximum electron concentration, thus allowing to detect sharp peaks and valleys in the electron density profile. This property can be used to see the propagation of atmospheric gravity waves in the thermosphere, as shown in Chapter 4. Normally the atmospheric gravity wave detection requires using filtering techniques to determine the periodicity. The variations observed in the plasma line provides the base period to create such a filter for a finer altitude resolution gravity wave detection. The advantage of using frequencies of gyro and the plasma lines is that the frequency measurements are more accurate than measuring the shape (area under the curve). Moreover, high spectral resolution observations of these lines can help observe weak layers and small period waves in the ionosphere that may be playing an important role in driving larger scale phenomena.

CHAPTER 2

GYRO LINE

2.1 Introduction

As noted in Chapter 1, the gyro line is weaker than to the ion line or even the plasma line, and due to its strong dependence on the angle between $\mathbf{k}$ and $\mathbf{B}$, it can, in theory, be observed at mid and high latitudes. At equatorial latitudes, the condition $m_e/m_i \ll \sin^2\phi$ is no longer true and the gyro line frequency can be approximated as the frequency for the lower hybrid waves ($\omega \approx \sqrt{\Omega_e \Omega_i}$).

The first reported measurements of the gyro line were made using the Arecibo radar by *Behnke and Hagen* (1978). It was a difficult detection that required 2 hours of integrating both day and night time incoherent scatter (IS) spectra (see figure 2.1 for daytime observations shown in this paper). Since it was difficult to observe the gyro line even with the most sensitive radar in the world and was generally considered devoid of any useful information, it was not studied in detail for quite a few years after these initial observations. Further theoretical and experimental research was conducted at the EISCAT radar facility by various researchers (*Bjørnå et al.*, 1990; *Malnes and Bjørnå*, 1993; *Malnes et al.*, 1996; *Shume*, 2000) with ambiguous results (see figure 2.2). Recently, for the first time, high spectral and temporal resolution spectra obtained using the Arecibo radar show a distinct presence of the gyro line (*Bhatt et al.*, 2006). These observations were followed by *Janches and Nicolls* (2007) showing diurnal variations in the gyro line frequency also using the Arecibo radar. This prompted revisiting

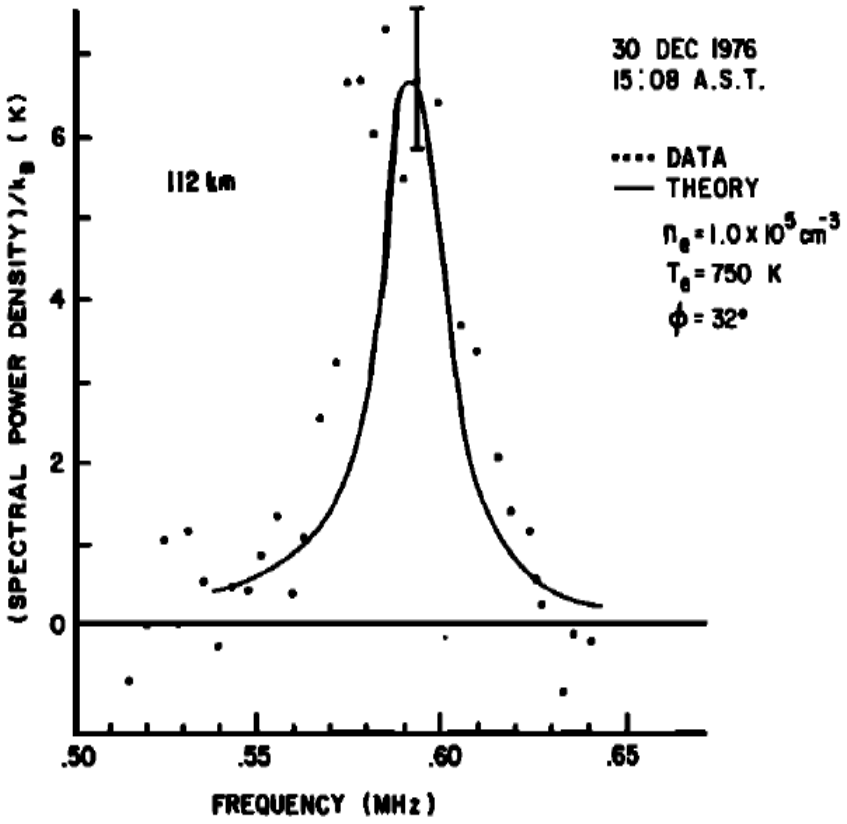

Figure 2.1: Figure 4 from *Behnke and Hagen* (1978) showing daytime observations of the gyro line from the E region after 2 hours of integration and a fit according to the calculations of *Perkins* (1963).

the original theory by *Salpeter* (1961) and numerical calculations of the same by *Perkins* (1963). This analysis suggested that during the low electron density conditions, namely dawn, dusk and most of the night, the gyro line frequency and intensity are very sensitive to the electron density. This property can be used to get absolute measurements of the electron density in the absence of the plasma line that is enhanced by the energetic photoelectrons. This chapter presents the data from multiple Arecibo experiments and comparison with the theory.

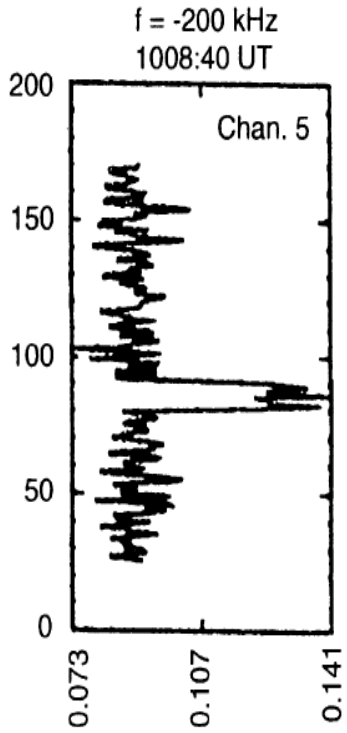

Figure 2.2: Figure 4 from *Malnes et al.* (1996) shows power profile observations of anomalous enhancement in E region at 200 kHz offset with the EISCAT UHF radar. The horizontal axis gives power in arbitrary units while the vertical axis shows altitude in km. The authors speculate the enhancement to be coming from the gyro line.

2.2 Experiments

Nearly thirty years after *Behnke and Hagen* (1978), a new set of gyro line experiments was carried out at the Arecibo Observatory during the PARS (Polar Aeronomy and Radio Science) Summer School in August 2004. These experiments were performed during the dawn hours on August 15 and 18. Since the gyro line is very weak in the spectrum, we transmitted an "uncoded" long pulse. This meant that the returned signal would be integrated over a range

of altitudes specified by the pulse length, thus enhancing the signal above the noise floor. The tradeoff is that while ensuring good signal-to-noise ratio, this pulse mode gives a poor altitude resolution. For this experiment, the pulse length was 500 μs giving a 75 km range resolution with an inter-pulse period (IPP) of 10 ms. The received signal was sampled every 200 ns, which means that the signal was received over 5 MHz bandwidth. The radar pointing was 349° in azimuth, corresponding to the declination of the magnetic field, and 19.6° offset from the zenith on Aug. 15. The dip angle at Arecibo is 49° and hence α was 60.6°. The bandpass for the received signal was from 427.5 to 432.5 MHz. On Aug. 18, all parameters were kept identical except for the angle α, which was 55.6°. The spectra from these experiments were integrated for 6 minutes initially (*Bhatt et al.*, 2006). Further analysis indicated that both the gyro and the plasma lines could be well distinguished in the spectra even with 20 seconds integration. More experiments followed in December 2005, November 2006, and August 2008.

2.2.1 Results

The incoherent scatter spectra were obtained from four different altitude regions depending on the radar pointing angle and range. For August 15, the altitude gates were centered at 141, 212, 282, and 353 km, with a resolution of $\pm$ 34 km. Figure 2.3 shows spectra from these four altitudes. Figure 2.4 shows a frequency-time-intensity image from two lower heights and figure 2.5 from two higher heights during the period 0554 - 0652 LT on Aug. 15 2004. All four

heights show ion line at the center frequency of 430 MHz, which is denoted in the images as 0 MHz offset. The strongest plasma and the gyro line returns were observed at 212 km range gate. Morning twilight at 282 km, 212 km, and 141 km occurred at 0458, 0531, and 0547 local time according to the US Naval Observatory sunrise/sunset calendar (`http://aa.usno.navy.mil/data/docs/RS_OneYear.php`). In fig. 2.4, a strong gyro line trace appears in both the range gates from the start of the experiment, while for the first 20 minutes of the experiment, the plasma line trace is only faintly visible. The gyro line frequency reaches 0.5 MHz by 0610 local time and remains steady till the end of the experiment. Note the relatively measurable change in the gyro line frequency that occurs while the electron density is lower as indicated by the frequency of the plasma line and the thickness of the ion line, both of which are proportional to the electron density.

Figure 2.6 shows spectra for 221 km altitude on Aug. 18 during the period 0533 - 0753 local time. The radar was pointing at 19.6° off zenith from 0533 - 0627 LT, and changed to 10.6° making $\alpha = 55.6^\circ$ at 0633 LT. With the change in angle, the gyro line offset changes from 500 kHz to 570 kHz, consistent with 1.23. Such a change in the gyro line frequency can only be attributed to the change in the angle since the change in the altitude with the angle is negligible and the value of $\mathbf{B}$ does not change drastically within 10 km.

Further observations of gyro line were carried out in December 2005 and November 2006. Radar parameters were the same as that on August 15, 2004. Upshifted spectra from the evening of Dec 23 are shown in figure 2.7. As the time

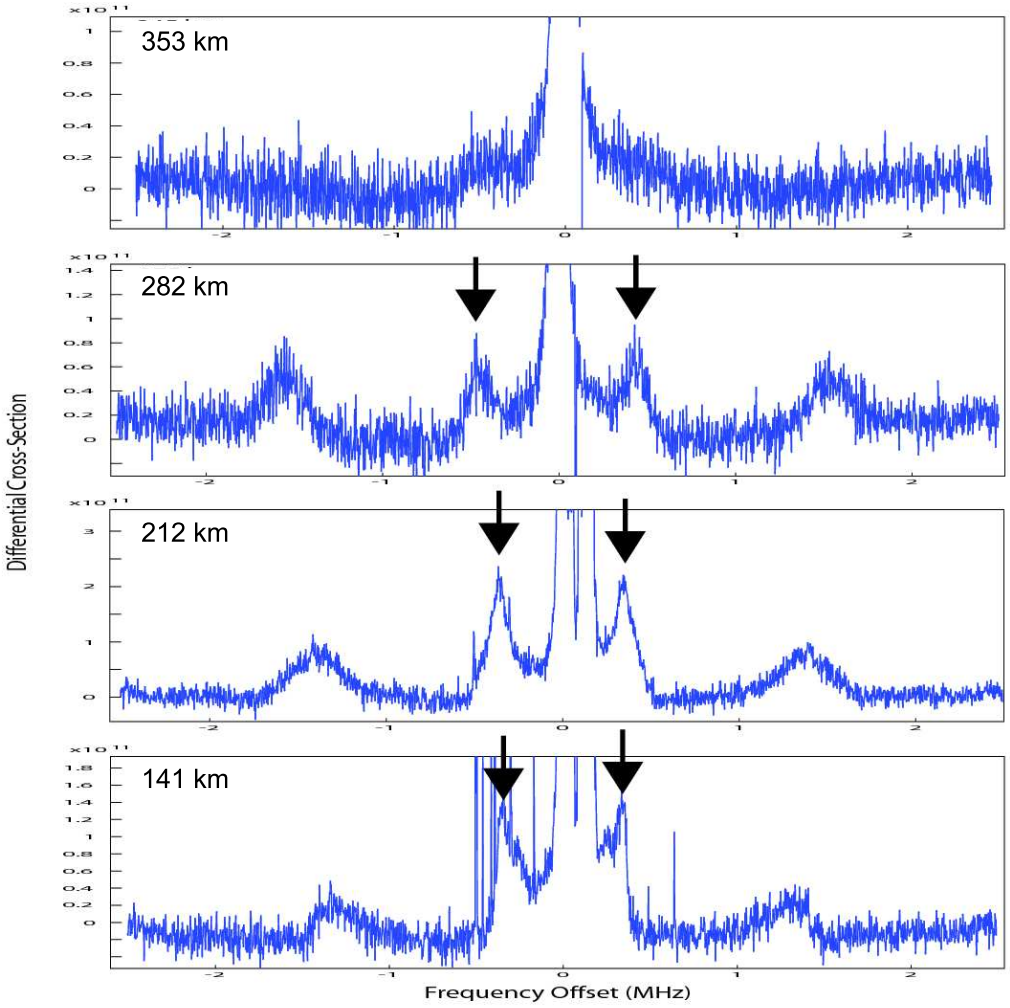

Figure 2.3: Spectra from August 15 experiment for four altitude bins. The up and down shifted gyro lines are visible at ≈ 400 kHz and are indicated with arrows, while the other up and down shifted resonance lines between 1 and 2 MHz are plasma lines. The gyro line intensity here ranges from 0.8 to 2.5×10^{11} in units of un-calibrated signal power minus noise depending on the altitude. These spectra have been integrated for 6 minutes

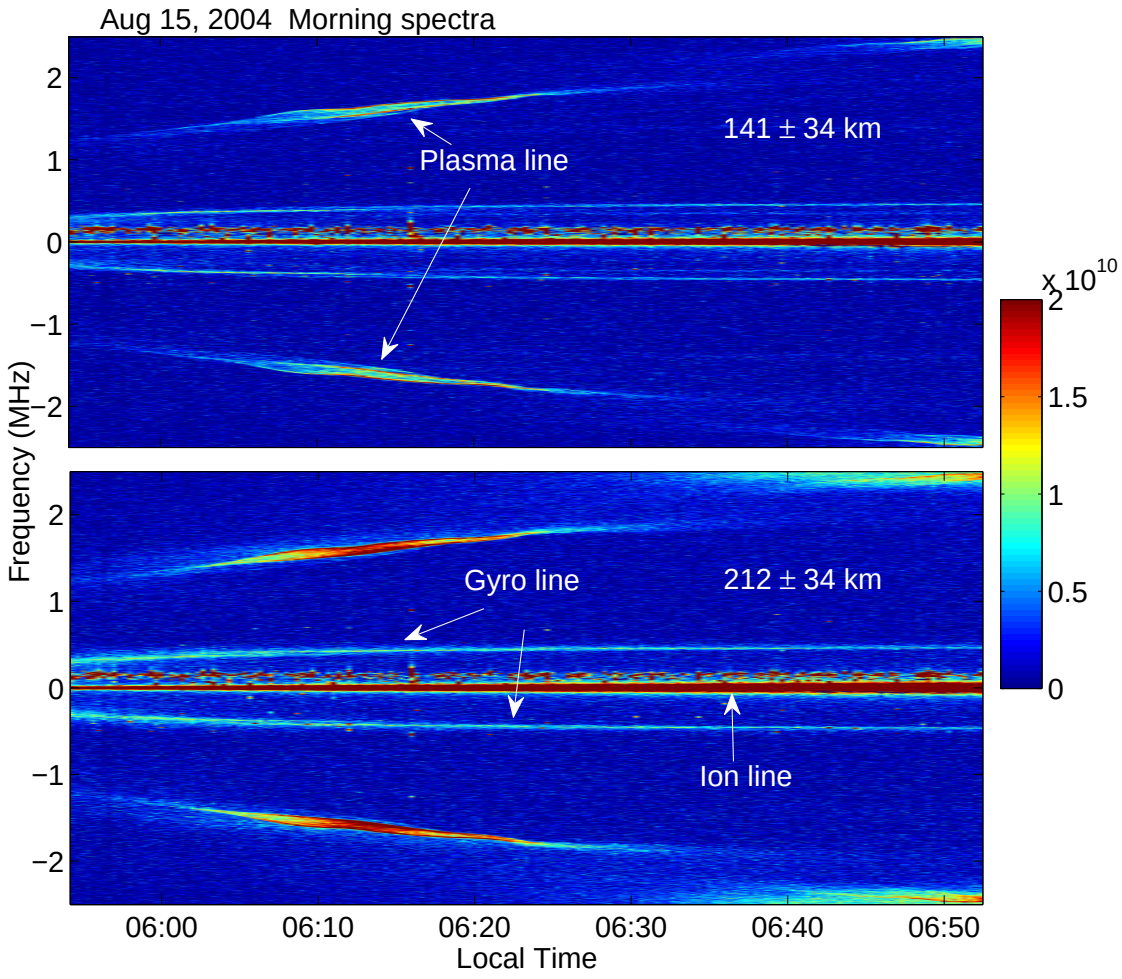

Figure 2.4: The spectra received at the lower two range gates that show the presence of the ion line at the center frequency, the plasma line from 1.2 MHz to 2.5 MHz, and the gyro line from 0.35 MHz to 0.5 MHz. The trace visible in both figures just above the ion line trace is interference from unknown sources. The color scale indicates un-calibrated signal power after noise subtraction.

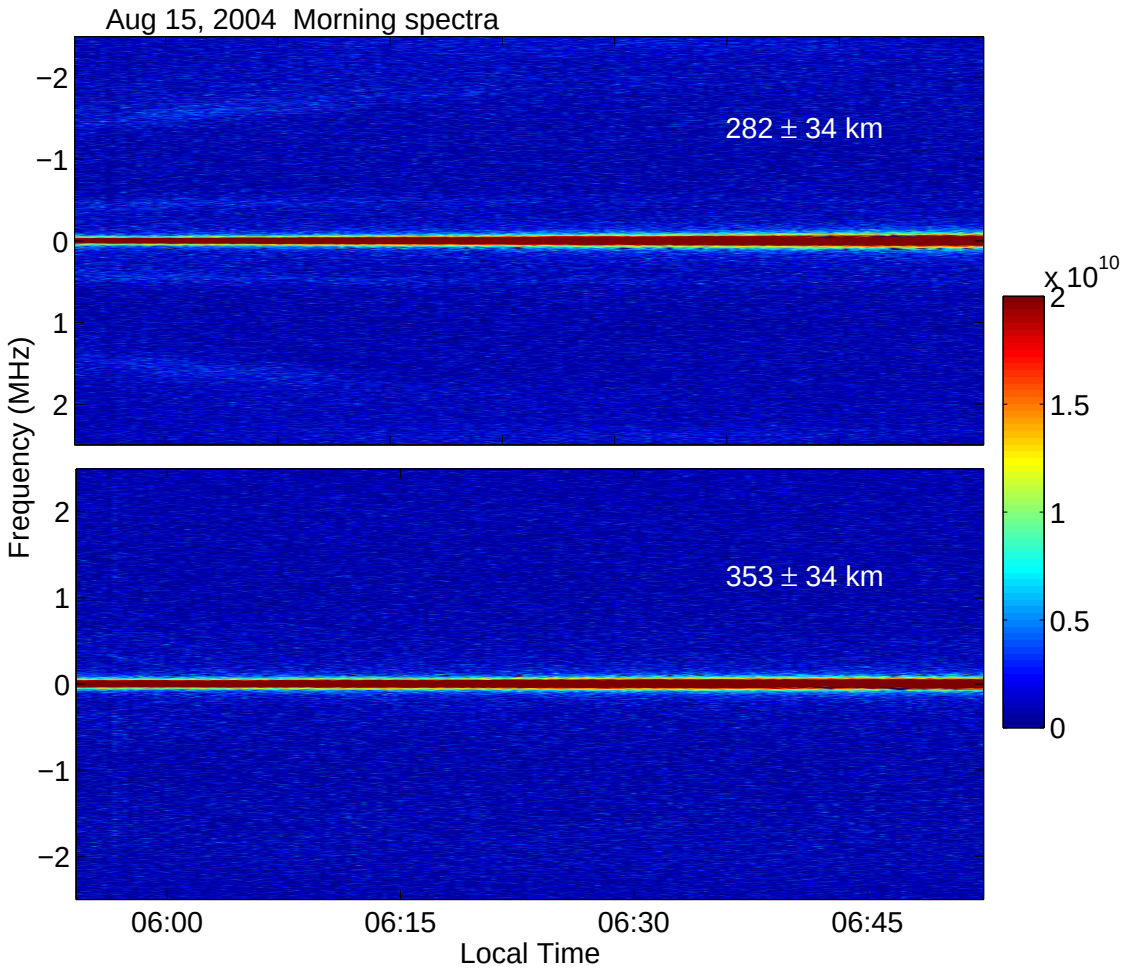

Figure 2.5: The spectra received at the higher two range gates. While the upper image from 282 km shows only faint traces of plasma and gyro lines along with a stronger trace for the ion line, the lower image from 353 km shows only the ion line in the center. The color scale indicates un-calibrated signal power after noise subtraction.

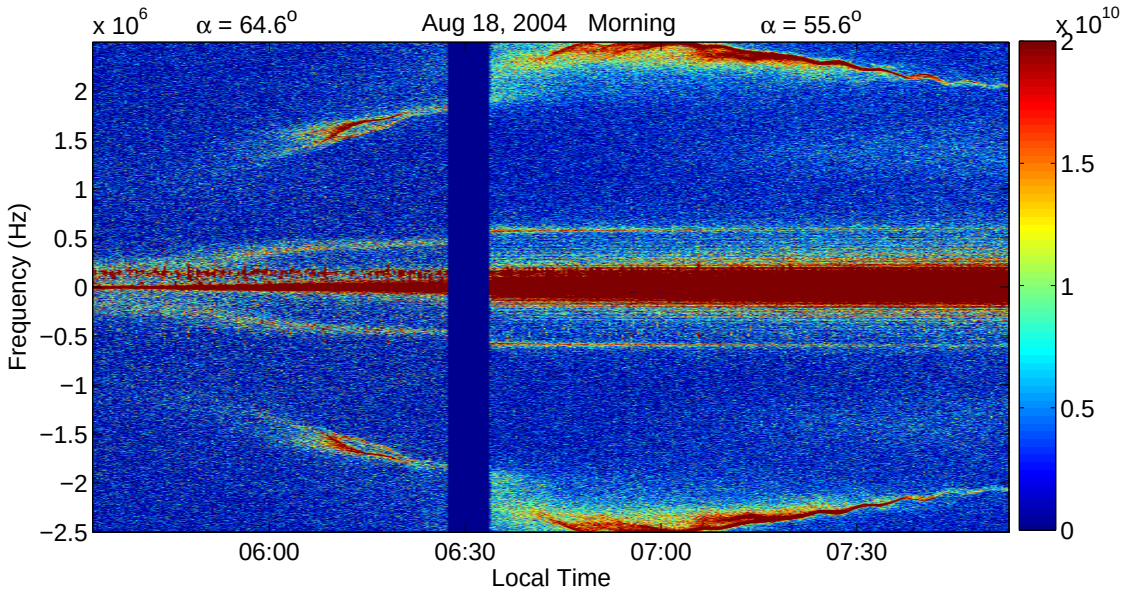

Figure 2.6: The spectra received on August 18 when the radar pointing angle was changed from $19.6°$ to $10.6°$ off zenith between 0627 and 0633 LT. The gyro line offset changed from 500 kHz to 570 kHz corresponding with the cosine of the angle α. The color scale indicates un-calibrated signal power after noise subtraction.

passes, the electron density decreases and is reflected in both the plasma and the gyro line offsets. The spectra plotted there are separated by 2 minutes. The figure indicates the change in the gyro line frequency is much slower than the change in the plasma line frequency, which is a direct measure of the electron density with minor corrections for electron temperature and magnetic field.

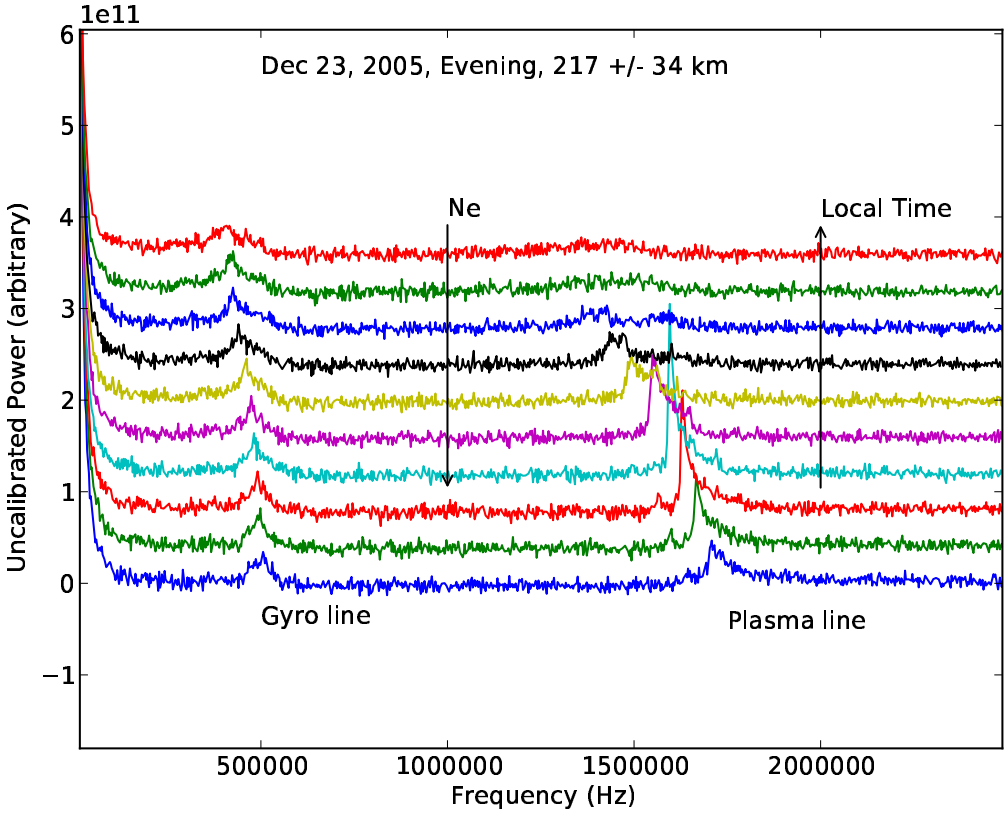

Figure 2.7: The spectra observed on December 23, 2005. The progression in time is indicated by increasing the intensity of the spectra by a constant. The y-axis thus has arbitrary units of intensity. The spectra plotted here are separated by 2 minutes in time that goes from 1730 to 1750 LT. Note that a distinct gyro line can be seen in these spectra after the plasma line has disappeared.

2.3 Sensitivity to electron density

Shume (2000) had explored the theoretical aspects of varying electron density and electron temperature on the gyro line cross-section for EISCAT conditions, based on the calculations in *Bjørnå et al.* (1990). The theoretical results arrived at by these authors however do not agree with the calculations or observations presented in this thesis. We used full spectrum analysis to compare with exper-

imental results, an example from which was shown in figure 1.7. This analysis was first employed by *Nicolls et al.* (2006) and has been used here to compare with the observations from all subsequent experiments. More accurate frequency offsets calculated using the full spectrum analysis are shown in figure 2.8. These calculations have assumed that $T_e = T_i = 863^o K$. The analytical equation 1.23 for gyro line works in a limited sense and fails to accurately mimic the full spectrum results for higher densities. Adding the thermal term in the analysis from the beginning leads to complicated terms that are difficult to take approximations for. Therefore we attempt to use two analytical solutions in different frequency regimes, based on the electron wave behavior in those regimes.

For $\omega_p < \Omega_e$

$$\omega_{GL}^2 = \omega_p^2 \sin^2 \phi \tag{2.1}$$

For $\omega_p \geq \Omega_e$

$$\omega_{GL}^2 = \Omega_e^2 \left[\frac{\omega_p^2}{(\Omega_e^2 + \omega_p^2)} + \frac{3}{2} \frac{k^2 v_{the}^2}{\Omega_e^2} \right] \sin^2 \phi \tag{2.2}$$

The resulting behavior is graphed in figure 2.8. This is estimated from the behavior of electron cyclotron wave in different frequency regimes. When $\omega_p < \Omega_e$, as ω approaches the resonance at Ω_e, the electron inertia limits the mobility of electrons along the magnetic field lines to neutralize the charge generated by the motion perpendicular to the magnetic field lines (*Stringer*, 1963). As the electron density increases, the frequency tends to $\omega_p \sin \phi$. As it further increases the electron pressure gradient becomes dominating restoring force, and the wave becomes electron acoustic wave with a frequency $\sqrt{3/2} k v_{the} \sin \phi$, which continues till ω reaches $\Omega_e \sin \phi$ (*Stringer*, 1963). The gyro line is part of the low frequency branch of the Whistler mode wave, and can be interpreted as a scat-

ter from electron cyclotron waves. An appropriate analytical expression for the resonance would then seem to be adding the electron acoustic wave to the resonance, which seems to give a better analytical approximation in this regime as indicated in figure 2.8.

The figure 2.8 shows multiple curves - full spectrum analysis including and excluding ions, and approximate gyro line expression with and without temperature. The ions correct the curve by $\approx 50kHz$ at low densities and $\approx 25kHz$ at higher densities. (Note: The electron temperature used in these plots has been estimated using the plasma line observations described in Chapter 3. The electron density derived from experimental values will be shown in Chapter 3, figure 3.6.) Conversely, we calculated the electron density from the gyro and the plasma line frequencies extracted from the computed spectrum, using equations 1.28, 2.1 and 2.2. The densities are shown in the figure 2.9. The 'jump' in the plasma line derived electron density is the subject of Chapter 3. Suffice it to say that using the plasma line to derive the low values of electron density requires more sophisticated fitting than simply using the plasma line frequency. The comparison is shown with the actual electron density used to compute the spectrum. For the values of 1×10^{10} to $4 \times 10^{10}/m^3$, the density derived using 2.2 is very close to the actual values. Below 1×10^{10}, the equation 2.1 gives much more reasonable densities, as indicated by the bottom panel in figure 2.9. Although the plasma line frequency also gives density values close to the actual values in this regime, these densities correspond to plasma line frequencies below 1 MHz that even the Arecibo radar cannot observe. These are also the densities occurring during dawn, dusk and night time. We know from *Janches and Nicolls* (2007) that the gyro line is present all night during various seasons.

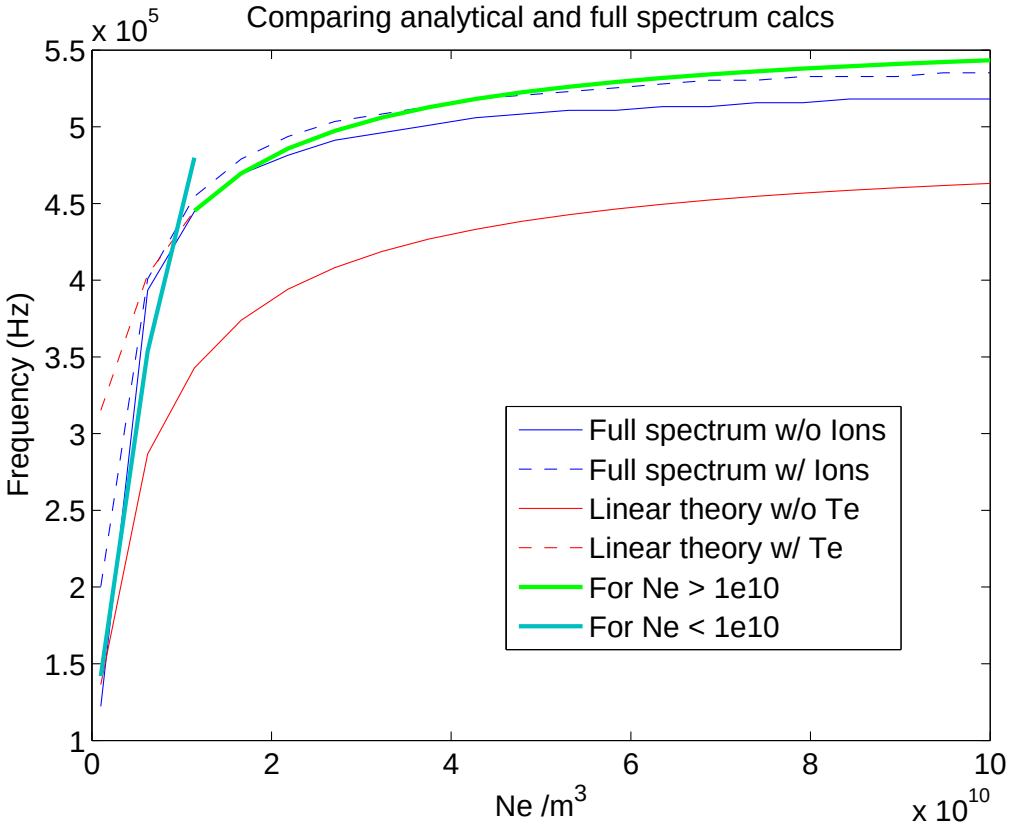

Figure 2.8: Gyro line frequency vs. varying electron density for $T_e = 863^o K$ and $\phi = 30^o$. The temperature is determined from the plasma line data in Chapter 3. The analytical expression has two parts. The approximate expression without T_e differs from the full spectrum analysis calculations by about 100 kHz. Adding thermal term for densities higher than $1 \times 10^{10}/m^3$ gives a better approximation for the gyro line frequency.

Next we derive electron density from the observed spectra on December 23, 2005 in the same way. The observed spectra are plotted in 2.10. The electron densities derived from resonance lines are plotted in 2.11.

The gyro line is better detected at low electron densities than plasma line. To compare the observed intensity values to the theoretical ones, we refer back

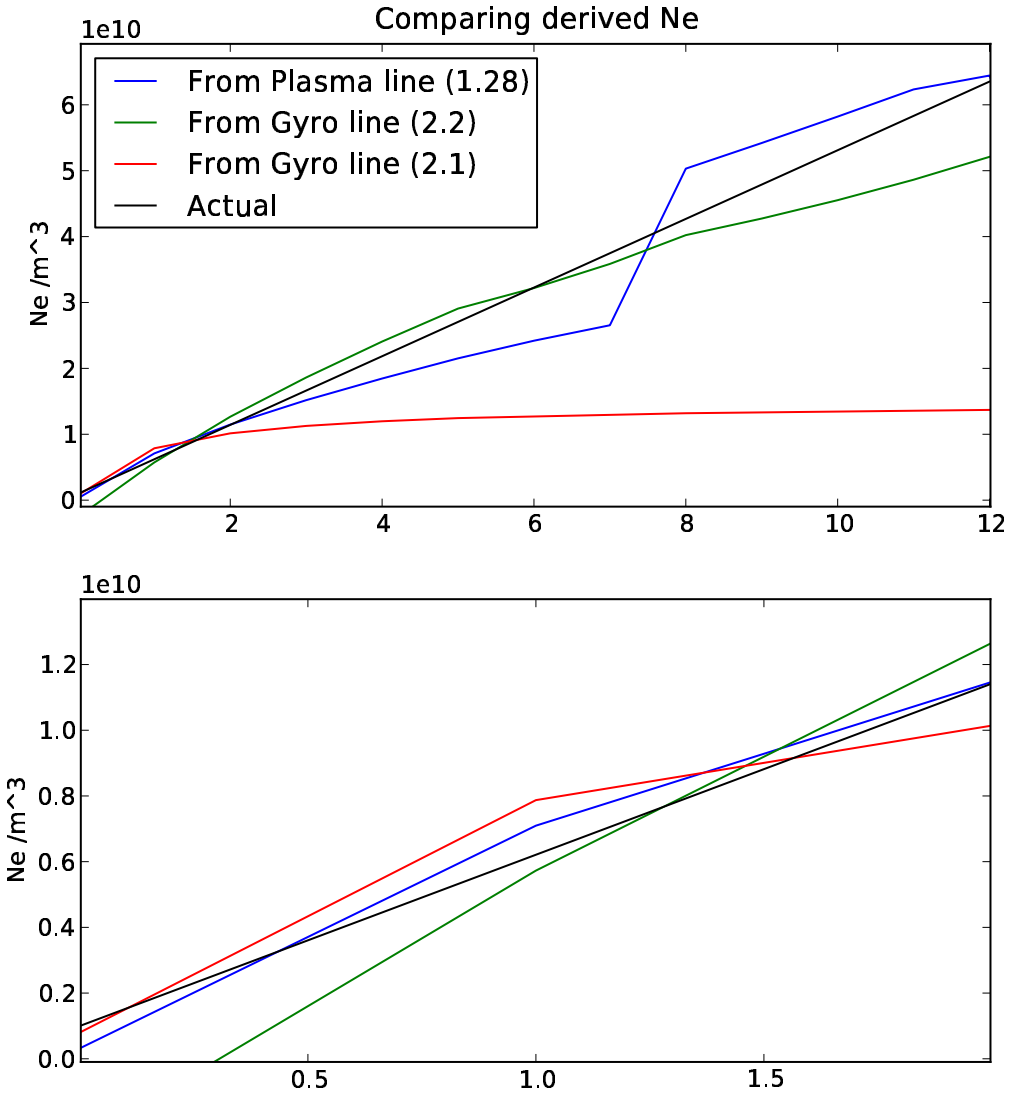

Figure 2.9: Comparing N_e derived using equations (3.1), (2.2), and (2.1) with actual values of N_e used to calculate the spectra from which the plasma and gyro line resonances were extracted. The jump in the plasma line derived N_e will be explained in Chapter 3.

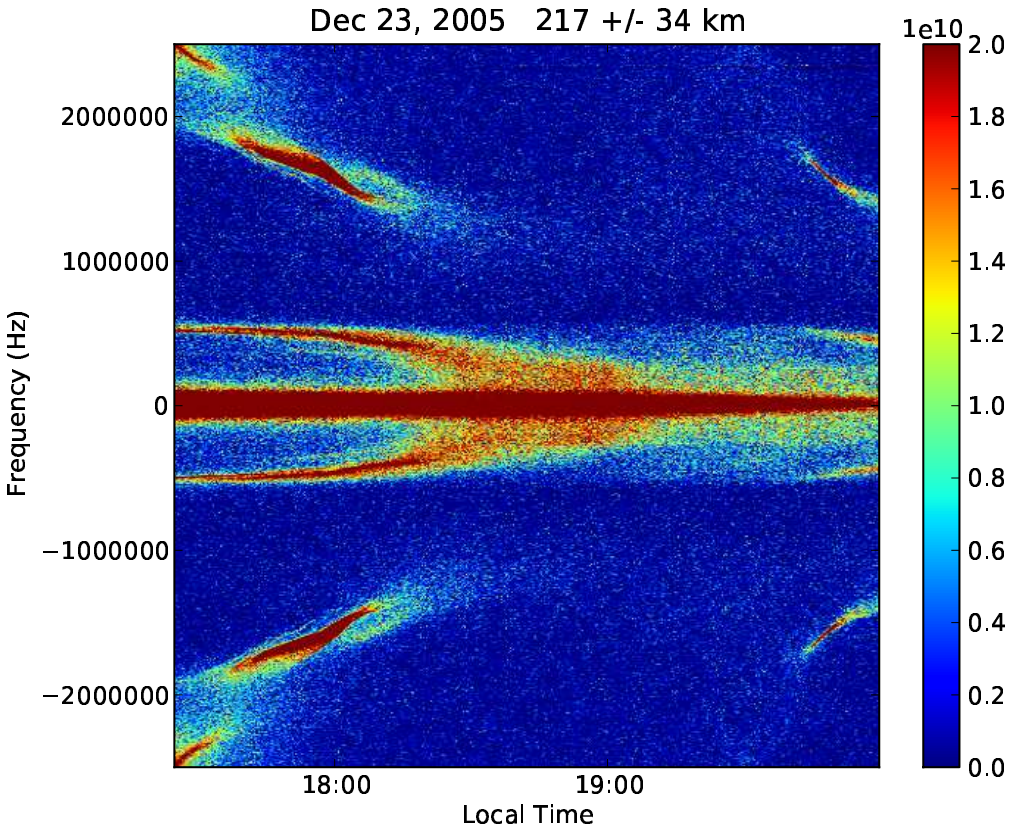

Figure 2.10: Observed spectra from December 23, 2005 at 217 km are plotted over time. The plasma line trace is visible at frequencies > 1 MHz and the gyro line trace is visible starting at 500 kHz. The line in the center is the ion line. The color scale indicates un-calibrated signal power after noise subtraction. The negative values on the colorbar are to increase the contrast in the image.

to equation 1.35. Chapter 1 described problems in calculating accurately the system constant for the Arecibo radar. We shall attempt to estimate a system constant anyway from the available data using the equation 1.35. We compared the computed spectra for electron density values shown in figures 2.8 and 2.9 with the observed ones, which indicated that the observed densities should be in the same range of values that the theoretical spectra are computed for. We

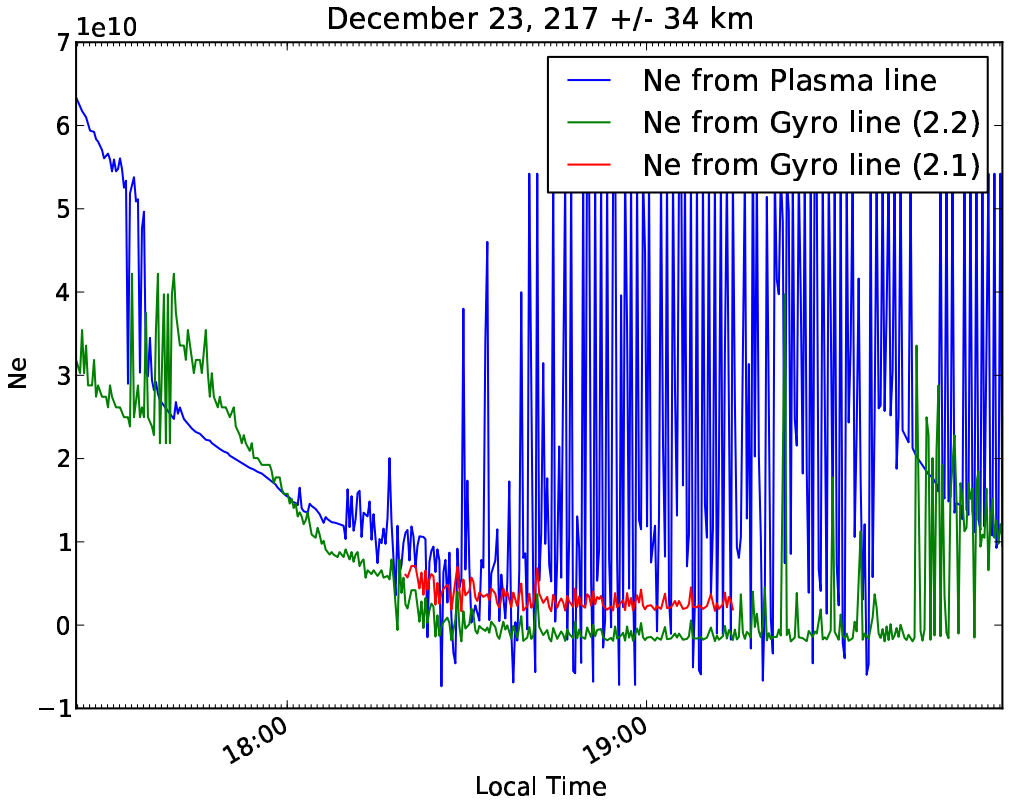

Figure 2.11: N_e derived from observed spectra on December 23, 2005 using analytical expressions for resonance lines. The jump in the plasma line (blue curve) derived N_e near the beginning of the plot will be explained in Chapter 3. After 1830 LT, it was difficult to detect the plasma line, which is indicated by noise-like values. The green curve shows the gyro line from eq. 2.2. It works close to $N_e = 10^{10}/m^3$, below that gives negative values. The red curve is N_e derived using eq. 2.1 and gives reasonable values until after the sunset, which was at 1915 LT at F-region altitudes.

took one value of electron density of the order of $10^{10}/m^3$, and same values for other parameters used to compute the theoretical spectra i.e. $T_e = 863^oK$, $B = 35000nT$. We used $P_T = 1.8MW$, $\tau = 500ns$, Range = $217km$, multiplied the right-hand side of the equation with number of pulses integrated to produce the experimental spectra = 2000 and used the power under the ion line in observed spectra as P_R. This P_R is simply Signal - Noise. It is not in the absolute units of Watts since no calibration pulses were inserted in these experiments. The received signal and the noise subtracted, both have some unknown parameters inherent to the system that cannot be determined accurately since no calibration pulse was injected for these experiments. This is the reason why the spectral intensity is listed as 'un-calibrated' signal power after noise subtraction in figures showing experimental data, and it is not in the absolute units of Watts. We estimate that the transmitted power should not have changed drastically during the period of the experiment on December 23, 2005 and that most unknown factors remained constant throughout the experiment. The K_{sys} should take care of some of these inherent factors, though not all. K_{sys} calculated thus is of the order of $0.5 - 1 \times 10^{16}[m^5/s \times Calibration factors]$. Figure 2.12 shows spectra computed with the full spectrum analysis scaled according to 1.35 and above mentioned values, compared with the observed spectrum for approximately the same value of electron density derived using the gyro line frequency. The resonance line intensities or widths do not compare absolutely because the theoretical spectrum is only scaled with radar parameters, while the observed spectrum has been affected by range smearing as described in Chapter 1. This is also the reason that the observed plasma line has a sharp edge consistent with a sharp gradient in the electron density profile, while the theoretical spectrum does not.

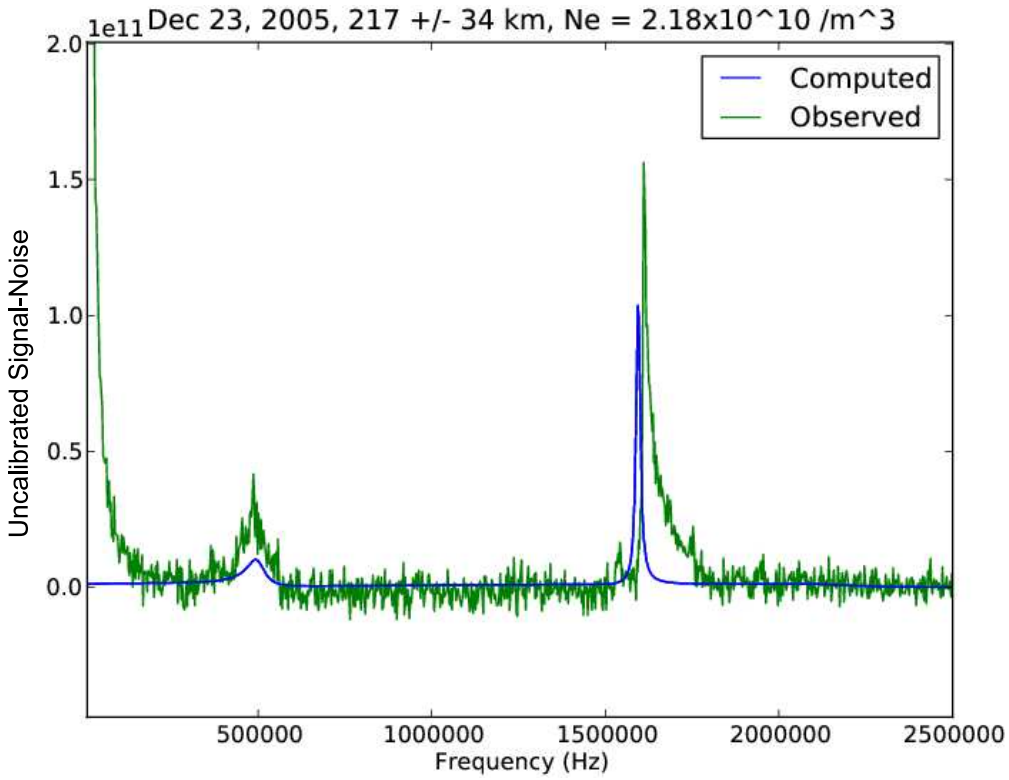

Figure 2.12: Theoretical spectrum compared with the observed spectrum for same value of electron density derived using the analytical expression for the gyro line. The y-axis here is [equivalent to] un-calibrated signal power after noise subtraction. Note that the intensities of the resonance lines do not compare absolutely.

Note that the theoretical spectra need to be corrected for N_e, i.e. scaled by the factor $N_e/(1+k^2\lambda_{de}^2)(1+k^2\lambda_{de}^2+T_r)$ in order to be compared with the observed spectra. Figures 2.13 and 2.14 present the theoretical spectra for various values of electron density uncorrected and corrected for N_e respectively. Figure 2.14 is also scaled by the system constant for Arecibo radar as estimated above. The parameters used to compute these are as above ($T_e = T_i = 863^oK$, $B = 35000nT$, $\phi = 30^o$). Note how the gyro line intensity is drastically affected by this scaling.

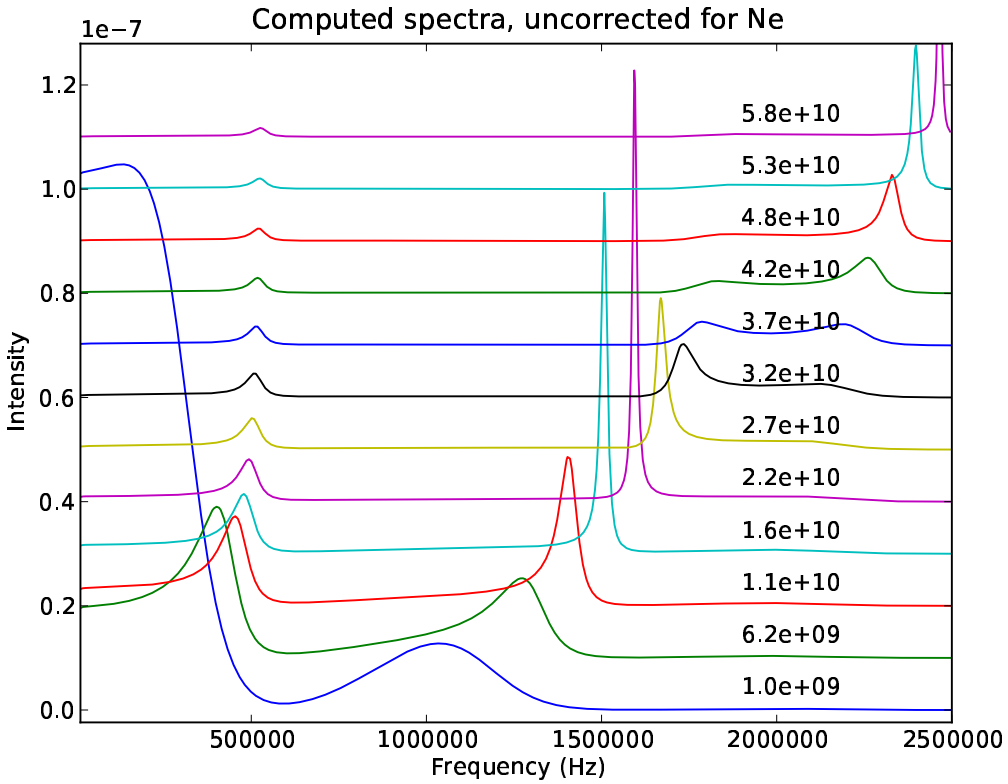

Figure 2.13: Theoretical spectra for a variety of electron density values and other geophysical parameters mentioned in the text. Note how the gyro line intensity changes with the electron density. The gap in the spectra at 2 MHz will be explained in Chapter 3. The spectral intensity on y-axis here is Cross section $\cdot Hz^{-1}$ and plotted arbitrarily.

Also note that only the resonance line intensities are affected by this scaling, and not the frequencies. This is consistent with spectra shown in fig. 2.7.

Figure 2.15 shows the intensities of both resonance lines over a range of electron densities observed. Though the absolute intensities do not match, the shapes of the curves do. To better see the shape for the gyro line intensity, the observed and theoretical values are plotted in figure 2.16.

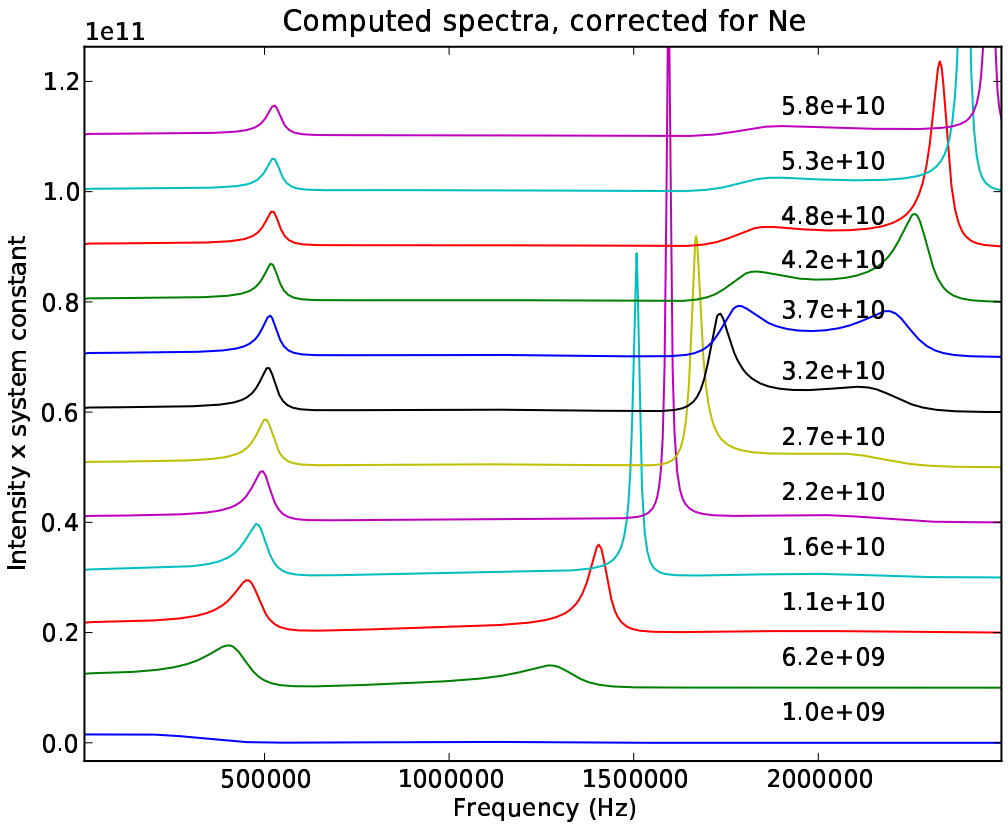

Figure 2.14: Theoretical spectra calculated for a variety of electron density values corrected for N_e and same parameters as fig. 2.13, with dimensionless intensity in fig. 2.13multiplied by the system constant estimated from observations. While the relative intensities of the plasma lines do not change compared with fig. 2.13, the gyro line intensity is most affected by this scaling. For $N_e < 1 \times 10^{10}/m^3$, the gyro line is easily detected compared with the plasma line. The y-axis here is in the same units as the data i.e. un-calibrated power , but with arbitrary values in order to show all spectra in one image.

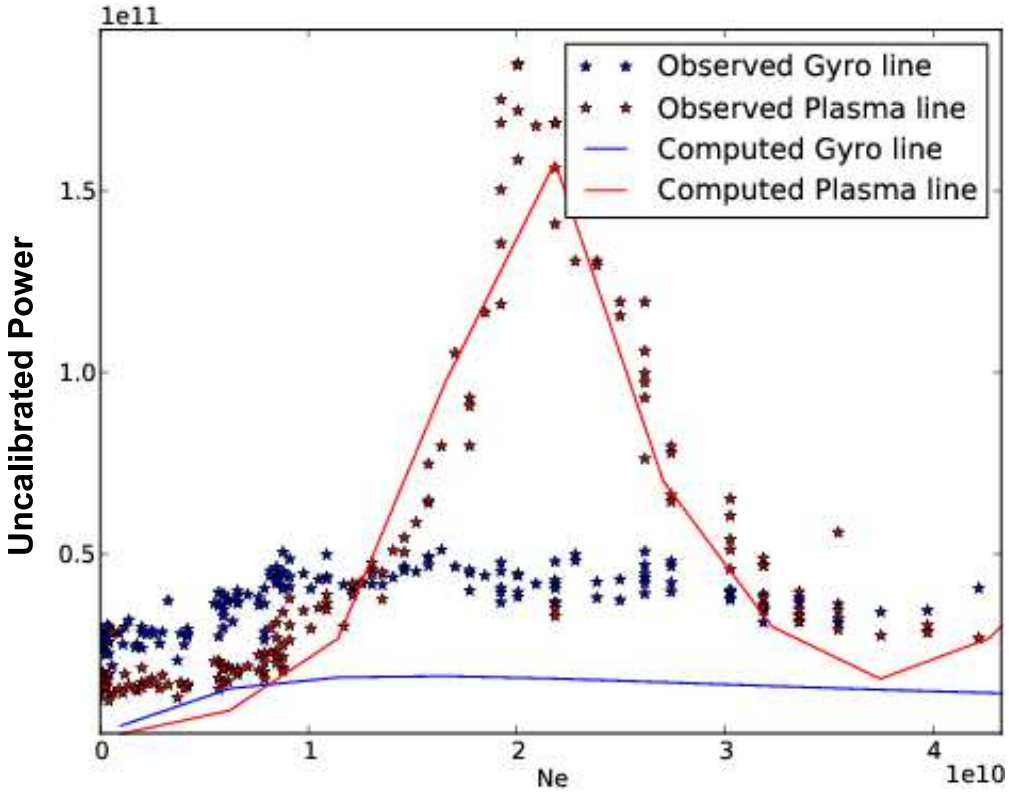

Figure 2.15: Comparison of computed gyro and plasma line intensities with those observed on Dec 23, 2005, evening time experiment. The y-axis is [equivalent to] un-calibrated signal power after noise subtraction. While the absolute intensities do not compare, the observed values follow the same shape as the computed ones. The electron density on x-axis is from fig. 2.11

We argue that the gyro line is better suited to derive the absolute value of electron density for dawn, dusk and night time. Figure 2.17 shows the resonance line intensities over time on December 23, evening time observations. The plasma line intensity decreases after 18:00 LT, but the gyro line intensity decreases some 20 minutes after that. It can also be detected until the end of the experiment. The plasma line ”reappears” in the spectrum at 19:45 LT and the

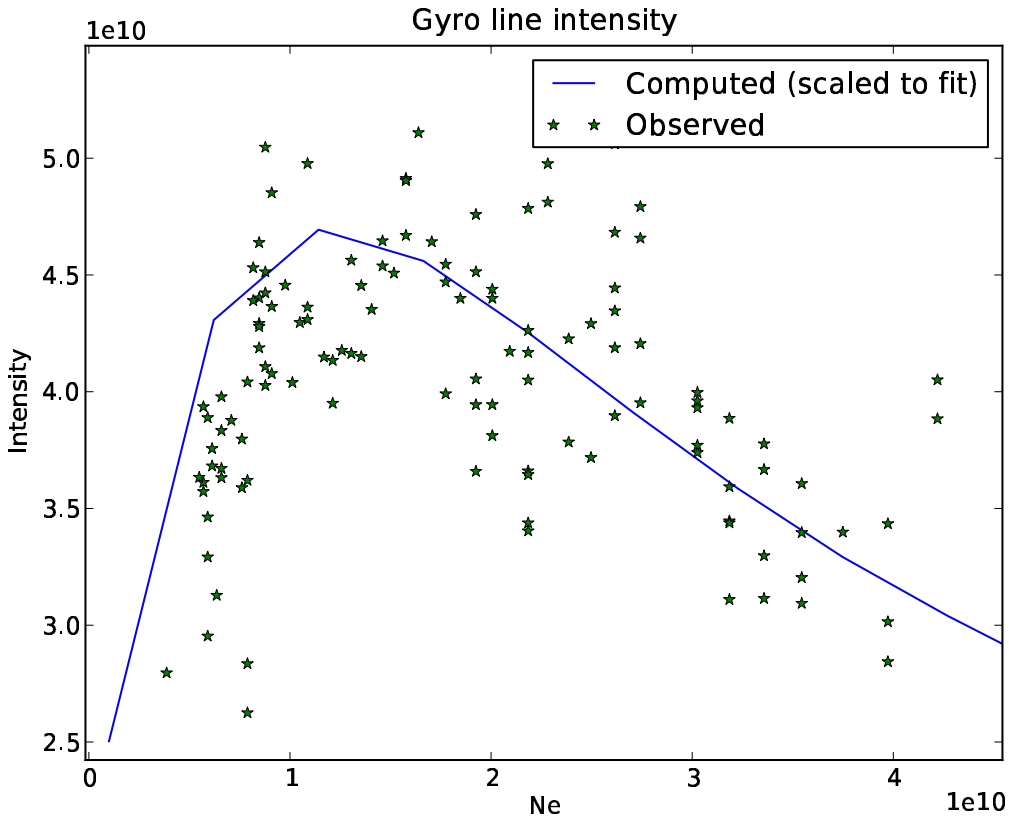

Figure 2.16: Observed and theoretical gyro line intensities plotted vs. electron density. The theoretical values are scaled to fit the observed values to better indicate the shape of the curve. The y-axis is [equivalent to] un-calibrated signal power after noise subtraction. The theory and experiment agree very well. Note that the observed density values are as derived in fig. 2.11.

gyro line intensity increases slightly after it has disappeared again. This reappearance is attributed to either a density layer drifting in the view of the radar in this frequency range, or conjugate photoelectrons. The local sunset in F-region was at 1915 LT, while the conjugate sunset was at 1924 LT at Arecibo.

Although the electron density may be derived with this method, to make a better use of this functionality, measurements with higher altitude resolution need

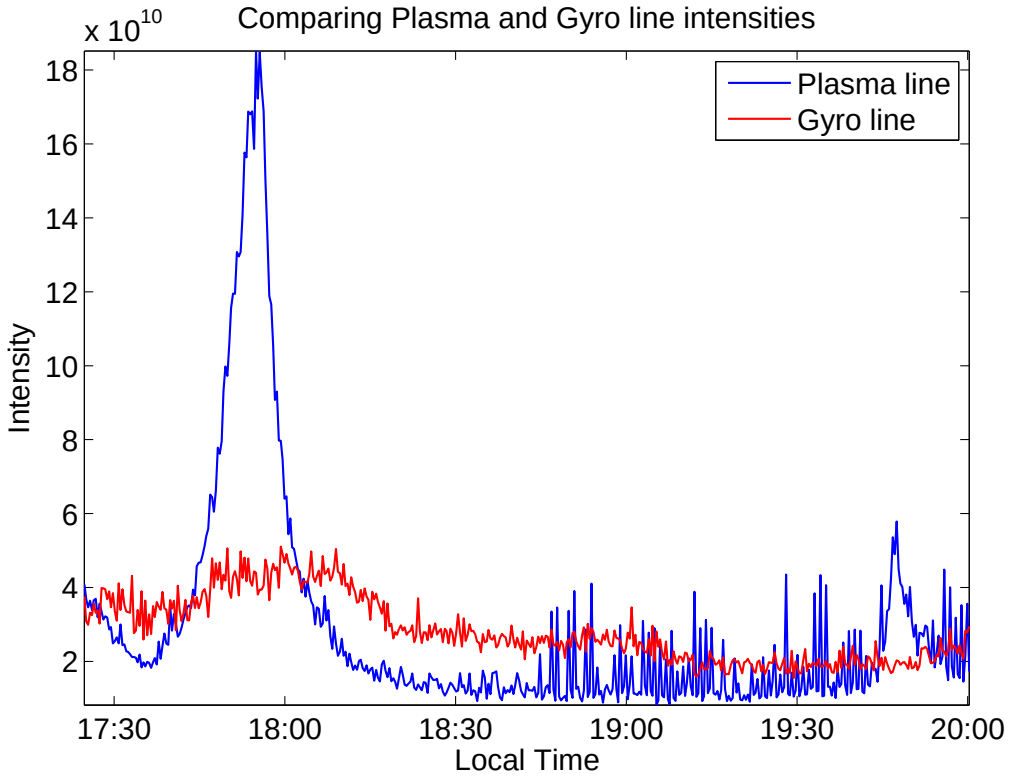

Figure 2.17: Power under the gyro and the plasma lines over time on December 23 evening for 217 km range gate. The intensity here is un-calibrated signal power after noise subtraction $\cdot Hz$. Note that the gyro line is accurately detected throughout the experiment time, while plasma line detection yields noise-like values between 18:45 - 19:45 LT.

to be achieved. While transmitting the radar pulse without any coding helps improve the signal-to-noise ratio markedly, the altitude resolution gets sacrificed.

2.3.1 Interpretation and usage

Figure 2.18 shows spectra during dawn time. The The dawn time spectra were received using two separate channels, each 5 MHz wide. A plasma line trace is present from the beginning of the experiment, which was 0400 LT, starting at 3 MHz, and a strong gyro line trace is also seen at the same time, starting at ≈ 0.5 MHz. However, looking closely, a weaker gyro line trace can be seen at an offset of ≈ 0.3 MHz. At 0700 LT, a plasma line trace appears at ≈ 1.5 MHz and at the same time, the frequency offset of the weaker gyro line trace increases to almost merge with the stronger gyro line trace mentioned above. The two traces, both in the plasma line and the gyro line, are indicative of intermediate layers in the mid-latitude E and lower-F region. These two intermediate layers have been observed regularly at dawn time in winter months.

During December 2005 experiments, both the gyro and the plasma lines disappeared after the local sunset in F-region. However, on most days they reappeared in the spectra after some time. Figure 2.19 shows the spectra for December 22. Both the resonance lines almost disappear by 1850 LT, plasma line before the gyro line. The local sunset in F-region was at 1914 LT, however both the plasma and the gyro line are present almost an after that time as well. The plasma line shows 2 distinct traces indicating two layers. The gyro line during the reappearance is also much stronger than the plasma line. The power under the ion line did not increase, indicating no increase in the ionization. This is also indicated in figure 2.20, where the spectra from another such event on December 23 are shown at four different altitudes and the gyro lines are more

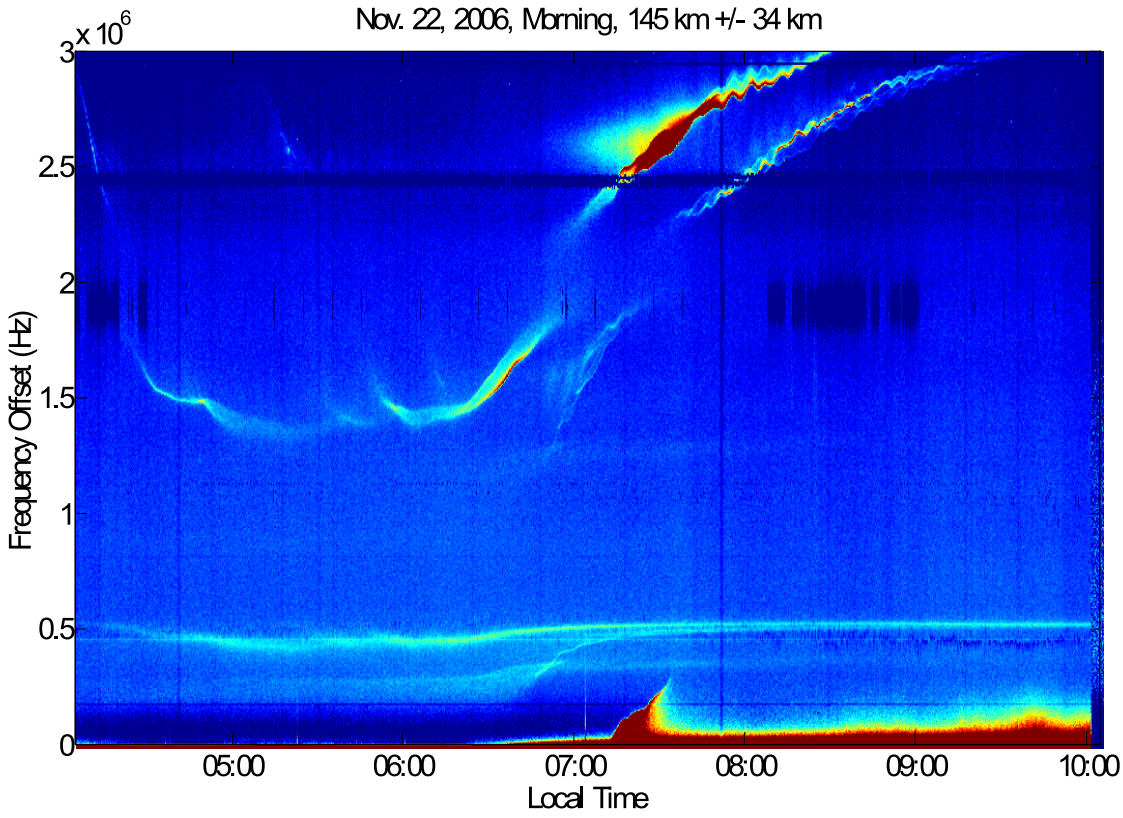

Figure 2.18: Dawn time IS spectra over time as observed using the Arecibo radar showing the upshifted gyro line and plasma line traces. Each gyro line trace corresponds to a plasma line trace. There are two plasma line traces, one beginning at 0400 LT at 3 MHz, and the other at $\approx 1.2MHz$ at 0650 LT. The corresponding gyro line trace for the former is visible from 0400 LT and with little change in the frequency. For the latter, the gyro line trace begins at 0500 LT, much earlier than the plasma line trace. The color scale for intensity indicates un-calibrated signal power after noise subtraction and is same as that in figs. 2.4, 2.5, and 2.10.

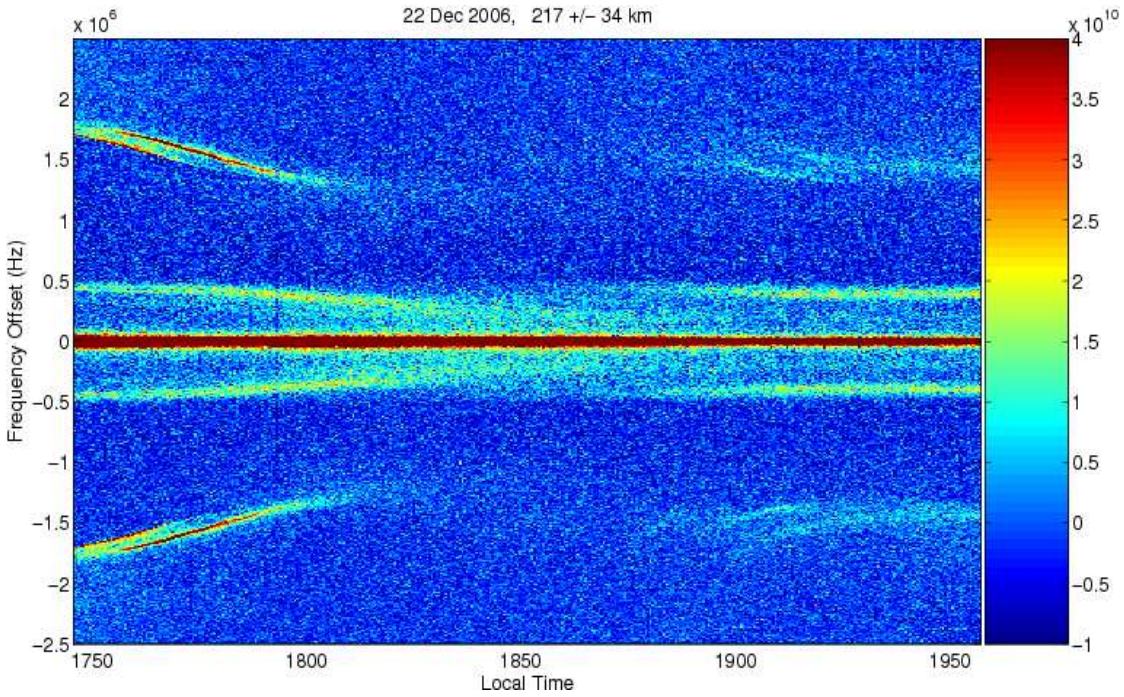

Figure 2.19: Dusk time spectra on December 22 showing the reappearance of gyro and plasma lines after sunset. The sunset in F-region was at 1914 LT. The figure also demonstrates how gyro line is much stronger and well defined than the plasma line during this reappearance. The color scale indicates un-calibrated signal power after noise subtraction.

prominently seen than the plasma lines. The F-region sunset on Dec 23 was at 1915 LT. We see very clear gyro lines at three bottom altitudes - 145, 217 and 289 km at 250, 450 and 500 kHz respectively. The plasma lines however are weaker compared to the gyro lines and can be clearly seen only in the spectrum at 217 km. Note how thin the ion line in the center is.

One speculation about the reappearance of these lines is the presence of conju-

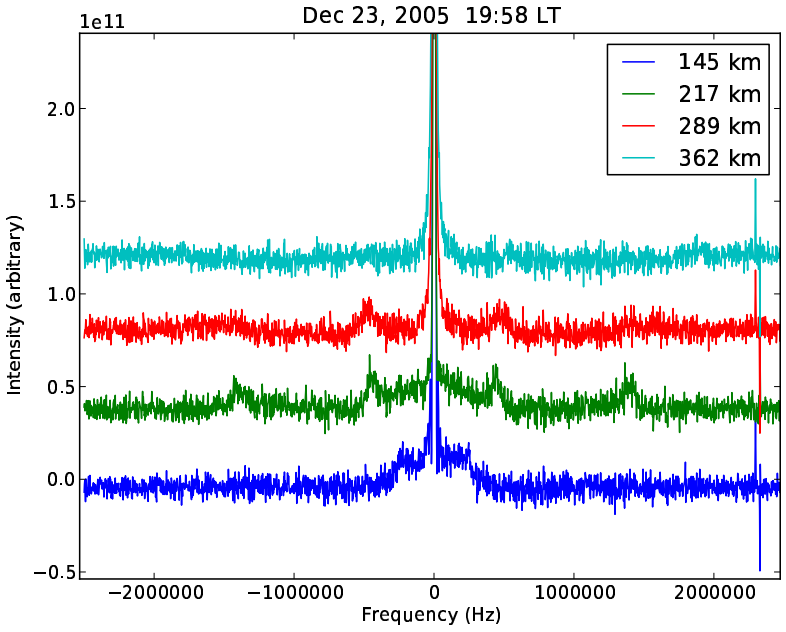

Figure 2.20: Dusk time spectra on Dec 23 from four altitudes centered at 145, 217, 289 and 362 km from bottom to top at 1958 LT. The x-axis is frequency in MHz and the y-axis is spectral intensity in arbitrary units since the values have been tweaked to make them appear on a single figure. We see no plasma line at 145 km, only gyro lines near 250 kHz, plasma line at 1.4 MHz at 217 km and the gyro lines at 450 kHz, extremely faint and broad plasma lines at 1.5 MHz at 289 km and prominent gyro lines at 500 kHz, and no clear lines at 362 km altitude. The intensity values are un-calibrated signal power after noise subtraction and arbitrary since they are tweaked to fit all spectra in one plot.

gate photoelectrons. Another possible cause may be that a layer of ionization drifted in the frequency band we were observing. The former seems somewhat unlikely since the conjugate F-region sunset (Arecibo's conjugate point is near Bahia Blanca on Argentine coast) was at 1924 Arecibo local time, not that different from the Arecibo F-region sunset time. If a layer indeed drifted in the frequency band, it seems to be a recurring phenomenon, and requires more observations.

2.4 Conclusion

Presented here are observations and theory of a resonance line in the IS spectrum that exists only in the presence of a magnetic field. In mid-latitude ionosphere, the gyro line is a ubiquitous feature at E and the lower F region, where the radar aspect angle can be matched to observe the line and the electron temperatures are low enough to ensure a sharper resonance line. At higher altitudes, as the electron temperature increases significantly, the line gets broader and requires much longer integration times to be detected. Observations presented in figures 2.3 to 2.5 were the first clear observations of the gyro line with the Arecibo radar. The gyro line seems to particularly get stronger at lower electron density values. The results described here seem to indicate a more closer relationship between the plasma and the gyro line energies than previously thought. At lower electron densities, when the plasma frequency gets closer to the electron gyro frequency, the plasma line essentially seems to transfer the energy into the gyro line resonance.

The gyro line during dawn and dusk can be used as a measure for absolute electron density. This technique can be used to calibrate the ion line power during night time. The gyro line can also be used to detect thin intermediate density layers and investigate their structure. These layers play a significant role in the dynamics of the mid-latitude ionosphere. Although the data presented here have indeed very coarse altitude resolution, the observation beg the need for a better observation technique that can yield higher range resolution without greatly compromising the frequency resolution.

So far, only the Arecibo radar has been able to unambiguously detect the gyro line. This is also true for low frequency plasma lines. Since low frequency resonance line intensities come from the thermal electrons primarily, the signal is relatively weaker as compared with the high energy photoelectrons enhanced plasma lines. The Arecibo radar has the largest power-aperture product of any known incoherent scatter facility. While other radars have been able to detect the plasma lines at higher frequencies successfully, the low signal-to-noise ratios resulting from lower power-aperture products do now allow them to detect the weak gyro line (and low frequency plasma line) signals above the noise floor.

CHAPTER 3

PLASMA LINE

3.1 Introduction

The plasma line is the larger root of the dispersion relation of the magnetized plasma and can be interpreted as scatter from the Langmuir (electron plasma) waves in the ionosphere, which are enhanced above their thermal energy level by the presence of energetic photo-electrons during the daytime (*Perkins et al.*, 1965). The plasma line frequency can be used as a precise measure for the plasma frequency and consequently the electron density (e.g., *Showen*, 1979; *Djuth et al.*, 1994), and also to obtain electron temperature using slight asymmetries in the up- and down-shifted lines (e.g., *Nicolls et al.*, 2006). Langmuir waves are electrostatic waves and are not affected by magnetic field changes. The plasma line resonance however, does have a magnetic field term in it and the frequency offset is slightly affected by the magnetic field at higher Doppler shifts. At low frequencies (near 2nd electron gyro harmonic), the frequency and the width of the plasma line are significantly affected by the magnetic field and the angle between the radar wave vector ($\mathbf{k}$) and earth's geomagnetic field lines ($\mathbf{B}$) (*Salpeter*, 1961; *Perkins*, 1963). These effects are predicted in the standard IS theory with the magnetic field included in it, but until recently had not been observed. This chapter presents first observations of the magnetic field effect on the plasma line frequency when the plasma frequency is close to the second electron gyro harmonic.

As described in Chapter 1, the approximated plasma line frequency can be given as,

$$\omega^2 = \omega_p^2 + \frac{3}{2}k^2 v_{the}^2 + \Omega_e^2 \cos^2 \phi, \tag{3.1}$$

This approximated frequency works as long as $\omega_p^2 \gg \Omega_e^2$, and the magnetic field plays a negligible role. When ω_p is close to Ω_e, the magnetic field and the angle with the magnetic field play a much larger role. When we consider the contributions from frequency bands not previously considered namely, those close to the electron gyro harmonic, it introduced strange behavior. The following sections discuss theoretical predictions along with the experimental evidence that near the second electron gyro harmonic, the plasma line essentially splits into two lines separated by $kv_{the}/2\pi$, if the right aspect angle condition is met.

3.2 Splitting of Plasma line

Experiments described later in this chapter were conducted during the morning and the evening periods during the winter months (December 2005 and November 2006) at Arecibo, to investigate the effects of conjugate photoelectrons on the electron component of the IS spectrum. The observations showed a split in the plasma line when the plasma frequency passes through the second electron gyro harmonic. This effect was predicted in the early days of incoherent scatter theory (*Salpeter*, 1961), when it was noted that the dispersion relation for electron plasma waves exhibits "frequency gaps" (no roots) at some multiples of the electron gyro frequency (*Gross*, 1951; *Bernstein*, 1958). Instead, two roots

appear, one on either side of the frequency gap (*Perkins*, 1963). The existence of these so-called "frequency gaps" in theory was met with doubt initially (*Oster*, 1960), despite theoretical confirmations using a different approach by *Salpeter* (1961). The practical implication of these predictions is that when the plasma frequency is near a gyro harmonic, the plasma line can split into two lines. First ever observations of this "split" are presented here with the supporting theory.

3.2.1 Predictions from theory

The expressions derived in Chapter 1 only took values of $|x_{ne}| \gg 1$ into account. Now if we try to estimate the contributions from $|x_{ne}| \leq 1$ in the low density regime, we find that it affects the intensity of the spectrum. Let us try to estimate the contribution to the spectrum from the frequency band $|n\varepsilon - x| \leq 1$. For $n \geq 2$, we can add the next order to the expression for $Y(x)$ from 1.20 (after rewriting $Y(x)$ to simplify taking the derivative) (*Perkins*, 1963; *Salpeter*, 1961),

$$Y(x) = 1 - \frac{a^2}{2}\left[\frac{\cos^2\phi}{x^2-\varepsilon^2} - \frac{\sin^2\phi}{x^2}\right] + a^2 \sum_{n=-\infty,\neq 0,1,-1}^{\infty} \left(\frac{\cos^2\phi}{4\varepsilon^2}\right)^{|n|} \frac{x}{|n|!}\frac{f(x_{ne})}{x_{ne}\sin\phi} \quad (3.2)$$

$Y'(x)$ is then given as,

$$Y'(x) = a^2 x\left[\frac{\cos^2\phi}{(x^2-\varepsilon^2)^2} + \frac{\sin^2\phi}{x^4}\right] +$$

$$a^2 \sum_{n=-\infty,\neq 0,1,-1}^{\infty} \left(\frac{\cos^2\phi}{4\varepsilon^2}\right)^{|n|} \frac{1}{|n|!} \left(\frac{f(x_{ne})}{x_{ne}\sin\phi} + \frac{2x}{\sin^2\phi}(f(x_{ne})-1)\right) \tag{3.3}$$

The function $P(x)$ will display resonances wherever slope of $Y(x)$, i.e. $Y'(x)$ is zero. This depends strongly on the angle ϕ. From the above equation, the condition for $Y'(x)$ to be zero at $x = n\varepsilon$ is,

$$n\varepsilon \left(\frac{\cos^2\phi}{\varepsilon^4(n^2-1)} + \frac{\sin^2\phi}{\varepsilon^4 n^4}\right) = \left(\frac{\cos^2\phi}{4\varepsilon^2}\right)^n \frac{2n\varepsilon}{n!\sin^2\phi} \tag{3.4}$$

Putting $n = 2$, the condition is,

$$\frac{\cos^4\phi}{\sin^2\phi(1+(7/9)\cos^2\phi)} = 1 \tag{3.5}$$

Or,

$$\phi = 34^\circ$$

For $\phi < 34^\circ$, the plasma line will split into two resonance lines when the plasma frequency is close to the second electron gyro harmonic. For $\phi > 34^\circ$, the plasma line will be broadened but not split. For higher values of n, ϕ requirement gets smaller and smaller giving 15° for $n = 3$ and 4° for $n = 4$. Later it was shown by *Perkins* (1963) that the split resonance lines are separated by $kv_{the}/2\pi$ and the energy gets distributed in those two lines. However, it does not create a discontinuity in the frequency spectrum, rather the frequency is the average of the two resonance line frequencies above and below the gap, as indicated in figures 2.9

and 2.11.

All the calculations in this analysis have been carried out with Arecibo radar parameters. In Fig. 3.1, plotted are the electron density spectra using the Full Spectrum Analysis method in the region of parameter space where the interesting behavior occurs. The density is varied and the spectrum is plotted for two different values of electron temperature, with constant $\phi = 30^\circ$. It is apparent that as the plasma line passes through the second harmonic of the gyro frequency (denoted by the dashed line), it is split into two resonances.

In the limit of probing angle approaching perpendicularity, harmonics should be observed at all gyro harmonics. We note that the limit of Arecibo scanning is $\phi \sim 30^\circ$, however other systems could look for other harmonics (although detecting the plasma line at low densities can be difficult with most IS systems).

In Fig. 3.2, plotted are the theoretical spectra for several values of $\alpha = 90^\circ - \phi$ at a constant electron density 4×10^{10} m^{-3} and $T_e = 1000$K. At about $\alpha = 55^\circ$ we see the presence of the double hump, as expected. The lines get narrow with increasing α. The separation of the humps is about $kv_{the}/2\pi$, but does vary slightly with α. The plasma line almost vanishing at $\alpha = 80^\circ$ is the result of $\sin\alpha$ in $\Im He$ approaching 0 as α is increased. However, the abrupt disappearance can be attributed to the limited computing power that directly translates into frequency resolution.

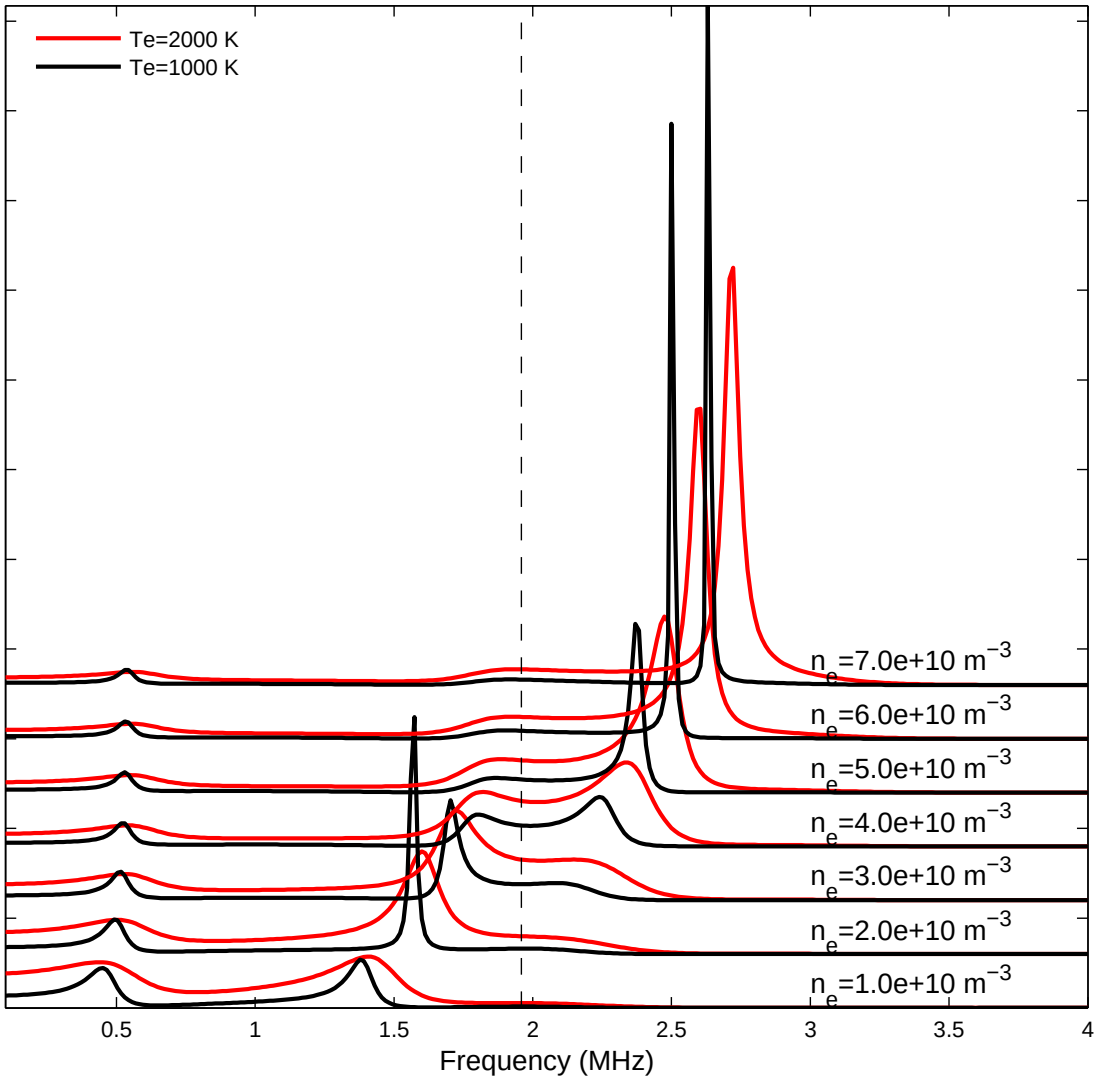

Figure 3.1: Theoretical spectra calculated for two different values of electron temperature, varying electron density, and $\phi = 30°$. The electron density increases from bottom to top. The split is shown by the dashed line. The y-axis has the same units as fig.1.7 in Cross section $\cdot Hz^{-1}$, but are tweaked to fit in the same plot and hence arbitrary.

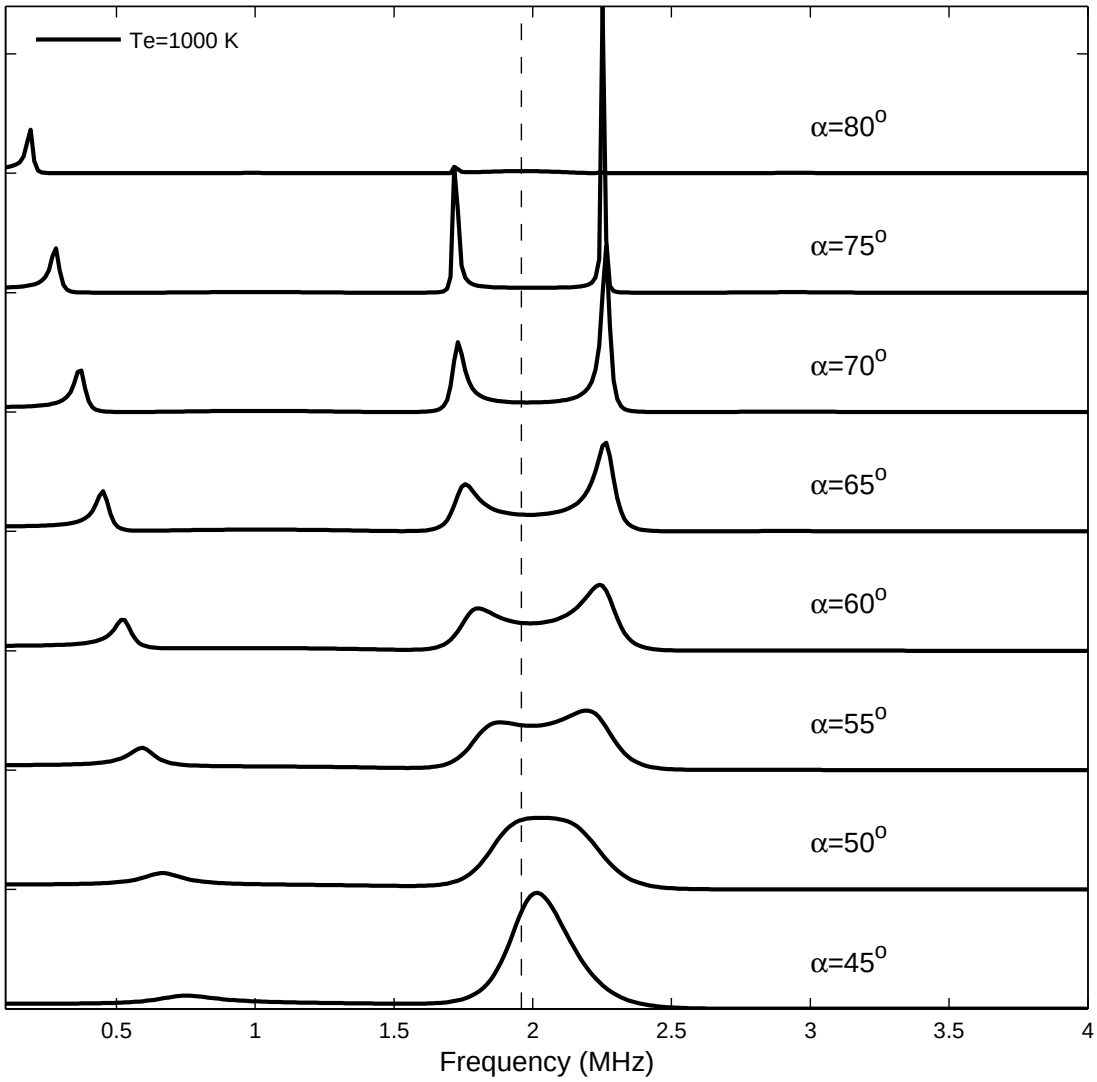

Figure 3.2: Theoretical spectra calculated for different values of α. These spectra are calculated for $T_e = 1000K$ and $N_e = 4.0 \times 10^{10} m^{-3}$. For Arecibo parameters, the split occurs only in the range of $55^o \leq \alpha \leq 75^o$. The y-axis here indicates Cross section $\cdot Hz^{-1}$ but the values are arbitrary and hence not shown.

3.2.2 Observations

The experiments described here were the same as those described in Chapter 2 and carried out using the Arecibo 430 MHz IS radar (18°20′ N, 66°45′ W) in Puerto Rico. A recap: In December 2005, evening experiments were conducted in the period 1700-2000 LT (UT=LT+4). A 500 μs uncoded long pulse (=75 km in range) with an inter-pulse period of 10 ms was transmitted to ensure a high signal-to-noise ratio (SNR) for the returned signal in order to study the weak features. The receiver bandwidth was 5 MHz (sampling rate = 0.2 μs). The radar was pointed 349° in azimuth, aligned with the magnetic meridian, and 15° offset from the zenith towards north. The dip angle at Arecibo is close to 45° at E- and F-region altitudes, hence the angle between the radar pointing and the magnetic field (α) was close to 60°. All the spectra shown here have been integrated for 20 seconds (2000 pulses).

The evening results reported here were taken on December 23 and are representative of the observations on other days. The spectra were computed at four independent altitude bins, centered at - 145, 217, 289, and 362 km. At 1700 LT, the electron density was low ($\leq 8 \times 10^{10} m^{-3}$, corresponding to a plasma frequency of ~ 2.5 MHz). The F-peak was around 250 km. The plasma lines were observed at the two lower altitudes. Fig. 3.3 is a frequency-time-intensity (FTI) plot at 217 km, showing the ion line centered at zero frequency offset, the gyro line starting at an offset of 500 kHz, and the plasma line starting at an offset of 2.5 MHz that decreases with time. The color scale indicates un-calibrated signal power after noise subtraction. The electron density decreases with time (plasma

line moves towards the center). The plasma line trace is seen from 2.5 MHz ending at ~ 2.3 MHz, reappearing at ~ 1.8 MHz and ending at ~ 1.25 MHz. The gap between the disappearance and the reappearance of the trace is ~ 450 kHz. The center frequency of this gap (where the split occurs) is ~ 2 MHz, which is close to the second electron gyro harmonic at this altitude, the magnetic field intensity being 35000 nT ($f_{ce} = 0.9MHz$). The local sunset at this altitude was at 1901 LT. The plasma line trace disappears ~ 30 minutes before sunset. The box inserted in Fig. 3.3 shows sample individual spectra at 1 minute intervals between 1726 to 1742 LT (time progressing upward). The split occurs close to 2 MHz.

Fig. 3.4 shows a frequency-time-intensity plot for a morning experiment on November 22, 2006 with considerably more spectral structure. The color scale in this figure also indicates un-calibrated signal power after noise subtraction. This experiment had the same parameters described above, except that the total receiver bandwidth was 10 MHz. The plasma line can be seen to increase in frequency from ~ 1.2 MHz beginning at 0430 LT. When it reaches ~ 2 MHz, the split occurs and the plasma line 'jumps' to an offset ~ 450 kHz higher. This plasma line indicates the presence of an intermediate layer of electron density, which typically occurs between the F and the sporadic E layers at night and is a result of the tidal oscillations in the neutral atmosphere (*Kelley*, 1989). Since we transmitted a long pulse, we were also able to see what we believe to be a second density layer occurring within the 75-km pulse, which starts to form around 0700 LT at an offset of 1.5 MHz. This can be seen more clearly in the subplot. The plasma line for this layer splits at 0730 LT, again at 2 MHz and

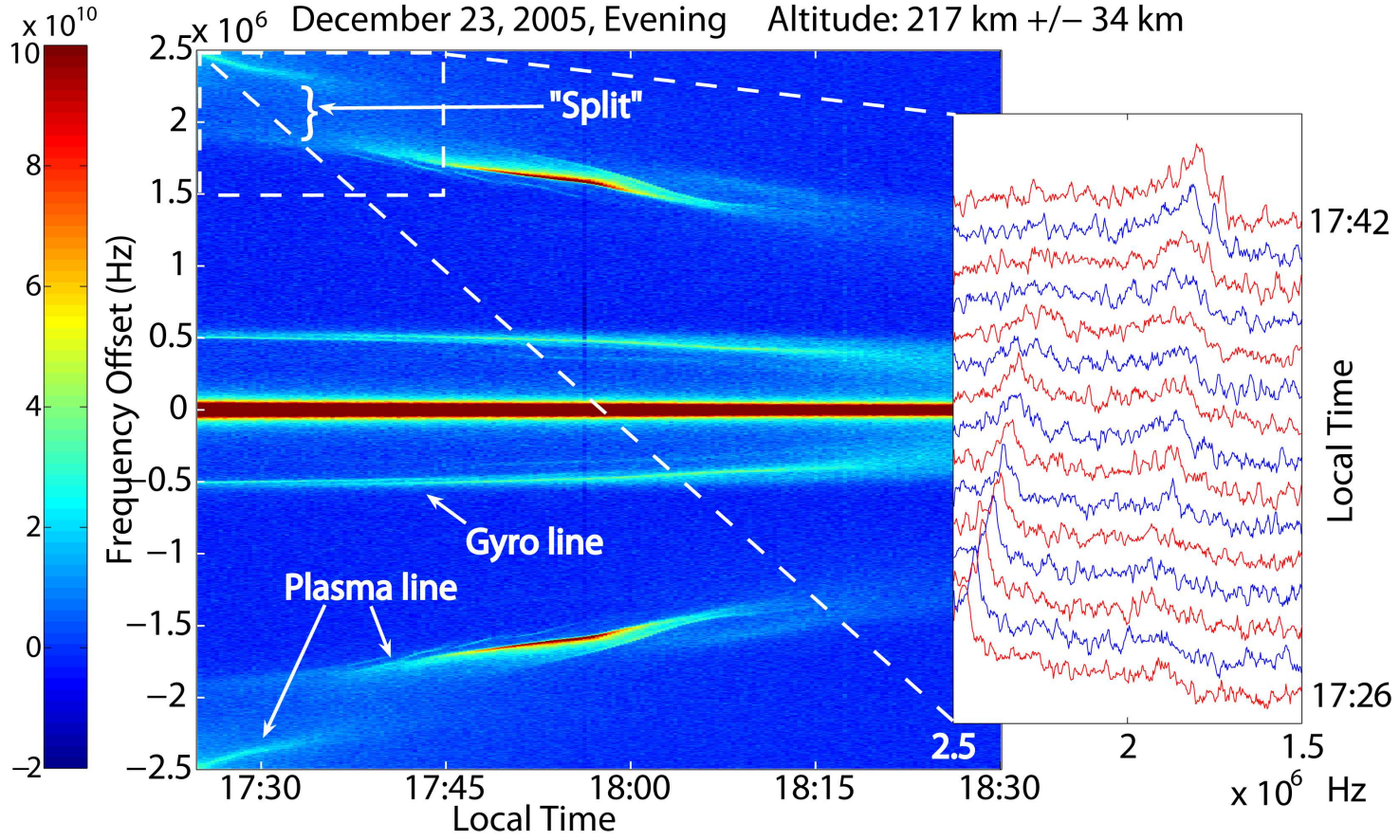

Figure 3.3: Frequency-time-intensity plot showing the plasma line on Dec 23, 2005. The insert shows individual spectra from the boxed region. Negative values in the color scale are for enhanced visibility of features.

it 'jumps' to an offset of 2.3 MHz at 0737 LT. Note the wavy activity characteristic of intermediate layers, which are sharp density layers consisting mainly of metallic and molecular ions confined to a narrow region in altitude. These observations, showing two independent plasma layers jumping in frequency at the second electron gyro harmonic at different times, provide evidence that this frequency is indeed a crucial parameter.

This behavior has been seen on several days. Figure 3.5 is a scatter plot of plasma line observations from three evenings in December 2005. The split and the enhancement in the plasma line intensity after it comes out of the split is visible on all three days. On some days, the plasma line reappeared in the spectra after disappearing at local sunset. This reappeared line was weaker than before but still exhibited the split at the second electron gyro harmonic.

Note that the gyro line does not seem to have any noticeable correlation with the split in the plasma line. The gyro line can be seen in both figures 1 and 2 and remains relatively constant in frequency close to the electron gyro frequency multiplied by $\cos\alpha$, near $\pm$0.5 MHz. This is also consistent with the IS theory.

3.2.3 Electron temperature measurements

As noted in the section 3.2.1, the split in the plasma line equal to $kv_{the}/2\pi$. This proportionality to the electron temperature can be used to infer absolute elec-

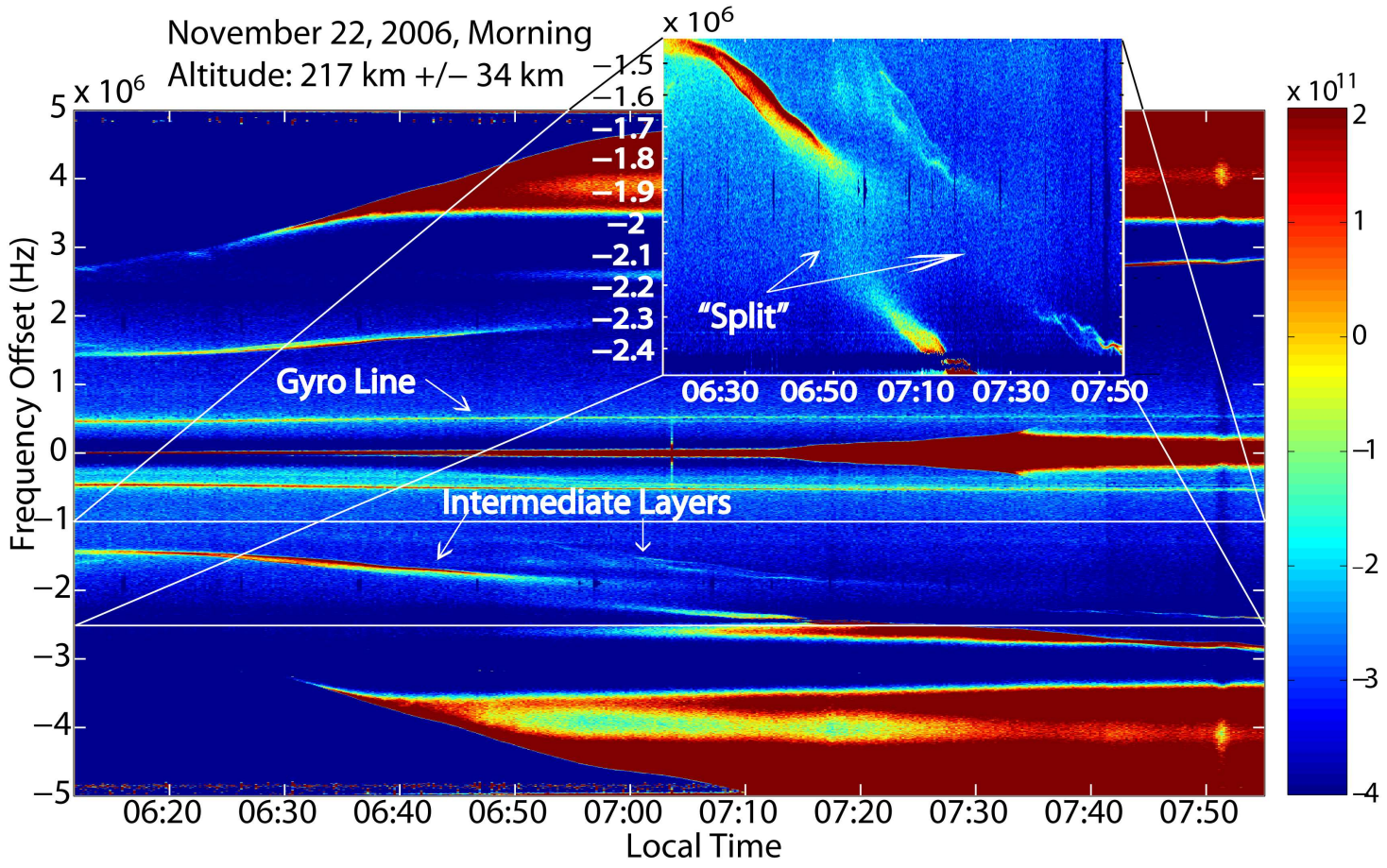

Figure 3.4: FTI from data obtained during the morning of November 22, 2006 for an altitude of 217 km. The sunrise was at 0602 LT at this altitude.

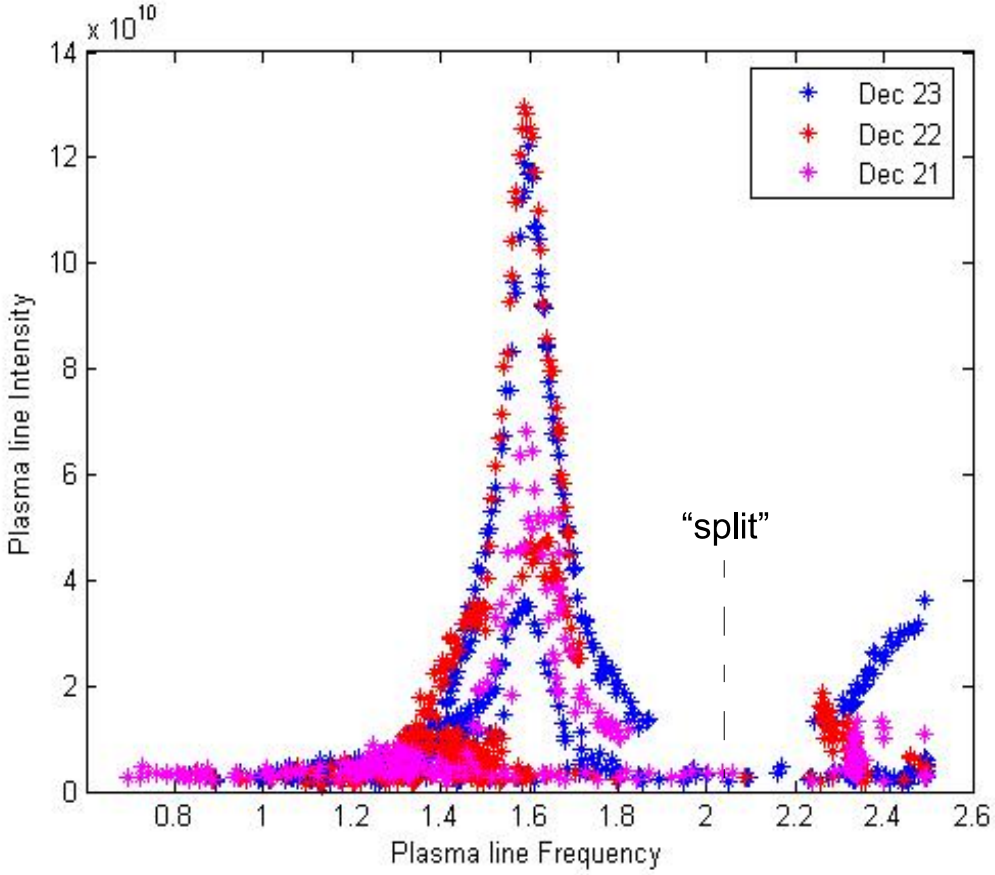

Figure 3.5: Observed plasma line frequency offsets from three consecutive evenings. The intensity on y-axis is un-calibrated signal power after noise subtraction $\cdot Hz$. This plot suggests that the plasma line split occurred everyday.

tron temperature for a particular value of electron density in the spectra. In the dawn time observations, we see multiple density layers present that display the split at different times and have different plasma line widths. Knowing the absolute electron temperature for these layers tell us the energy of the electrons that help form these layers. This temperature can also be used to calibrate the gyro line frequency for electron densities. The advantage of using the split over the intensities of lines is that the frequency is a more precise measure than the

shape.

From the split displayed in figure 3.3, the dusk time temperature of this layer is $\approx 863^oK$, a value used for calculating the gyro line frequency in Chapter 2. The electron densities calculated from the gyro line offsets using this temperature is displayed in figure 3.6. The figure shows electron density derived from the equation 2.1 then input into the full spectrum analysis and plotted alongside the approximated values. Temperatures derived from the split during the dawn time in two layers are different from each other, which tells us which layer is from what altitude range. The split in the stronger layer, that appears earlier in the spectra gives the temperature of $\approx 724^oK$ and the other layer gives $\approx 500^oK$. This indicates that the weaker layer is from a lower altitude while the stronger layer was from a higher altitude range. This information will be used for a more sophisticated fitting routine in the future.

3.3 Discussion

Presented here were results obtained from evening and morning time experiments at the Arecibo Observatory, where we were able to make observations of the entire IS spectra at low electron densities. As predicted by the IS theory, when the plasma frequency is near the second gyro harmonic, the plasma line splits into two resonances, and is greatly enhanced when it comes out of the split. Our observations also indicate that the split occurs regardless of the energy in (intensity of) the plasma line. The split plasma line in weak intermediate layers have been observed during morning experiments, when the layer

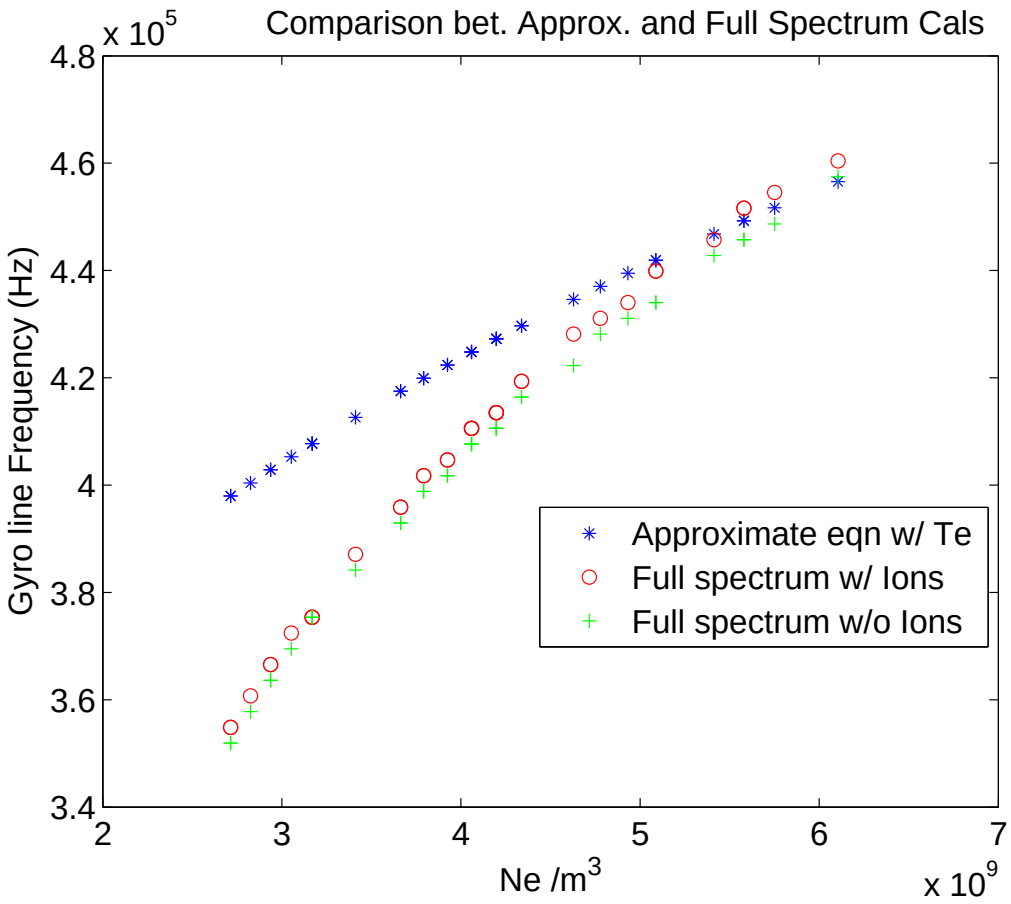

Figure 3.6: Electron density derived from the gyro line frequency using the temperature derived from the plasma line split with equation 2.1. The derived density values are then input into the full spectrum analysis to compare with the predictions of approximate equation. The data used are obtained on Dec 23 between 18:03 to 18:16 LT during the hour before local sunset.

passes through second gyro harmonic. The split indicates damping that is consistent with Landau damping (see (e.g., *Chen*, 1984) for description of Landau damping)in the presence of a magnetic field. *Yngvesson and Perkins* (1968) gave a detailed treatment of Landau damped plasma line for different conditions. For thermal Maxwellian plasma, in weak magnetic field, i.e. $\omega_p > \Omega_e$, the Landau damping for angles $0^\circ < \alpha < 90^\circ$ can be significantly greater than when there is no magnetic field and depends strongly on the angle that is α. The Landau damping including the magnetic field is derived from $\Im He$ (*Yngvesson and Perkins*, 1968; *Salpeter*, 1961),

$$\gamma_B = \omega_p \left(\frac{\pi}{8}\right)^{1/2} a^3 \sum_{n=-\infty}^{\infty} \frac{\chi_{ne}}{\sin\phi} \exp(-x_{ne}^2) \tag{3.6}$$

The frequency shift here are in the multiples of gyro frequency. However, this is still Landau damping because the electrostatic field of the wave interacts with the electron motion. If after one gyro period, if an electron has the same phase relationship with the electron plasma wave, then the wave-particle interaction is stronger. For smaller frequencies and at intermediate angles, the thermal Landau damping depends strongly on the angle α. Figure 3.7 shows a graph of γ_B for the experimental parameters and $n = 2$ for a varying α. At higher angles between k and $\mathbf{B}$, the damping is much greater. At $k \perp \mathbf{B}$, the Landau damping vanishes.

For values of $\varepsilon \gg 1/\sqrt{2}$, or angles nearly perpendicular to B, or both, the Landau damping strongly depends on whether the plasma line is close to an electron gyro harmonic. For our case described here, $\varepsilon = 2 \gg 1/sqrt2$ and the angles of interest are $55^\circ < \alpha < 65^\circ$. So we would expect to see significant Landau

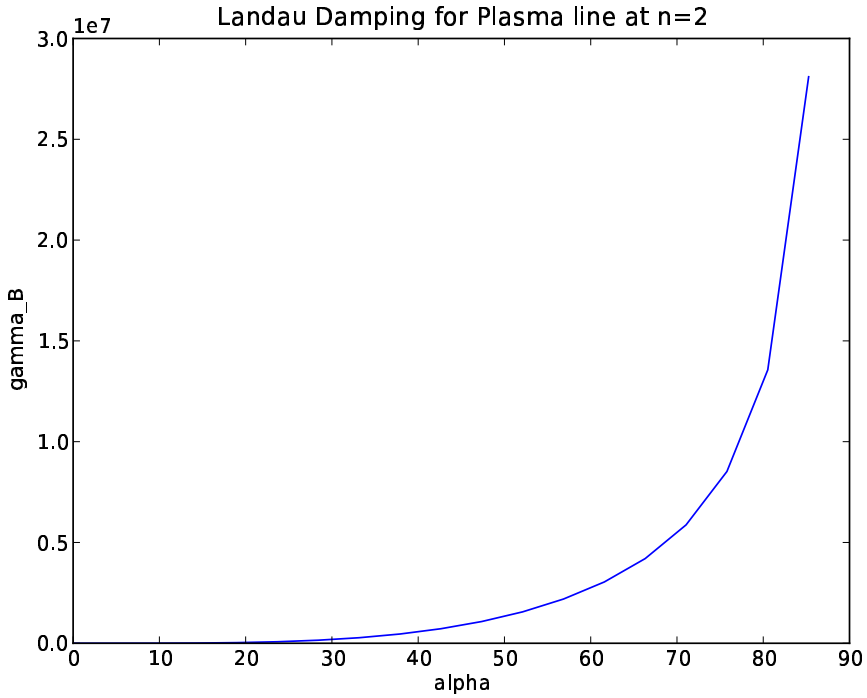

Figure 3.7: Landau damping for $x = 2\varepsilon$ for a range of angles between k and B. γ here is in the units of s^{-1}. It is much greater for angles $> 30°$. The relevant values for the experiments described here are $56°$ and at $60°$.

damping. Figure 3.8 shows Landau damping for $n = 2$ and $\alpha = 56°$ vs. the plasma line frequency. At these points, the spectrum shows either the split of a broadened line depending on the angle.

Our observations pertain only to electrons with thermal energies, as observed by *Yngvesson and Perkins* (1968). For the angles possible with the Arecibo radar, the non-thermal contribution to the spectrum starts at frequencies $> 4.5MHz$. Similar observations for non-thermal energy distribution were carried out by *Fremouw et al.* (1969), where frequency gaps or "bite-outs" in IS spectra using 1290 MHz Stanford radar (presently at Sondrestrom, Greenland) were observed

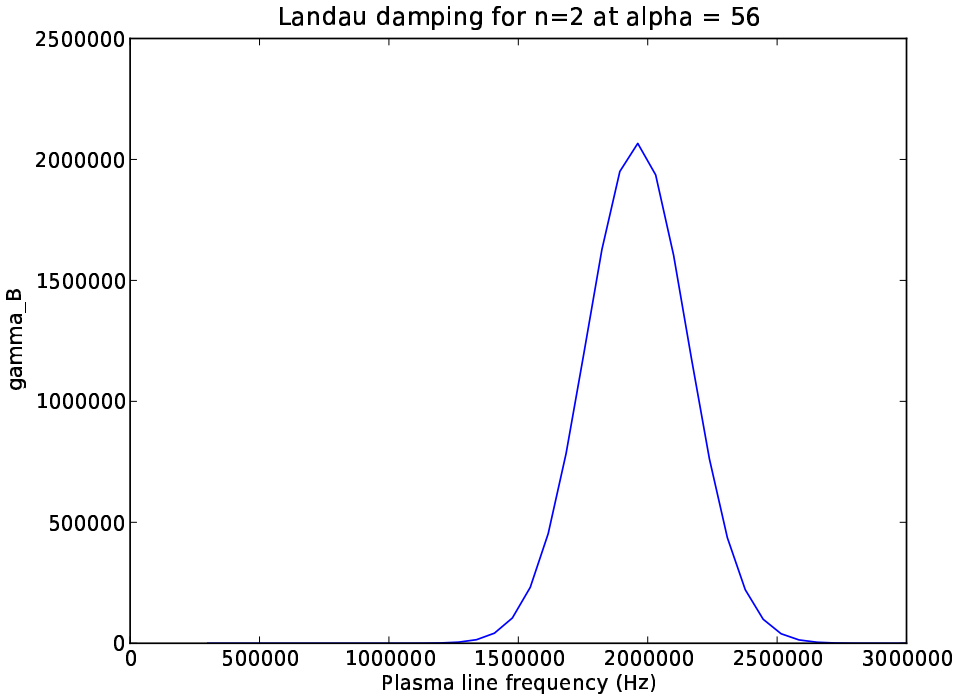

Figure 3.8: Landau damping for $x = 2\varepsilon$ for $\alpha = 56°$ plotted against the plasma frequency. γ_B is in the units of s^{-1}. As the plasma line frequency nears the 2nd gyro harmonic, the Landau damping increases and the frequency spectrum shows the "split" or broadening of the line.

for $\alpha > 80°$. These experiments were carried out by tuning the center of the receiver to the plasma frequency of interest. Results showed that at multiples of electron gyro frequency, the received signal showed significant damping. The damping is attributed to the Landau damping process.

In recent years, high latitude ionospheric modification experiments done at the second gyro harmonic have produced some interesting results using optical diagnostics (*Kosch et al.*, 2005; *Djuth et al.*, 2005). An enhancement in the artificial air glow has been observed while heating the ionosphere at second gyro har-

monic. It has been suggested that the Langmuir waves participate in the electron cyclotron acceleration when the local plasma and electron gyro frequencies match (*Mishin et al.,* 2005). We plan to make further observations to investigate this effect using an ISR as a diagnostic tool for an ionospheric modification experiment.

CHAPTER 4

ATMOSPHERIC WAVE STUDIES WITH PLASMA LINE

4.1 Introduction

Since the plasma line is a measure of the electron density in the ionosphere, any modulations in the electron density are readily reflected in the plasma line frequency. Atmospheric pressure waves routinely propagate up to the ionosphere and cause the electron density to bunch up at periodic spatial and temporal intervals. These waves are important in understanding the coupling between the atmospheric regions, since they also transfer the momentum flux from lower atmosphere to the upper (e.g., *Vadas*, 2007; *Vadas and Fritts*, 2005). Characterizing the temporal and spatial scales of these waves are crucial in order to understand their velocity, propagation and dissipation. This chapter describes two examples of how plasma line observations can assist the investigations of such waves in the ionosphere. The following section gives a background on the buoyancy or gravity waves, as they are more commonly known.

4.2 Introduction to Gravity Waves

Gravity waves are buoyancy waves, where a parcel of fluid is displaced and is restored by gravity. The process of restoring the parcel towards equilibrium results in oscillations about the equilibrium state, which are observed as density

fluctuations in a fluid medium. The characteristic frequency of these oscillations is called the Brunt-V$\ddot{a}$is$\ddot{a}$l$\ddot{a}$ or the buoyancy frequency, which is a low frequency branch of the acoustic waves. Only the waves with frequencies less than the buoyancy frequency would propagate. A variety of gravity wave (GW) signatures can be observed in the oceans, the clouds (e.g. figure 4.1), and also the upper atmosphere. These GWs create variations in the neutral fluid density, temperature, pressure, and wind velocity. In the ionosphere, the GWs originated in the neutral atmosphere cause the plasma to converge along the magnetic field lines forming density layers in horizontal and vertical directions at altitudes primarily below 200 km (*Kelley*, 1989). These waves are mainly observed in the ionosphere as traveling ionospheric disturbances or TIDs. A characteristic of observed wave-layer structuring is that the layers are downward propagating, which indicates a downward phase progression for an upward group velocity and is predicted in the gravity wave theory (*Kelley*, 1989). The typical wave periods for such GWs are from ≈ 6 to 180 minutes (*Vadas*, 2007). The horizontal and vertical wavelengths vary with altitude.

The TIDs have been detected by a variety of techniques including ionosondes, air glow imagers, and radars. Recently first observations of the TIDs from Poker Flat incoherent scatter radar (PFISR) have been reported (*Nicolls and Heinselman*, 2007; *Vadas and Nicolls*, 2008), where GWs were detected using ion line in the incoherent scatter (IS) spectrum. The Arecibo radar is the most sensitive facility of its kind and has been used by *Djuth et al.* (1997, 2004) to provide high temporal and spatial resolution electron density fluctuations at 1% level. The height dependence of the vertical wavelength in these measurements were compared

Figure 4.1: Gravity waves in tropospheric clouds.

with damping mechanisms as described by *Hines* (1960), who treated dissipating effects of kinematic viscosity and thermal diffusivity separately. A different approach was taken by *Vadas and Fritts* (2005), which involves both the kinematic viscosity and thermal diffusivity in a single anelastic dispersion relation. This dispersion relation has led to explore in detail the thermospheric response to lower atmospheric sources (*Vadas*, 2007) provided that enough GW characteristics (vertical and horizontal wavelengths and periods, background neutral winds and temperatures) are measured properly. A detailed account of theoretical work on the GWs is given in *Vadas* (2007).

4.3 Gravity waves at High latitudes

The Advanced Modular Incoherent Scatter Radar (AMISR) at the Poker Flat Research Range near Fairbanks in Alaska ($65.12^oN147.47^oW$) is a new facility capable of detecting the plasma line using a long pulse. Here we describe using the plasma line observed thus to infer vertical parameters of upward propagating gravity waves that manifest themselves as plasma density fluctuations. Though this method doesn't give a very good height resolution, the ability to detect these waves at high latitudes is of potential importance for our understanding of the high latitude ionosphere. Furthermore, the measurements obtained at the Poker Flat IS radar (PFISR) during the International Polar Year (IPY) provide an opportunity to study these effects using plasma lines on a regular basis.

4.3.1 Poker Flat Incoherent Scatter Radar

PFISR shown in figure 4.2 is a 449 MHz phased array with a pulse-to-pulse steering capability. This allows the radar to make high time resolution measurements in a single direction and reasonable time resolution measurements in multiple directions. The data shown in this thesis are taken only in a single direction - radar pointed towards the magnetic zenith at Poker Flat ($-154.3^oAz.77.5^oEl.$). A $480\mu s$ long pulse was transmitted and received signal was sampled every $143\mu s$, giving a range resolution of 21.5 km. The receiver bandwidth was 3.56 MHz.

Figure 4.2: Poker Flat Incoherent Scatter Radar (image courtesy: Craig Heinselman, SRI International)

4.3.2 Observations

Figure 4.3 shows a series of frequency-time-intensity images for the June 15, 2007 from 0814 - 1842 LT (UT-9) for altitudes from 158 to 242 km. The color scale indicates calibrated signal power after noise subtraction in [Watts].The signal of interest here is the temporally fluctuating enhancement in the intensity above the noise floor. The experiment technique here to transmit a long pulse to observe plasma lines is known as plasma line cutoff technique, where the received signal comes from a sharp gradient in the electron density profile in a given range gate (*Showen*, 1995). The transmit pulse gives the resolution of 72 km. We will call this the range gate. The received signal here is sampled at a higher rate than the transmitted signal to achieve apparent higher range resolution of 20

km. We will call this the range bin. In essence, the received signal comes from chopping a range gate into multiple range bins, regardless of the actual range resolution (72 km in this case). Each image in this figure thus shows the largest return in a particular range bin, though the actual signal is still integrated over the entire range gate. The result of this is that the same signal may appear in multiple 20 km range bins, and signal from multiple range gates may appear in a single range bin. The spectra shown here are integrated for ~ 2 minutes. Notice that the plasma line trace seen in the lowest two altitude bins is qualitatively different from that seen in upper two altitude bins. This means that the bottom two and the top two range bins come from non-overlapping range gates. The lower trace has the strongest signal at 179 km, and the upper trace is strongest at 242 km. So it is reasonable to assume that there are two extrema in the electron density profile at $h_1 = 179 \pm 10$ km and $h_2 = 242 \pm 10$ km. At 200 km, both traces are present due to the range gate overlapping in this range bin, which enables us to see the phase relationship between the lower trace and the upper trace. The upper trace has the same period as the lower trace with a phase shift of $\sim 180^o$. This difference is shown in more detail in fig. 4.4. The color scale here is also in the units of calibrated signal power after noise subtraction in [Watts].

Since the radar beam is aligned with the magnetic field lines, the plasma density variation cannot be due to an imposed electric field effect, as such fields map along the magnetic field lines. It is also highly unlikely that production or loss would vary in the manner seen along magnetic field. We conclude that the variability must be due to an internal gravity wave interaction with the medium. The induced amplitude of the plasma line frequency variation was 3% at the

upper height and considerably less below. The increase with altitude is also a good evidence for a GW interpretation.

As a further evidence for the characteristic downward phase propagation of the GW, we compared the density fluctuations seen in the plasma line with the electron density estimates obtained from the ion line. Figure 4.5 shows electron density estimated from the ion line using Te/Ti correction but neglecting Debye length variations with Te and Ne in the upper panel. The lower panel shows electron density fluctuations $\delta Ne/Ne$, after filtering out high-frequency components from Ne. This figure shows 30-40 min. period perturbations in the electron density, which match with those seen in the plasma line.

Calculating Gravity wave vertical parameters

Taking the wave period to be $\tau = 37$ min., which is greater than the buoyancy period (7-11 min.) at these altitudes. The phase delay between the lower altitude wave and the higher altitude wave is $\delta t = 10$ min., which is almost certainly due to the downward phase propagation. Using this information, we derive the vertical wavelength $\lambda_z = (h_2 - h_1)\tau/\delta t \approx 233 \pm 10$ km, and vertical phase velocity of -105 m/s.

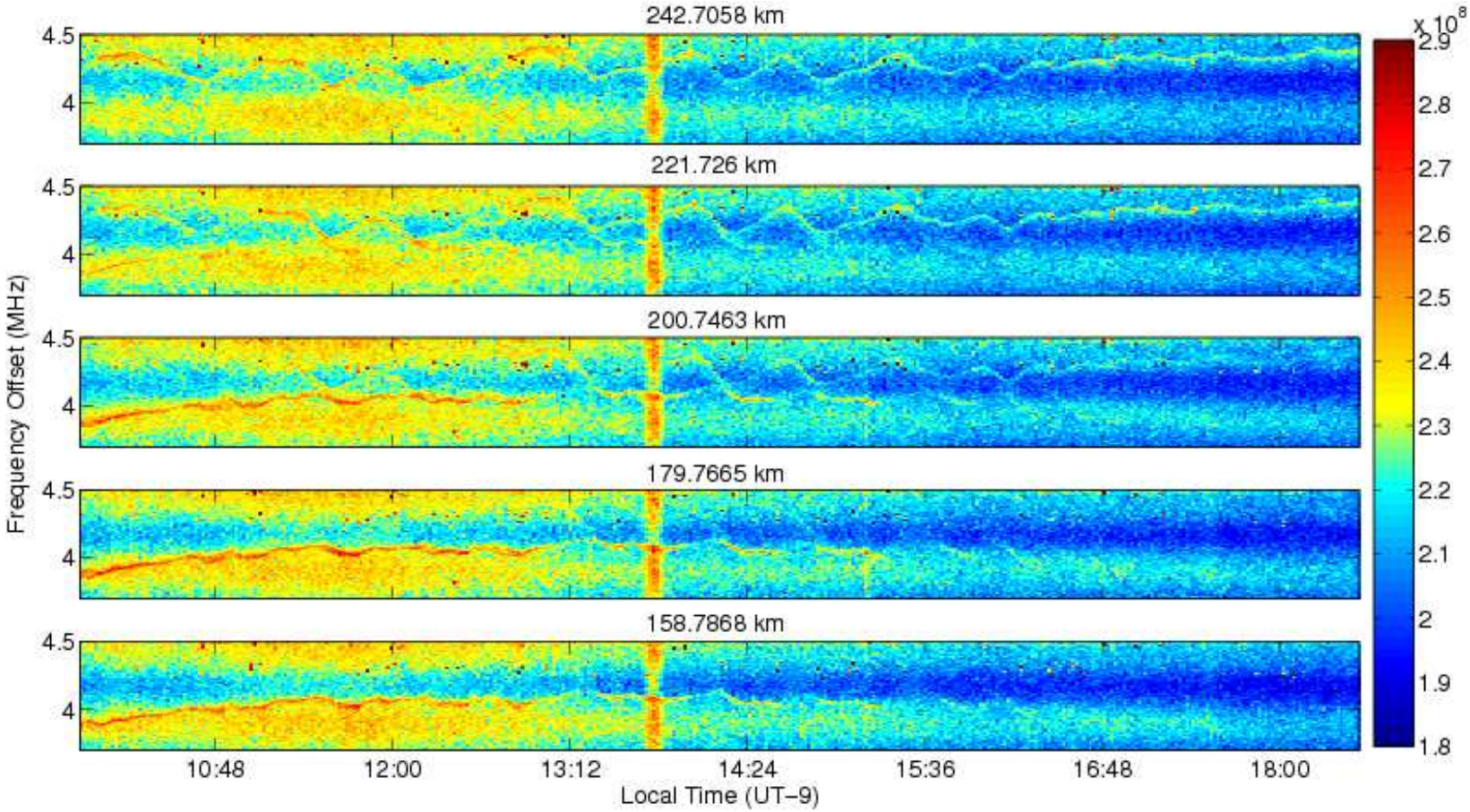

Figure 4.3: Plasma line frequency over time for altitudes from 158 km to 242 km. Notice two different plasma line traces in lower two and upper two altitude bins, which overlap at 200 km, indicating a downward phase progression. See text for details.

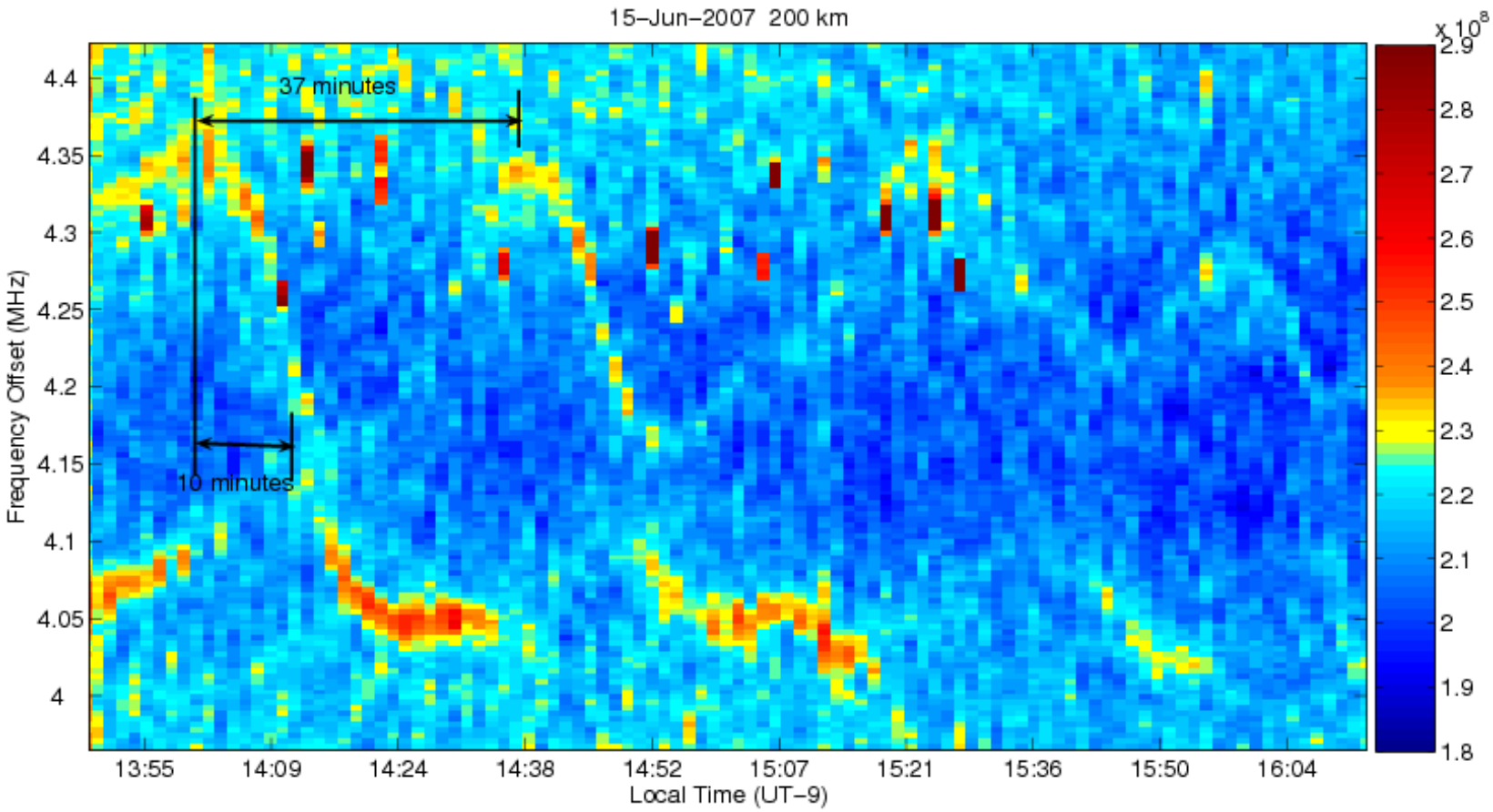

Figure 4.4: A zoomed in image for 200 km that shows GW in both lower and upper density layers, with $\sim$ 37 min wave period and phase delay of 10 min. The amplitude of GW has grown from lower to higher altitude by 65%.

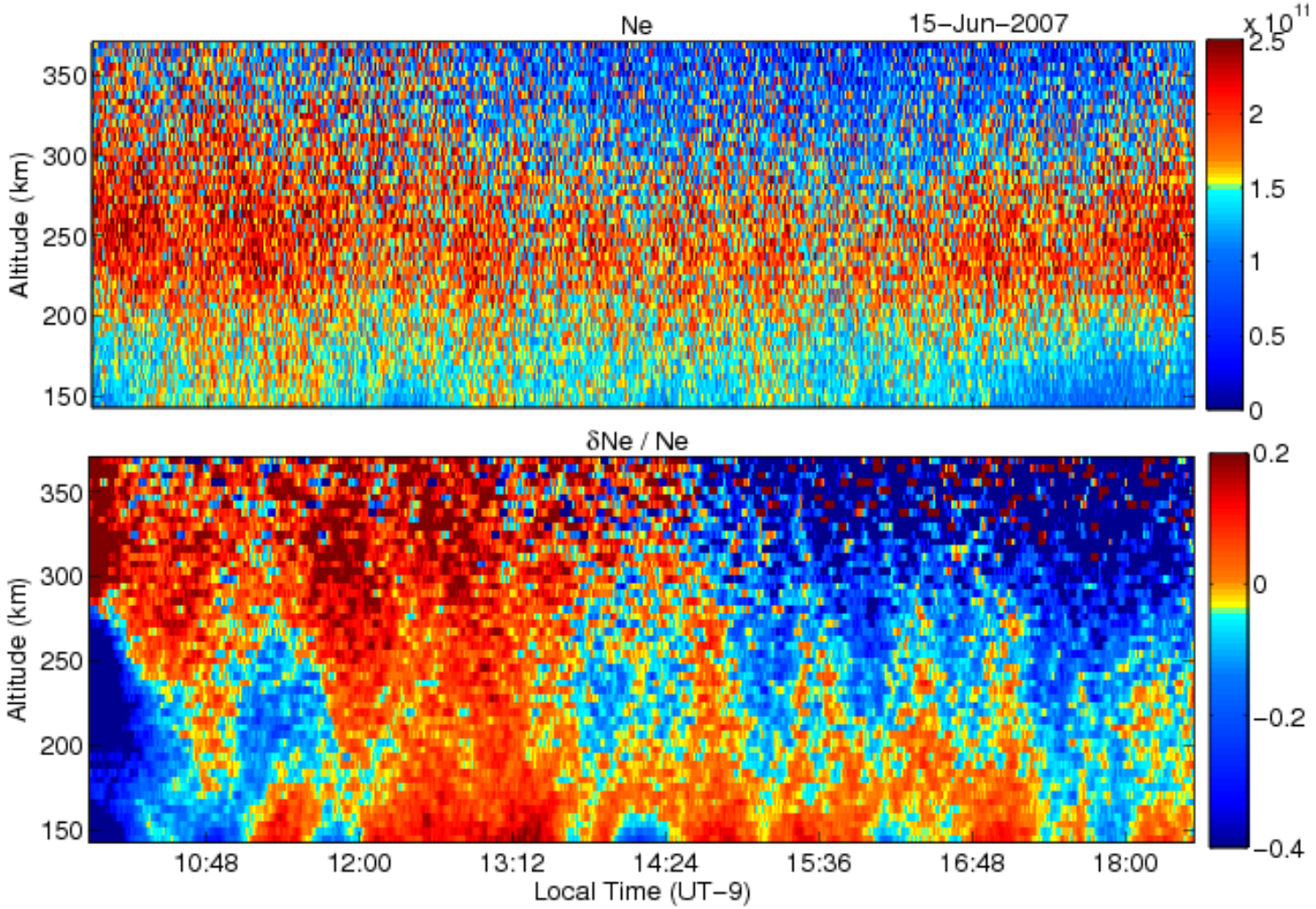

Figure 4.5: Top panel shows electron density estimate [$/m^3$], while bottom panel shows $\delta Ne/Ne$.

4.4 Density fluctuations at Mid-latitudes

In addition to the GW observations presented here with the Poker Flat IS radar, the plasma line cutoff technique at Arecibo radar has also revealed significant periodic density perturbations in the morning period. The morning time observations taken during November 2006 have indicated the presence of two spectrally thin intermediate layers at lower F region heights, oscillating with a period of 6-10 minutes. Figure 4.6 observations from one such morning. At lower altitude of 145 km, two traces indicating layers are seen at frequency offsets between 2.5 to 3.5 MHz. These oscillations are not only limited to the thin layers. The period of oscillation is 6 minutes. These layers were present on every consecutive morning from November 21-23, 2006, with the same period. The broad plasma line return between 3.5 and 5 MHz is not smooth, but shows striations spanning over several frequencies and varying in time. Since the returned signal is integrated over 75 km range gate, and the highest return comes from where the density gradient is sharpest, returns at higher plasma frequencies may be interpreted as coming from higher altitudes. If this is the case, the top panel in fig. 4.6 indicates that the same neutral density variation is affecting both layers and the ionosphere at higher altitudes. However, it is important to note here that the plasma line at lower frequency offsets (¡ 4 MHz) may come only from purely thermal electrons while that at the higher offsets also has a contribution from high energy photoelectrons (*Yngvesson and Perkins*, 1968). The bottom panel in fig. 4.6 shows plasma line fluctuations in topside (above the F region peak) ionosphere. These fluctuations are on top of the background density as shown in figure 4.7. The fluctuations increase in the frequency, stay at the same offset for about 40 minutes, then decrease in the frequency. This behavior was

also seen on all three mornings of observation. Now it is known that gravity waves are a ubiquitous feature at mid-latitudes (e.g. *Djuth et al.*, 2004). However, the sources for the various period waves are unknown. Several sources have been hypothesized including the ocean waves, the tropospheric pressure fluctuations, solar terminator driven effect and magnetospheric sources. Precise measurements of the various period electron density perturbations can certainly help in the process of determining the sources.

4.5 Discussion and Conclusion

Here we have presented a method using plasma lines to detect GWs and infer the vertical wavelength and period of the same. GWs were observed using the fluctuations in the electron density and hence in the plasma line frequency over time at different altitudes. It also allowed for a sensitive measurement of the GW amplitude, which increased by 65% in ~ 63 km. Using these plasma line density estimates with electron and ion temperature estimates obtained using the ion line could, combined with the GW theory, help determine the fluctuating thermospheric wind. In addition the height variation with altitude will provide a good test for the damping mechanisms for these waves. We would like to note that the plasma line method provides a much cleaner way to detect the GW fluctuations and eliminates the need for additional data processing. At Arecibo radar, it may also help distinguish between the fluctuations in thermal and non-thermal electrons densities in combination with the gyro line measurements in low-density environment.

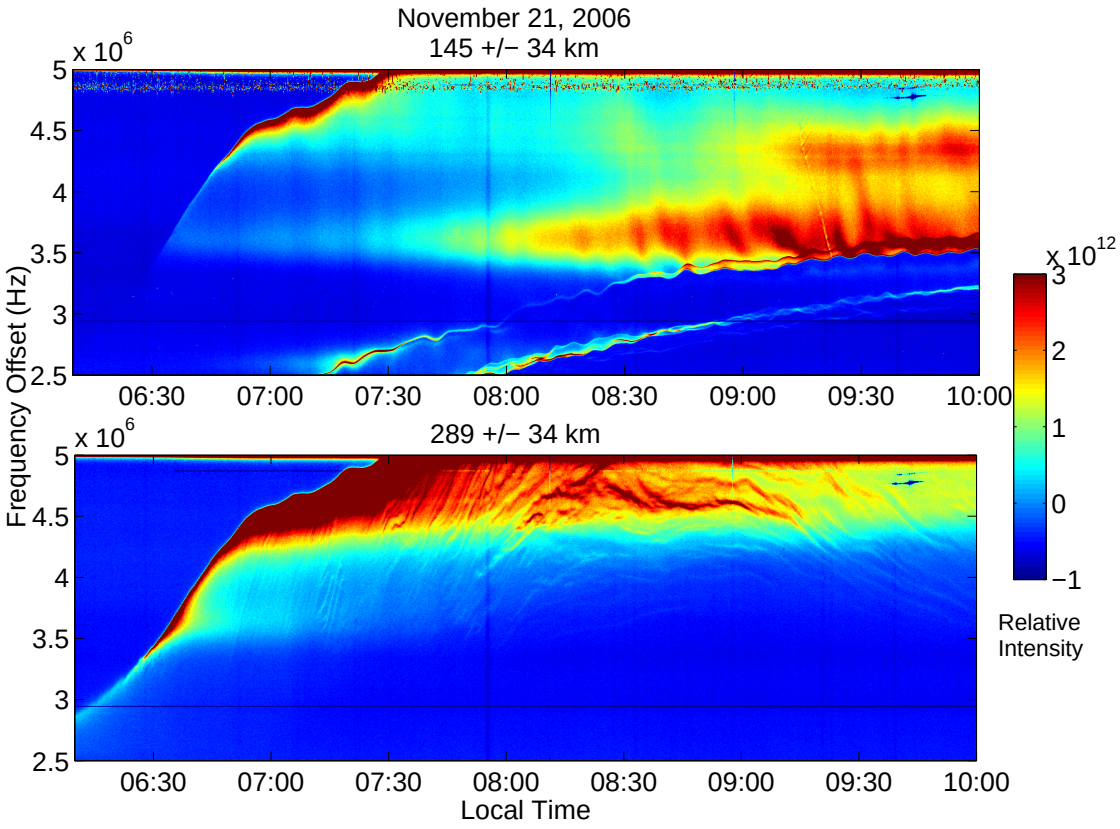

Figure 4.6: Plasma line spectra taken on the morning of November 21, 2006. It shows the presence of two intermediate layers indicated by two different plasma line traces in the top panel, which are oscillating with 6-10 minute period. These layers were present on every morning during November 21-23, 2006. The bottom panel shows the spectra at a higher altitude, where the dark traces are the plasma density perturbations on top of the background density. The characteristic increase in the frequency, relative steadiness for 40 minutes, and eventual decrease in the frequency were seen on other days as well. This could be part of a larger period gravity wave. The color scale indicates un-calibrated signal power after noise subtraction and negative values are to enhance contrast.

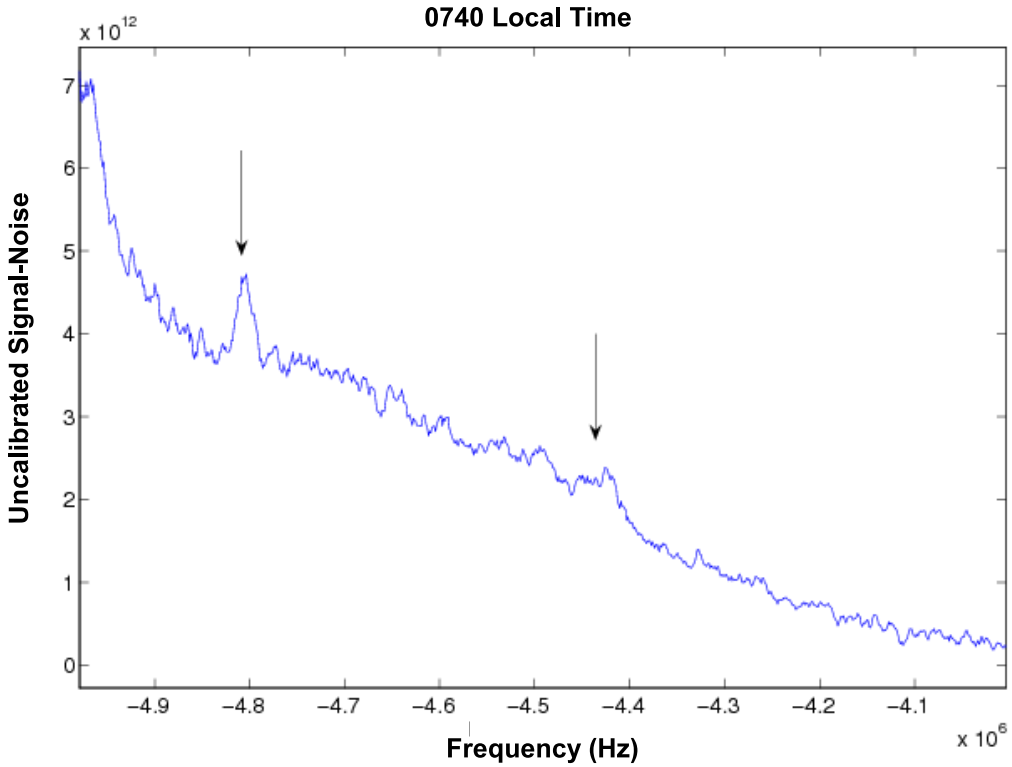

Figure 4.7: Plasma line spectrum taken on the morning of November 21, 2006 at 0740 LT. The arrows show the fluctuations in the plasma line power on top of the broad plasma line resulting from the long pulse. These fluctuations are at 10% of the background plasma line power.

We have looked at the plasma line data from February to August 2007 and we have found such fluctuations in the plasma line nearly 50% of the time. Determining source mechanisms for these periodic fluctuations is an active area of research. The significance of the work presented here is that plasma line can be easily used to determine the nature of such fluctuations that can provide the means to understand the source mechanism for them.

At high latitudes, auroral precipitation, electric fields, and plasma instabilities add to the complex nature of the ionosphere and make it difficult to find the source of GWs in the thermosphere. The electron plasma waves, which create the resonance line known as plasma line, have velocities near the tail of the Maxwellian distribution and get enhanced by energetic particles such as photoelectrons. Auroral precipitation gives rise to superthermal electron flux, which is difficult for particle detectors. There have been several previous successful attempts to measure auroral plasma lines (*Valladares et al.*, 1988; *Kirkwood et al.*, 1995; *Nilsson et al.*, 1996). In addition, according to *Yngvesson and Perkins* (1968)The plasma line technique described can prove to be a useful tool to augment the studies of these processes.

CHAPTER 5

SUMMARY AND FUTURE WORK

We have presented here new ionospheric applications using the technique of incoherent scattering. The experiments and theoretical discussions presented pertain to the resonance lines in the electron component of the incoherent scatter (IS) spectrum, namely the gyro line and the plasma line. These resonance lines have been explored theoretically since 1960's, when the IS theory was developed by various authors. The experimental exploration began primarily at the Arecibo Observatory when it became possible to observe wide bandwidth spectrum. In recent years, the development in the radar hardware and software has made it feasible to make high time and range resolution observations of these lines, which has led us to discover several applications using them. In this thesis, we have described a technique to infer the night-time electron density and detection of intermediate layers at mid-latitudes using the gyro line, and detecting gravity wave signatures using the plasma line at high latitudes. In addition, also presented are experimental observations of frequency gap in the IS spectrum at second electron gyro harmonic, a feature that was predicted in the IS theory but observed for the first time at the second gyro harmonic. The summary and the future explorations of the work presented here are discussed in the following sections.

5.1 Electron component in incoherent scatter spectrum

The technique of incoherent scatter (IS) from the ionosphere has over the years been primarily used to derive electron density and temperature information from the bulk electron motion while disregarding the magnetic field. Hence, the primary focus of various observing facilities around the world is to make ion line measurements because the power under the ion line is directly proportional to the electron density in the ionosphere. The ion line in the spectrum results from the up and the down going ion acoustic waves in the ionosphere and is not affected by the magnetic field, except at angles perpendicular to the magnetic field, namely equatorial latitudes (e.g. Jicamarca Radio Observatory). In recent years the IS radars around the world have added advanced hardware and developed compatible radar modes to be able to detect the scattering from the higher velocity plasma waves, mainly Langmuir (electron plasma) waves (e.g., *Showen*, 1979; *Djuth et al.*, 1994). These higher velocity waves result from the electron motion in the ionosphere, since ions are relatively slower and therefore do not produce high Doppler shift of the order of MHz in the spectrum. The electron component of the IS spectrum is composed of such waves with higher velocity that cause resonance lines in the spectrum at wave frequencies.

5.1.1 Gyro line

A unique feature that came out of the IS theory after including the magnetic field was the gyro line. It was first observed by *Behnke and Hagen* (1978) using

the Arecibo radar during the day time, but it involved integrating for 2 hours to see the gyro line signal above the noise. Since then a multitude of efforts have taken place to observe and discover the usefulness of this resonance line, mainly at the Arecibo (*Behnke and Hagen*, 1978; *Sulzer and Gonzalez*, 2002) and at the EISCAT (*Bjørnå et al.*, 1990; *Malnes and Bjørnå*, 1993; *Shume*, 2000) IS radars. For a long time, the gyro line was considered devoid of any useful information. The theoretical work carried out after initial detection primarily investigated the effects of the superthermal electrons. *Shume* (2000) did explore the gyro line frequency dependence on various ionospheric parameters, however the parameter values considered were for daytime ionosphere and much higher temperature, when the gyro line becomes very broad and is difficult to detect. The work reported in this thesis concentrates primarily on the gyro line observations during the dawn and the dusk conditions, when the electron density and temperature are relatively low and rapidly changing. The gyro line persists for much of the day at lower altitudes but remains difficult to detect at higher altitudes with much higher temperatures. These measurements were made with high spectral resolution, which requires transmitting a long pulse. As a result, the altitude resolution was poor; the received signal was integrated over 75 km in range. The advantage was that the gyro line could be detected at frequencies as low as 200 kHz. Such low frequency measurements also suggest that the energy in the gyro line comes from thermal electrons. Efforts to measure gyro line with a "coded" pulse that gives a much higher range resolution have not succeeded so far.

These measurements and the calculated theoretical spectra for observed

ionospheric conditions indicated that the gyro line is strongest for the electron density between 1×10^9 and 1×10^{11} $/m^3$. This has provided another tool to measure the absolute value of the electron density during the night time. Usually at IS radar facilities where the plasma line measurements are possible, the ion line spectra are normalized using the electron density from plasma line. Most plasma line measurements are taken during the day time. However, the plasma line measurements are difficult during the night time owing to the absence of the energetic photoelectrons. The above mentioned property of the gyro line is thus useful in obtaining the absolute value of the electron density, especially for the very low density layers regularly observed at mid-latitudes. It has been known that the intermediate layers are a common occurrence in the nighttime Arecibo ionosphere (*Riggin et al.*, 1986). These layers typically occur between the F and the sporadic E layers at night and may indicate a presence of metallic ions. The structuring of the layer is a result from tidal oscillations in the neutral atmosphere (*Kelley*, 1989). These layers are also very thin in altitude and low in electron density. Our observations show such layers both in the plasma line and the gyro line during the dawn period in November. The layers seemed to appear earlier in the gyro line traces and later in the plasma line traces. Also, like the plasma line, the shape of the gyro line is indicative of the electron temperature. If the gyro line can be measured with enough spectral accuracy, it is a very useful measure to investigate the night time dynamics in mid-latitude ionosphere.

5.1.2 Plasma line

As noted in the Chapter 1, the plasma line is one of the solutions of the dispersion relation for the magnetized plasma. The frequency of the plasma line is the most sensitive measure for the electron density with a nominal correction for the electron temperature and the magnetic field. This however, changes somewhat in the domain where electron plasma frequency is close to multiples of the electron gyro frequency. The dispersion relation for waves in magnetized plasma exhibits gaps at these frequencies. Instead of a resonance line at these frequencies, two roots appear, one on the either side of the gap. The separation between the two roots is $kv_{the}/2\pi$. This effect was first noted by *Gross* (1951) and *Bernstein* (1958) but was met with doubt initially (*Oster*, 1960). However, it was proven later using a different technique by *Salpeter* (1961). Soon after, *Perkins* (1963) provided numerical calculations for the electron component of the IS spectrum and showed that the plasma line splits into two separate resonances. Much of the approximate theoretical work shown in this thesis is based on these early calculations.

In the IS theory, this "split" is only present when magnetic field is included in the calculations. The presence of the split depends on the angle between the radar wave vector and the magnetic field. However, the width of the gap itself depends on the electron temperature. This provides an additional measure for the electron temperature. According to the theory, such frequency gaps should also be present at the higher gyro harmonics, though the angle requirements for those are severe with Arecibo parameters as noted in Chapter 3. The discussion in this thesis concentrates solely on the effects on thermal electrons. The effects

at radar wavelengths other than Arecibo or AMISR have not been explored either.

5.2 Gravity waves

We have shown here that the high spectral resolution plasma line can be used to measure some of the properties of the thermospheric gravity waves (GWs). The GWs propagating into the thermosphere cause the electron density displacement in the plasma. Numerous previous measurements have suggested that the thermospheric GWs are a ubiquitous feature at mid and high latitudes. The advantage of the high spectral resolution plasma line is that the density perturbations of all periods can be detected with high precision, the frequency being a more precise measure than the power. The electron component can also be used to observe the evolution of thin density layers that are often modulated with gravity waves propagating up from lower atmosphere. We haven't been able to explain the features observed during November 2006 mornings with the Arecibo radar very well, and more observations are needed.

5.3 Conclusion and Future work

The work reported in this dissertation involves measuring the complete IS spectrum and using it to derive important geophysical parameters. While the

plasma line is a much widely known feature in the spectrum that has been used to make a variety of sensitive measurements (e.g. *Djuth et al.*, 1994; *Nicolls et al.*, 2006), this was the first time a plasma line has been measured at a frequency offset of as low as 1.2 MHz. These measurements helped validate the IS theory including the magnetic field by showing that the plasma line indeed "splits" at the second gyro harmonic (*Salpeter*, 1961; *Perkins*, 1963).

The ionospheric electron density is often modulated by the small and the large scale waves and instabilities in the upper atmosphere. These waves could either be the result of the gravity waves from the lower atmosphere or the solar-magnetospheric sources. The large scale instabilities such as the sporadic-E instability and the Rayleigh-Taylor instability can also cause the fluctuations in the electron density. However, it is very difficult to determine the source of the observed fluctuations in the electron density. The plasma line measurements can help in two ways to aid this research. First, high spectral and temporal resolution plasma lines are the best way to measure the periodicity of the waves. This also helps to find if there are multiple periods that need to be taken into consideration. The plasma line technique at the most IS radar facilities (Arecibo, AMISR facilities - PFISR and RISR, and EISCAT Svalbard) has been refined to make reasonably high spectral and temporal resolution measurements to make this possible. Second, at high latitudes, the energetic auroral electrons enhance the plasma lines. Such auroral plasma lines can be used to determine the auroral influx and the effect of magnetospheric sources on the ionospheric electron density. The IPY dataset discussed in this thesis has revealed significant density fluctuations about 50% of time using the Poker Flat IS radar. A comparison between the simultaneous plasma line measurements taken during the IPY at

other high latitude IS radars, such as the EISCAT radar will be used to gain some insight into the sources of these fluctuations.

The gyro line, the lesser known cousin of the plasma line was measured first in 1978 (*Behnke and Hagen*, 1978), then thrust largely into obscurity (barring a few attempts using the EISCAT radar) due to the belief that it is useless in deriving any geophysical information. The work described here reports first clear observations of the gyro line in an IS spectrum, and was detected with a 20 second integration. These measurements also confirmed the theoretical results about a rapid change in the gyro line frequency when the electron density is changing in the range of $10^9 - 10^{10}/m^3$. The gyro line intensity is about twice as much during this electron density range as it is at the higher densities, so it is easier to detect. Of course the detection also depends on the electron temperature. The broadening caused by much higher temperatures make it nearly impossible to detect at higher altitudes, but it can still be seen at lower altitudes even during the daytime. The gyro line measurements during the dawn and the dusk hours, when the electron density and temperature are rapidly changing, can thus be used to derive an absolute value of the electron density. This is of particular importance since the plasma line, which usually provides the absolute electron density, is not available before the sunrise due to the lack of the high-energy photoelectrons as noted above. The gyro line can fill this gap. The mid-latitude IS radars should be able to measure the gyro line with reasonable sensitivity and temporal resolution. At Arecibo, an attempt to measure high altitude resolution gyro line is already in progress and the same will be undertaken with the Millstone Hill radar in near future, though may prove to be much more difficult.

BIBLIOGRAPHY

Behnke, R. A., and J. B. Hagen (1978), Incoherent scattering of radio waves by whistler mode oscillations in the ionosphere, *Radio Sci.*, *13*(1), 215–218.

Bernstein, I. B. (1958), Waves in a plasma in a magnetic field, *Phys. Rev.*, *109*(1), 10–21.

Bhatt, A. N., E. A. G. Kendall, M. C. Kelley, M. P. Sulzer, and E. B. Shume (2006), Observations of strong gyro line spectra at arecibo near dawn, *Geophys. Res. Let.*, *33*, L14105, doi:10.1029/2006GL026139.

Bhatt, A. N., M. J. Nicolls, M. P. Sulzer, and M. C. Kelley (2008), Observations of plasma line splitting in the incoherent scatter spectrum, *Phys. Rev. Lett.*, *100*, 045,005, doi:10.1103/PhysRevLett.100.045005.

Bjørnå, N., B.-T. Esjeholm, and T. L. Hansen (1990), Gyro line observations with the $EISCAT\ VHF$ radar, *J. Atmos. Terr. Phys.*, *52*(6-8), 473–482.

Bowles, K. L. (1958), Observations of vertical incidence scatter from the ionosphere at 41 mc/s., *Phys. Rev. Lett.*, *1*, 454–455.

Bowles, K. L., G. R. Ochs, and J. L. Green (1962), On the absolute intensity of incoherent scatter echoes from the ionosphere, *J. Res. Nat. Bur. Standards.*, *66D*, 395–407.

Chen, F. F. (1984), *Introduction to Plasma Physics and Controlled Fusion Volume 1: Plasma Physics*, Plenum Press.

Djuth, F. T., M. P. Sulzer, and J. H. Elder (1994), Application of the coded long pulse technique to plasma line studies of the ionosphere, *Geophys. Res. Let.*, *21*(24), 2725–2728.

Djuth, F. T., M. P. Sulzer, J. H. Elder, and V. B. Wickwar (1997), High-resolution studies of atmosphere-ionosphere coupling at arecibo observatory, puerto rico, *Radio Sci.*, *32*, 2321–2344.

Djuth, F. T., M. P. Sulzer, S. A. Gonzalez, J. D. Mathews, and J. H. Elder (2004), A continuum of gravity waves in the arecibo thermosphere?, *Geophys. Res. Let.*, *31*, L16,801, doi:10.1029/2003GL019376.

Djuth et al., F. T. (2005), Ionospheric modification at twice the electron cyclotron frequency, *Phys. Rev. Let*, *94*, doi:10.1103/PhysRevLett.94.125001.

Dougherty, J. P., and D. T. Farley (1960), A theory of incoherent scattering of radio waves by a plasma, *Proc. Roy. Soc.*, *A359*, 79–99.

Farley, D. T., J. P. Dougherty, and D. W. Barron (1961), A theory of incoherent scattering radio waves by a plasma ii. scattering in a magnetic field, *Proc. Roy. Soc. A.*, *263*, 238–258.

Farley, D. T., J. P. McClure, D. L. Sterling, and J. L. Green (1967), Temperature and composition of the equatorial ionosphere, *J. Geophys. Res.*, *72*(23), 5837–5851.

Fejer, J. A. (1960), Scattering of radio waves by an ionized gas in thermal equilibrium, *Can. J. Phys.*, *38*, 1114–1133.

Fremouw, E. J., J. Petriceks, and F. W. Perkins (1969), Thomson scatter measurements of magnetic field effects on the landau damping and excitation of plasma waves, *Phys. Fluids*, *12*, 869–875.

Gordon, W. E. (1958), Incoherent scattering of radio waves by free electrons with application to space exploration by radar, *Proc. of the IRE*, pp. 1824–1829.

Gross, E. P. (1951), Plasma oscillations in a static magnetic field, *Phys. Rev.*, *82*(2), 232–242.

Hagfors, T. (1961), Density fluctuations of a plasma in a magnetic field with applications to the ionosphere, *J. Geophys. Res.*, *66*, 1699–1712.

Hines, C. O. (1960), Internal atmospheric gravity waves at ionospheric heights, *Can. J. Phys.*, *38*, 1441–1481.

Janches, D., and M. J. Nicolls (2007), Diurnal variability of the gyro resonance line observed with the arecibo incoherent scatter radar at e- and f1-region altitudes, *Geophys. Res. Let.*, *34*, L01,103, doi:10.1029/2006GL028510.

Kelley, M. C. (1989), *The Earth's Ionosphere: Plasma Physics and Electrodynamics*, Academic Press Inc.

Kirkwood, S., H. Nilsson, J. Lilensten, and M. Galand (1995), Strongly enhanced incoherent-scatter plasma lines in aurora, *J. Geophys. Res.*, *100*(A11), 21,343–21,355.

Kosch et al., M. J. (2005), Artificial optical emissions at haarp for pump frequencies near the third and second electron gyro-harmonic, *Ann. Geophys.*, *23*, 1585–1592.

Kudeki, E., and M. Milla (2006), Incoherent scatter spectrum theory for modes propagating perpendicular to the geomagnetic field, *J. Geophys. Res.*, *111*, A06306, doi:10.1029/2005JA011546.

Malnes, E., and N. Bjørnå (1993), Enhancement of incoherent scatter gyro lines by suprathermal electrons, *J. Atmos. Terr. Phys.*, *55*(4-5), 667–674.

Malnes, E., N. Bjørnå, and T. L. Hansen (1996), Anomalous echoes observed with the eiscat uhf radar at 100-km altitude, *Ann. Geophys.*, *14*, 1328–1342.

Mishin, E. V., M. J. Kosch, T. R. Pedersen, and W. J. Burke (2005), Hf-induced airglow at magnetic zenith: Thermal and parametric instabilities near electron gyroharmonics, *Geophys. Res. Let.*, *32*, doi:10.1029/2005GL023864.

Nicolls, M. J., and C. J. Heinselman (2007), Three-dimensional measurements of traveling ionospheric disturbances with the poker flat incoherent scatter radar, *Geophys. Res. Let.*, *34*, L21,104, doi:10.1029/2007GL031506.

Nicolls, M. J., M. C. Kelley, A. J. Coster, and S. A. González (2004), Imaging the structure of a large-scale TID using ISR and TEC data, *Geophys. Res. Let.*, *31*, L09812, doi:10.1029/2004GL019797.

Nicolls, M. J., M. P. Sulzer, N. Aponte, R. Seal, R. Nikoukar, and S. A. González (2006), High-resolution electron temperature measurements using the plasma line asymmetry, *Geophys. Res. Let.*, *33*, L18107, doi:10.1029/2006GL027222.

Nilsson, H., S. Kirkwood, J. Lilensten, and M. Galand (1996), Enhanced incoherent scatter plasma lines, *Ann. Geophys.*, *14*, 1462–1472.

Oster, L. (1960), Linearized theory of plasma oscillations, *Rev. Mod. Phys.*, *32*(1), 141–168.

Perkins, F. W. (1963), Numerical calculations of the electronic contribution to electron density fluctuations in a plasma with a uniform magnetic field, *Tech. Rep. CRSR 145-I*, Cornell University, Ithaca, NY.

Perkins, F. W., E. E. Salpeter, and K. O. Yngvesson (1965), Incoherent scatter from plasma oscillations in the ionosphere, *Phys. Rev. Lett.*, *14*, 579–581.

Riggin, D., W. E. Swartz, J. Providakes, and D. T. Farley (1986), Radar studies of long-wavelength waves associated with mid-latitude sporadic e layers, *J. Geophys. Res.*, *91*(A7), 8011–8024.

Rodrigues, F. S., M. J. Nicolls, and D. L. Hysell (2007a), Improved electron density measurements at jicamarca, *J. Geophys. Res.*, *112*, A11,315, doi:10.1029/2007JA012598.

Rodrigues, F. S., M. J. Nicolls, R. Woodman, D. L. Hysell, J. L. Chau, and S. A. Gonzálex (2007b), Ion gyroresonance observations at jicamarca revisited, *Geophys. Res. Let.*, *34*, L13,107, doi:10.1029/2007GL029680.

Rosenbluth, M. N., and N. Rostoker (1962), Scattering of electromagnetic waves by a nonequilibrium plasma, *Phys. Fluids*, *5*(7), 776–788.

Salpeter, E. E. (1960), Electron density fluctuations in a plasma, *Phys. Rev.*, *120*, 1528–1535.

Salpeter, E. E. (1961), Plasma density fluctuations in a magnetic field, *Phys. Rev.*, *122*, 1663–1674.

Showen, R. L. (1979), The spectral measurements of plasma lines, *Radio. Sci.*, *14*(3), 503–508.

Showen, R. L. (1995), Spectral plasma lines at sondrestrom, *Radio. Sci.*, *30*(6), 1841–1853.

Shume, E. B. (2000), Simulation of gyro lines for the $EISCAT$ svalbard radar, Master's thesis, University of Tromsø, Tromsø, Norway.

Stringer, T. E. (1963), Low-frequency waves in an unbounded plasma, *J. Nucl. Energy Part C*, *5*, 89–107.

Sulzer, M. P., and S. A. Gonzalez (1999), The effect of electron coulomb collisions on the incoherent scatter spectrum in the f region at jicamarca, *J. Geophys. Res.*, *104*(10), 22,535.

Sulzer, M. P., and S. A. Gonzalez (2002), Electron and gyro-lines, *NAIC/AO Newslet.*, *34*.

Vadas, S. L. (2007), Horizontal and vertical propagation and dissipation of gravity waves in the thermosphere from lower atmospheric and thermospheric sources, *J. Geophys. Res.*, *112*, A06,305, doi:10.1029/2006JA011845.

Vadas, S. L., and D. C. Fritts (2005), Thermospheric responses to gravity waves: Influences of increasing viscosity and thermal diffusivity, *J. Geophys. Res.*, *110*, D15,103, doi:10.1029/2004JD005574.

Vadas, S. L., and M. J. Nicolls (2008), Using pfisr measurements and gravity wave dissipative theory to determine the neutral, background and thermospheric winds, *Geophys. Res. Let.*, *35*, L02,105, doi:10.1029/2007GL031522.

Valladares, C. E., M. C. Kelley, and J. F. Vickrey (1988), Plasma line observations in the auroral oval, *J. Geophys. Res.*, *93*(A3), 1997–2003.

Woodman, R. F. (2004), On a proper electron collision frequency for a Fokker-Planck collision model with Jicamarca applications, *J. Atmos Solar-Terr. Phys.*, *66*(17), 1521–1541.

Yngvesson, K. O., and F. W. Perkins (1968), Radar thomson scatter studies of photoelectrons in the ionosphere and landau damping, *J. Geophys. Res.*, *73*(1), 97–110.